



Modelling and validation of wind
turbine wake superposition
Using wind farm data

Ottelien H.G. Bossuyt

Modelling and validation of wind turbine wake superposition

Using wind farm data

by

Ottelien H.G. Bossuyt

to obtain the degree of

Master of Science in Aerospace Engineering at Delft University of Technology,
Master of Science in Engineering (European Wind Energy) at The Technical University of Denmark

to be defended publicly on Wednesday, the 15th of August 2018.

Student number: 4624351

Project duration: 1st of November 2017 – 15th of August 2018

Supervisors: Dr.ir. Michiel B. Zaaijer TU Delft, Assistant Professor

Dr. Søren J. Andersen DTU, Assistant Professor

Nicolai G. Nygaard Ørsted, Lead Specialist

Chairman: Dr.ir. Carlos J. Simão Ferreira TU Delft, Associate Professor

An electronic version of this thesis is available at <http://repository.tudelft.nl/>.

Preface

This MSc Thesis marks the end of completing the European Wind Energy Master, and therefore also of my student life. I am very grateful I got the chance to be part of this interesting program, to study at universities widely known for their expertise in aerodynamics and wind energy and, above all, to meet very inspiring, helpful and dedicated people. Writing a MSc Thesis is not something you do in one day and you definitely come across some obstacles along the way. Luckily, as sung by thousands of people before, “You’ll never walk alone” and therefore, I would like to thank some people in particular.

Firstly, I would like to express my gratitude to my supervisors, Søren Andersen, Michiel Zaaijer and Nicolai Nygaard. The bi-weekly meetings were a source of inspiration and a motivation to look critically at the results from another point of view. To Michiel, for the comprehensive feedback. To Søren, whose door was always open and who made sure I had LES results to work with. To Nicolai, who gave me the opportunity to write this MSc Thesis in collaboration with Ørsted and who provided the BEACon measurement data.

Thank you to all the people who make the EWEM program possible. I am sure the program would not be as it is now without the administration and coordinating people. It was also a pleasure to get the chance to work more closely together with some of them, both as an Aeolus board member and as student assistant.

I also want to thank my friends. The new ones and the old ones. The ones living close to me and the ones living in another country. The ones with motivating words and the ones with funny stories. The ones I worked closely together with and the ones you can always count on.

Last but not least, I would like to thank my parents and boyfriend for their love and support. They encouraged me, each in his/her own way, when I needed it the most. Thank you.

*Ottelien Bossuyt
24th of July 2018*

Abstract

The wind field and, more importantly, the power production change when downstream wind turbines are located in the wake of an upstream wind turbine. Wind farms become larger and therefore the field becomes more complex. Turbines will experience the influence of the wake of multiple wind turbines. The interaction of these wakes can be modelled using different approaches. Using numerical solvers is very computationally costly and accordingly, there is a need for simple engineering wake models which represent the wind field in a good way.

The focus of this MSc Thesis project is to find a superposition method in combination with the Jensen/Park model, which is in good agreement with a representative reference for mixed wakes in reality. This reference could be either Large Eddy Simulations (LES) or large-scale measurements data from the BEACON campaign, carried out by Ørsted. Comparisons between some datasets showed that more research is needed to identify the discrepancies between the wake fields of both datasets.

Studies have been carried out in literature, but mostly focussing on wind speeds below rated wind speed. Therefore, cases with an inflow wind speed just above and below rated wind speed are considered. The superposition methods looked at are linear superposition, quadratic superposition and the maximum deficit method. The modelling of the wake boundary, rotor averaged wind speed and power are discussed. Some superposition methods are in good agreement with the LES results, but because a uniform profile is modelled, more research is needed to assess if these conclusions also hold for sheared inflow wind profiles.

Apart from examining the combination of superposition methods and the Park wake, a study is also carried out to examine if single LES wakes can be superposed to mimic LES wake fields with multiple wind turbines. Based on the available single LES wakes, there are still essential differences in the results, but these might be overcome if more single LES wakes can be used. As the proposed superposition methods are not necessarily "true", a preliminary study is carried out in which the superposition method is optimized. This gives an insight in the number of upstream wakes that need to be included and the possible scaling or improvement of the superposition methods.

Contents

Preface	iii
Abstract	v
List of Figures	xi
List of Tables	xvii
1 Introduction	1
1.1 State of the Art & Historical Development of Single Wake Models	1
1.2 State of the Art of Wake Superposition Methods	2
1.3 Full Farm Models	3
1.4 Problem Analysis & Research Questions	4
1.5 Thesis Outline	4
2 Research Methodology	7
2.1 Overview	7
2.2 Calculation methods	8
2.2.1 Data planes	8
2.2.2 Rotor averaged wind speed	8
2.2.3 Wake boundary	11
2.2.4 Quantification system	11
2.3 Radar - BEACon	13
2.3.1 BEACon measurement campaign	13
2.3.2 Westermont Rough offshore wind farm	14
2.4 Large Eddy Simulation	15
2.4.1 Navier-Stokes equations	15
2.4.2 LES	15
2.4.3 EllipSys3D solver	16
2.4.4 Actuator line and turbine modelling	16
2.4.5 Inflow wind profile and turbulence	16
2.4.6 Post-processing	17
3 Wake Superposition Methods	19
3.1 Single Wake Models and Superposition Methods	19
3.2 Literature Review	19
3.3 Choice of Engineering Model	20
4 Engineering Models	23
4.1 Development of the Park Model	23
4.1.1 Jensen wake model	23
4.1.2 Park 1 model	23
4.1.3 Modified Park model (Peña, 2013)	24

4.1.4	Park 2 model: revised WAsP Park model	24
4.2	Implementation of the Park Model	25
4.2.1	Yaw misalignment	25
4.2.2	Correction factor	26
4.2.3	Wake reflection	26
4.2.4	Superposition methods	27
4.2.5	Park wake example	27
4.3	Sensitivity Study of the Park Model	30
4.3.1	Influence of superposition method	30
4.3.2	Influence of correction factor	31
4.3.3	Difference between Park 1 and Park 2	32
4.3.4	Summary	33
5	Defining the Reference	35
5.1	Test case	35
5.2	Wind Field	37
5.3	Power Production	40
5.4	Summary	41
6	Case Studies & Data	43
6.1	Case Studies	43
6.2	Data Generation	43
6.2.1	Wind turbine	43
6.2.2	Inflow conditions & boundary conditions	44
6.2.3	Cases	45
6.2.4	Grid spacing and domain	46
6.2.5	LES data planes	47
7	Comparison LES & Engineering Models	49
7.1	Calibration of Single Park Wake	49
7.2	Park Superposition	53
7.2.1	Inflow wind speed at rated wind speed	53
7.2.2	Inflow wind speed below rated wind speed	61
7.3	Quantification	63
7.4	Summary	65
8	Superposition of single LES wakes	67
8.1	Single wakes	67
8.2	Methodology for LES superposition	68
8.2.1	Induction zone	68
8.2.2	LES Superposition	69
8.3	Results	70
8.3.1	Case A5: 6 wind turbines	70
8.3.2	Case A6: 13 wind turbines	75
8.4	Summary	77

9 Optimization superposition method	79
9.1 Methodology	79
9.1.1 Method A	80
9.1.2 Method B	81
9.2 Discussion	82
9.2.1 Method A	82
9.2.2 Method B	86
9.3 Summary	90
10 Conclusions	91
References	95
A Sensitivity study of the Park model	99
A.1 Influence of wake decay coefficient and spacing	99
A.2 Influence of thrust coefficient	100
B Calibration of single Park wake	103
B.1 Case A1: $U_0=14 \text{ m.s}^{-1}$	103
B.2 Case B1: $U_0 = 11.2 \text{ m.s}^{-1}$	103
C Comparison LES and Park	105
C.1 Inflow wind speed at rated wind speed	105
C.1.1 Case A2: 3 wind turbines	105
C.1.2 Case A3: 4 wind turbines	106
C.1.3 Case A4: 5 wind turbines	107
C.1.4 Case A5: 6 wind turbines	109
C.1.5 Case A6: 13 wind turbines	110
C.2 Case B: $U_0 = 11.2 \text{ m.s}^{-1}$	112
C.2.1 Case B3: 3 wind turbines	112
D LES superposition	113
D.1 Case A5	113
D.2 Case A6	115
E Optimization method	119
E.1 Methodology	119
E.2 Method A: Interpolation of α -coefficients	119

List of Figures

1.1	Illustration of the local inflow wind speeds, used in the superposition methods.	3
2.1	Illustration of the different data planes, coordinate system and domain	8
2.2	Example of (a) a horizontal velocity profile and (b) a weighting function for a wind turbine with a rotor diameter of 80 m.	10
2.3	Rotor averaged wind speed, calculated as spatial average and with the weighting function.	10
2.4	Illustration of the different quantification measures.	12
2.5	Illustration of the quantification method.	13
2.6	Example of radial velocity measured by the two single Doppler radar systems (left and middle) and the corresponding Cartesian velocity (right).	14
2.7	Schematic overview of (a) the BEACon measurement set-up and (b) the lay-out of the Westermost Rough offshore wind farm with indications of wind turbine spacings and row directions (based on Ørsted data).	15
3.1	Normalized power in an interior row at the Horns Rev wind farm for the wind direction sector $270^\circ \pm 2.5^\circ$ (left) and for the wind direction sector $270^\circ \pm 15^\circ$ (right).	21
3.2	Lillgrund power deficit in a row with (a) 3.3D spacing, 2 missing wind turbines and (b) 4.3D spacing, 1 missing turbine.	21
3.3	Normalized velocity deficit at hub height as a function of the normalized distance downwind of a wind turbine for the Jensen, Frandsen, Bastankhah model and LES result.	21
4.1	Situation sketch of the Park model with an indication of the wind speeds U_0 , U_m and U_{mn} , the locations x_m , x_n , dx and the rotor diameter D_m (top view).	24
4.2	Illustration of the overlapping area, used in the Park model revised by Rathmann et al.	25
4.3	Normalized wake centerline lateral offset Δy_{yaw} as a function of the distance to the wind turbine for different yaw angles $\Delta\gamma$ for a C_T value of 0.75 and $\beta = 0.1$	26
4.4	Illustration of the ‘underground mirror’ wind turbine technique or wake reflection (side view). The region in which wake reflection has an influence is shaded in blue.	27
4.5	Example of (a) a horizontal wind speed field with three wind turbines and (b) a horizontal wind profiles at $4D$, $6D$ and $8D$ downstream of the first wind turbine.	27
4.6	General flow chart of the Park model.	28
4.7	Flow chart of the Park model, with a detailed description of calculating the wake deficit at the wind turbine locations.	29
4.8	C_T -curves of the wind turbines in the sensitivity study.	30
4.9	Wind farm lay-out used in the sensitivity study of the Park model.	30
4.10	Wake deficit at each wind turbine for different superposition methods in combination with including wake reflection or not.	31

4.11	Wake deficit at each wind turbine (a) with wake reflection and (b) without wake reflection. In both cases the results are shown with and without the implementation of the correction factor.	32
4.12	Wake deficit at the wind turbines for the Park 1 and Park 2 model, implemented in WAsP.	33
5.1	(a) Power curve and (b) thrust coefficient curve of the scaled DTU 10MW wind turbine.	35
5.2	(a) Mean vertical wind speed inflow profile with an indication of the mean wind speed at hub height for the BEACon dataset and (b) mean wind direction profiles with indication of the mean wind direction at hub height for the BEACon dataset.	37
5.3	Wind field in a horizontal plane at a height of 100 m for (a) the BEACon data and (b) LES results.	39
5.4	Streamwise wind speed at a streamwise line through the first wind turbine at a height of 100 m.	39
5.5	Horizontal profiles of the BEACon and LES datasets. The horizontal profiles shown are at a height of 100 m and $4D$, $5D$ or $6D$ downstream of the first or second wind turbine.	40
5.6	Wind speed $1R$ upstream of the hub (left) and electrical power (right) as a function of time for the three wind turbines of the LES results.	41
6.1	(a) Power curve and (b) thrust coefficient curve of the NM80 wind turbine.	44
6.2	Illustration of the calculation of the mean wind speed and turbulence intensity at the location of the second wind turbine in ‘single wake 1’. The first and second wind turbine are indicated in black and blue respectively.	45
6.3	Illustration of the LES grids for (a) a horizontal plane and (b) a vertical plane. The location of the first wind turbine and wind turbine rotor are indicated in red. The domain used in the calculations is indicated in green.	47
7.1	Wind field in a horizontal plane at hub height of a single wake with $U_0 = 14 \text{ m.s}^{-1}$ of (a) LES simulation (b) Park model with $k = 0.04$	49
7.2	Wake boundary of the single LES wake ($U = 0.98U_0$) and different single Park wakes ($U = U_0$).	50
7.3	Absolute difference between the wake boundary of the single LES wake and the different single Park wakes.	50
7.4	Centerline wind speed U_C of the single LES wake (Case A1) and the different single Park wakes.	51
7.5	Horizontal profiles of the single LES wake (Case A1) and different Park wakes at hub height and $4D$, $6D$, $8D$ or $10D$ downstream of the wind turbine.	51
7.6	Vertical plane $7D$ downstream of the single LES wake (Case A1). The rotor area is indicated in black.	52
7.7	Rotor averaged wind speed U_R of the LES simulation and single Park wakes for an inflow wind speed of 14 m.s^{-1} (Case A1).	52
7.8	Rotor averaged wind speed U_R of the LES simulation and single Park wakes for an inflow wind speed of 11.2 m.s^{-1} (Case B1).	53
7.9	Horizontal wind field at hub height of the LES simulation and Park model for Case A4, with the Park model ran with the quadratic superposition method and correction factor (CF).	54
7.10	Wake boundary of the LES simulation and Park model for Case A3, A4 and A5.	55

7.11	Rotor averaged wind speed U_R for Case A3 with four wind turbines and an inflow wind speed of 14 m.s^{-1} . The wake coefficient k of the Park model equals 0.03.	56
7.12	Rotor averaged wind speed U_R for Case A4 with five wind turbines and an inflow wind speed of 14 m.s^{-1} . The wake coefficient k of the Park model equals 0.03.	57
7.13	Rotor averaged wind speed U_R for Case A5 with six wind turbines and an inflow wind speed of 14 m.s^{-1} . The wake coefficient k of the Park model equals 0.03.	57
7.14	Rotor averaged wind speed U_R for Case A6 with 13 wind turbines and an inflow wind speed of 14 m.s^{-1} . The wake coefficient k of the Park model equals 0.03.	58
7.15	(a) Rotor averaged wind speed $U_{R,WT}$ just upstream of the wind turbine locations and (b) averaged rotor averaged wind speed $\overline{U}_{R,WT}$ for Case A5.	59
7.16	Rotor averaged wind speed $\overline{U}_{R,WT}$ at the wind turbine locations for (a) Case A4 and (b) Case A6.	59
7.17	Power of the LES results and Park models for Case A5.	60
7.18	Power of the LES results and Park models for Case A6.	60
7.19	Wake recovery for Case A5.	61
7.20	Horizontal wind field at hub height of the LES simulation and Park model for Case B3, with the Park model ran with the quadratic superposition method and correction factor (CF).	62
7.21	Rotor averaged wind speed for Case B3 (3 wind turbines).	62
7.22	(a) Rotor averaged wind speed at the wind turbine locations $U_{R,WT}$ and (b) averaged rotor averaged wind speed $\overline{U}_{R,WT}$ for Case B3.	63
7.23	The different weight sets used in the quantification of the Park model.	63
7.24	The measures Q_i for all superposition methods, shown as $(1 - \text{RMSE}_Q)$.	64
7.25	The total scores for Case A6 making use of three different weights sets.	64
7.26	The total scores for Case A6 making use of three different weights sets.	65
8.1	Rotor averaged wind speed of single wakes A1, B1, B2 and C1.	67
8.2	Induction zone length Δx_I for different wind turbine spacings. The results of the study of Andersen et al. are shown together with the induction zone length based on the streamwise velocity at hub height U_C and the rotor averaged wind speed U_R of Case A5 and A6.	69
8.3	Illustration of the single wakes at the location of the different wind turbines. The mean wind speed field and normalised mean wind speed field are shown on the left and right side respectively, for an inflow wind speed of (a)(b) $U_0 = 14 \text{ m.s}^{-1}$, (c)(d) $U_0 = 11.2 \text{ m.s}^{-1}$ and (e)(f) $U_0 = 8.6 \text{ m.s}^{-1}$. The wind turbines and the start of the induction zone are indicated with a black dot and dashed line.	69
8.4	Horizontal wind speed fields at hub height of (a) the full LES wake, followed by the superposed LES wakes, making use of (b) linear, (c) quadratic and (d) maximum deficit superposition. The LES superposition is carried out making use of the single LES wakes of Case A1, B2 and C1.	71
8.5	Difference in the horizontal wind speed fields at hub height of the full LES wake results and the superposed LES wakes, making use of (a) linear, (b) quadratic and (c) maximum deficit superposition. The LES superposition is carried out making use of the single LES wakes of Case A1, B2 and C1.	71
8.6	Horizontal profiles at hub height of the original LES simulation with six wind turbines (Case A5) and the fields constructed out of single LES wakes. The LES superposition is carried out making use of the single LES wakes of Case A1, B2 and C1.	72

8.7	Rotor averaged wind speed of the full LES wake (Case A5) and the wakes constructed out of single LES wakes. The LES superposition is carried out making use of the single LES wakes of Case A1, B2 and C1.	73
8.8	Rotor averaged wind speed at the wind turbine locations $U_{R,WT}$ of the full LES wake (Case A5) and the superposed wake fields. The LES superposition is carried out making use of the single LES wakes of Case A1, B2 and C1.	73
8.9	Wake boundary of the full LES wake (Case A5) and the superposed wake field, making use of the single LES wakes of Case A1, B2 and C1.	74
8.10	Rotor averaged wind speed of the full LES wake (Case A5) and the wakes constructed out of single LES wakes. The LES superposition is carried out making use of the single LES wakes of Case A1 and B2.	75
8.11	Rotor averaged wind speed at the wind turbine locations $U_{R,WT}$ of the full LES wake (Case A5) and the superposed wake fields. The LES superposition is carried out making use of the single LES wakes of Case A1 and B2.	75
8.12	Illustration of the calculation of the mean wind speed and turbulence intensity at the location of the second wind turbine with a spacing of $3.3D$ and inflow wind speed of 14 m.s^{-1} (Case A1). The first and second wind turbine are indicated in black and blue respectively.	76
8.13	Rotor averaged wind speed of the full LES wake (Case A6) and the wakes constructed out of single LES wakes. The LES superposition is carried out making use of the single LES wakes of Case A1 and B2.	77
8.14	Rotor averaged wind speed at the wind turbine locations $U_{R,WT}$ of the full LES wake (Case A6) and the superposed wake fields. The LES superposition is carried out making use of the single LES wakes of Case A1 and B2.	77
9.1	Illustration of the single wakes W_n , moved to the wind turbine locations, making use of a single (a) LES and (b) Park wake.	80
9.2	Illustration of the regions, used in optimization method B, for single LES wakes.	81
9.3	Result of optimization method A with a single LES wake for Case A5 as the target.	82
9.4	α -coefficients for (a) $f_{A,L}$ and (b) $f_{A,Q}$ for different wind turbine spacings if a single LES wake is used.	83
9.5	Contribution of the single wakes for Case A5 with the α -coefficient for $f_{A,L}$. The blue dashed line indicates the location of the wind turbines.	83
9.6	The coefficients α_1 to α_5 as a function of the spacing.	84
9.7	Result of optimization method A with a single Park wake for Case A5 as the target.	84
9.8	α -coefficients for (a) $f_{A,L}$ and (b) $f_{A,Q}$ for different wind turbine spacings if a single Park wake is used.	85
9.9	The coefficients α_1 to α_5 as a function of the spacing for optimization method A making use of a single Park wake.	85
9.10	Comparison of the α -coefficients for (a) $f_{A,L}$ and (b) $f_{A,Q}$ if a single Park and single LES wake are used (for Case A5 and A6).	86
9.11	Result of optimization method B with a single LES wake for Case A5 as the target.	86
9.12	β -coefficients for f_B and a single LES wake if the regions (a) do not include an induction zone and (b) include the induction zone.	87
9.13	β_1 to β_5 as a function of the wind turbine spacing if the regions (a) do not include an induction zone and (b) include the induction zone. Optimization method B is carried out with using a single LES wake.	87
9.14	Result of optimization method B with a single Park wake for Case A5 as the target.	88

9.15	β -coefficients for f_B and a single Park wake if the regions (a) do not include an induction zone and (b) include the induction zone.	88
9.16	β_1 to β_5 as a function of the wind turbine spacing if the regions (a) do not include an induction zone and (b) include the induction zone. Optimization method B is carried out with using a single Park wake.	89
9.17	Results for method B for Case A5 if $\beta_4 = \beta_5 = \beta_6 = 0$ for (a) a single LES wake and (b) a single Park wake.	90
A.1	Wind farm lay-out for the sensitivity study of the wake decay coefficient and wind turbine spacing.	99
A.2	Wake deficit at third wind turbine for different wind turbine distances S_x and wake coefficients k (a) without wake reflection and (b) with wake reflection.	100
A.3	Difference in wake deficit between including and not including wake reflection.	100
A.4	Wind farm lay-out for the sensitivity study of the wake decay coefficient and wind turbine spacing.	101
A.5	Wake deficit at $7D$ behind wind turbine for different values of C_T and k	101
A.6	Wake deficit at the wind turbines for an upstream wind speed of (a) 8 m.s^{-1} , (b) 10 m.s^{-1} and (c) 12 m.s^{-1}	102
B.1	Horizontal wind speed field at hub height for the LES results of Case A1 and the single Park wakes with different wake decay coefficients.	103
B.2	Single wakes with an inflow wind speed of 11.2 m.s^{-1} (Case B1) of (a) LES simulation and (b-f) single Park model with different wake coefficients k	104
B.3	Wake boundary of the LES simulation and Park model results with different wake coefficients k for Case B1.	104
B.4	Difference in wake boundary between the LES results and Park model results with different wake coefficients k for Case B1.	104
C.1	Horizontal wind speed field at hub height for Case A2 (three wind turbines with a spacing of $7.4D$).	105
C.2	Horizontal wind speed field at hub height for Case A3 (four wind turbines with a spacing of $4.9D$).	106
C.3	Power of the LES simulation and Park models for Case A3.	107
C.4	Horizontal wind speed field at hub height for Case A4 (five wind turbines with a spacing of $3.7D$). The white areas indicate where a negative wind speed is obtained.	108
C.5	Power of the LES and Park models for Case A4.	108
C.6	Horizontal wind speed field at hub height for Case A5 (six wind turbines with a spacing of $7.4D$).	110
C.7	Horizontal wind speed field at hub height for Case A6 (13 wind turbines with a spacing of $3.3D$). The white areas indicate where a negative wind speed is obtained.	111
C.8	Horizontal wind speed field at hub height for Case B3 (three wind turbines with a spacing of $7.4D$).	112
D.1	Horizontal profiles at hub height of the original LES simulation with 6 wind turbines (Case A5) and the fields constructed out of single wake LES simulations. The LES superposition is carried out making use of the single LES wakes of Case A1, B2 and C1.	114

D.2	Difference in the horizontal wind speed fields at hub height of the full LES wake and the superposed LES wakes, making use of (a) linear, (b) quadratic and (c) maximum deficit superposition. The second to the sixth single wake have an inflow wind speed of 11.2 m.s^{-1} and turbulence intensity of 8.6%.	115
D.3	Wake boundary of the full LES wake (Case A5) and the superposed wake field, making use of the single LES wakes of Case A1 and B2.	115
D.4	Illustration of the calculation of the mean wind speed and turbulence intensity at the location of the third wind turbine with respect to the first wind turbine ($3.3D$) in the single LES wake with an inflow wind speed of 11.2 m.s^{-1} and $\text{TI}=8.6\%$ (Case B2).	116
D.5	Horizontal wind speed fields at hub height of (a) the full LES wake, followed by the superposed LES wakes, making use of (b) linear, (c) quadratic and (d) maximum deficit superposition. The LES superposition is carried out making use of the single LES wakes of Case A1 and B2.	117
D.6	Difference in the horizontal wind speed fields at hub height of the full LES wake results and the superposed LES wakes, making use of (a) linear, (b) quadratic and (c) maximum deficit superposition. The LES superposition is carried out making use of the single LES wakes of Case A1 and B2.	118
D.7	Wake boundary of the full LES wake (Case A6) and the superposed wake field, making use of the single LES wakes of Case A1 and B2.	118
E.1	Linear extrapolation of a single LES wake (Case A1).	119
E.2	The original α -coefficients for $f_{A,L}$ are plotted in full lines. The interpolated coefficients are plotted in black for (a) $3.3D$, $3.7D$ and $7.4D$ known (interpolation 1) and (b) $3.3D$ and $7.4D$ known (interpolation 2).	120
E.3	Solution of the rotor averaged wind speed deficit with interpolated α -coefficients for $4.9D$ with the coefficients for (a) $3.3D$, $3.7D$ and $7.4D$ known (interpolation 1) and (b) $3.3D$ and $7.4D$ known (interpolation 2).	120
E.4	The original α -coefficients for $f_{A,Q}$ are plotted in full lines. The interpolated coefficients are plotted in black for (a) $3.3D$, $3.7D$ and $7.4D$ known (interpolation 1) and (b) $3.3D$ and $7.4D$ known (interpolation 2).	121
E.5	Solution of the rotor averaged wind speed deficit with interpolated α -coefficients of $f_{A,Q}$ for $4.9D$ with the coefficients for (a) $3.3D$, $3.7D$ and $7.4D$ known (interpolation 1) and (b) $3.3D$ and $7.4D$ known (interpolation 2).	121

List of Tables

2.1	Westermost Rough offshore wind farm data [2, 1, 36].	14
4.1	Input parameters for sensitivity study of superposition method and wake reflection.	31
4.2	Input parameters for sensitivity study of superposition method, wake reflection and correction factor.	31
4.3	Input parameters for sensitivity study of the Park1 and Park 2 model.	32
5.1	Wind turbine characteristics of the Siemens SWT-6.0-154 [1, 36, 37] and scaled DTU 10MW wind turbines	35
6.1	Wind turbine characteristics [3]	44
6.2	Overview of LES datasets.	46
6.3	Locations of the data planes of the LES simulations	47
9.1	RMSE of the original solution and the solution with $\beta_4 = \beta_5 = \beta_6 = 0$	90
A.1	Input parameters for sensitivity study of the wake decay coefficient and wind turbine spacing.	99
A.2	Input parameters for sensitivity study of the thrust coefficient.	100
E.1	Original α -coefficients for $f_{A,L}$ and the coefficients calculated by interpolation, together with the RMSE for all solutions.	120
E.2	Original α -coefficients for $f_{A,Q}$ and the coefficients calculated by interpolation, together with the RMSE for all solutions.	121

List of Symbols and Abbreviations

Symbols

Symbol	Description	Units
Greek		
α	Optimization coefficient for optimization method A	-
β	Optimization coefficient for optimization method B	-
γ	Yaw angle	deg
$\Delta\gamma$	Yaw misalignment	deg
θ	Wind direction	deg
κ	von Kármán constant	-
ν	Kinematic viscosity	$\text{m}^2 \text{s}^{-1}$
ν_{SGS}	Sub-grid stress viscosity	$\text{m}^2 \text{s}^{-1}$
ξ_{init}	Initial skew angle of the wake	deg
ρ	Density	kg.m^{-3}
ψ	Stability correction function	-
Roman		
A	Rotor area	m^2
$A_{overlap,mn}$	Partial wake overlap of wind turbine m on rotor are n	m^2
C	Scaling factor	m or -
C_s	Smagorinsky constant	-
C_T	Thrust coefficient	-
D	Rotor diameter	m
f	Body/external forces	m s^{-2}
H	Hub height	m
k	Wake decay coefficient	-
L	Obukhov length	m
p	Pressure	N m^{-2}
P	Power	W
Q	Quantification measure	-
r	Radial distance	m
R	Rotor radius	m
R_w	Rotor wake radius	m
S	Score	m
S_{ij}	Stress-strain tensor	s^{-1}
S_x	Wind turbine distance	m
t	Time	s
δt	Sampling time	s
T_{ij}	Sub-grid stress tensor	s^{-1}
u	Actual wind speed field	m s^{-1}

u'	Sub-grid scale wind speed field	m s^{-1}
\tilde{u}	Filtered wind speed field	m s^{-1}
u_*	Friction velocity	m s^{-1}
U	Horizontal streamwise wind speed	m s^{-1}
U_0	Free stream wind speed	m s^{-1}
$U_{0,m}$	Free stream wind speed upstream of wind turbine m	m s^{-1}
U_C	Centerline wind speed at hub height	m s^{-1}
U_{field}	Horizontal wind speed field	m s^{-1}
U_{mn}	Wind speed at/downstream of wind turbine n due to the wake of wind turbine m	m s^{-1}
U_n	Wind speed at wind turbine n	m s^{-1}
U_R	Rotor averaged wind speed	m s^{-1}
U_{WB}	Wake boundary wind speed	m s^{-1}
$U_{R,WT}$	Rotor averaged wind speed at the wind turbine locations	m s^{-1}
ΔU	Wake deficit	m s^{-1}
w	Weigth	—
x	Streamwise location coordinate	m
x_m, x_n	Streamwise wind turbine coordinate of wind turbine m / n	m
Δx_I	Induction zone length	m
X	Streamwise domain length	m
ΔX	Streamwise grid spacing	m
y	Cross-stream location coordinate	m
y_{bottom}	Cross-stream location of the bottom wake boundary	m
y_{top}	Cross-stream location of the top wake boundary	m
Δy_{yaw}	Wake centerline lateral offset due to yaw error	m
Y	Cross-stream domain length	m
ΔY	Cross-stream grid spacing	m
z	Vertical location coordinate	m
z_0	Surface roughness	m
Z	Vertical domain length	m
ΔZ	Vertical grid spacing	m

Abbreviations

Abbreviation	Description
CDS	Central Difference Scheme
CF	Correction Factor
CFD	Computational Fluid Dynamics
DNS	Direct Numerical Simulation
DWM	Dynamic Wake Meandering
IWFBL	Internal Wind Farm Boundary Layer
LES	Large Eddy Simulations
NS	Navier-Stokes
QUICK	Quadratic Upwind Interpolation for Convective Kinematics
RANS	Reynolds Averaged Navier-Stokes
SCADA	Supervisory Control And Data Acquisition
TI	Turbulence Intensity
WB	Wake Boundary
WF	Wind Farm
WMR	Westermost Rough
WT	Wind Turbine

Chapter 1

Introduction

When downstream wind turbines are located in the wake of an upstream wind turbine, the wind profile and turbulence intensity change. Due to the velocity deficit, the power output changes as well. Nowadays, wind farms become larger and larger and therefore the wind field within a wind farm becomes more complex. Turbines will experience an influence of not only one, but multiple wind turbines. These wakes interact with each other and different models exist to superpose the wakes of different wind turbines.

A distinction is made between the near wake and the far wake. The near wake is usually considered to be the region where the presence of the rotor is felt directly and dependent on the rotor characteristics. Therefore the near wake is the region where vortices formed are stable as they are directly related with the radial variation of the bound vortices on the blade [39, 43]. The near wake usually extends two to four rotor diameters downstream of the rotor.

In the far wake, the flow field is fully developed, independent of the rotor characteristics and governed by small-scale turbulence. Because wind turbines in a wind farm are mostly located some distance from the upstream wind turbines, the focus of this MSc Thesis project is on the wind speed (deficit) in the far wake.

1.1 State of the Art & Historical Development of Single Wake Models

Several models exist to compute the wind profile and wake deficit behind a single wind turbine. The results of these models can then be used in different wake superposition approaches to calculate the wind field in a wind farm.

The Park model, based on the wake model developed by Jensen (1983) [14] and Katić et al. (1986) [16], is implemented in WAsP [26]. The model assumes an axisymmetric flow, no rotation, no turbulence and a top-hat speed deficit inside the wake. The wake expansion is linear and defined by a wake decay coefficient k , which is often set to 0.04 for large wind farms [10]. Peña et al. (2013) [31] developed a modified version of the Park model, in which k is dependent on the atmospheric stability or turbulence intensity. Rathmann et al. (2017) [33] revised the WAsP Park model. A top-hat speed deficit profile is still used, but the wake deficit formulation is adapted.

The single wake model developed by Ainslie (1987) [4] is based on the thin shear layer approximation of the Navier-Stokes equations. The shear stresses are a function of the eddy viscosity, which is in its turn a function of the downstream distance, centerline velocity and the atmospheric stability. The wake is considered to be axisymmetric, fully turbulent, stationary in time and a flow with zero circumferential velocities.

In the first wake model developed by Larsen (1988) [18], the wind shear is neglected and the flow is considered to be incompressible and stationary. The wake region is described by Prandtl's turbulent boundary layer equations and the Navier-Stokes equations, simplified for large Reynolds numbers, are solved in combination with the momentum balance and by assuming that the axial wind velocity deficit is zero at the wake boundary. In a later version of the Larsen model (2009) [19], the boundary conditions are adapted, based on the results of full-scale experiments.

Frandsen et al. (2006) [9] developed a wake deficit model with a top-hat shape velocity deficit. Unlike the Jensen model, the model is based on both the mass and momentum conservation laws.

Bastankhah and Porté-Agel (2014) [7] developed a wake model based on both the mass and momentum conservation. The wake deficit has a Gaussian profile, compared to other top-hat shaped velocity deficit models (e.g. Jensen [14, 16], Frandsen [9]). The velocity deficit is a function of the coordinates, the thrust coefficient and a growth rate. The growth rate is the change of the standard deviation of the Gaussian velocity deficit profile with the streamwise distance behind the wind turbine.

Most models, some of which shortly discussed above, focus mainly on the velocity deficit, expressed in the power deficit, or on load aspects. The Dynamic Wake Meandering (DWM) model combines static and dynamic modelling, which means that the wind speed deficit and turbulence modelling are connected [20]. This way, both power deficit and the effect on loading can be addressed. The hypothesis behind the DWM model is that the wake acts as a passive tracer, driven by the large-scale turbulent structures in the atmospheric boundary layer. The DWM model consists out of three aspects: (1) the quasi-steady wake deficit, (2) a wake meandering model and (3) an added wake turbulence model, caused by the wind turbine rotor [20, 21].

1.2 State of the Art of Wake Superposition Methods

The methods to compute the wind profile and wake deficit behind a single wind turbine can be combined with a superposition method. Different superposition methods are proposed in literature to calculate the wind profile at a wind turbine, influenced by multiple wakes [12, 34]:

$$\text{Linear summation} \quad \left(1 - \frac{U_n}{U_0}\right) = \sum_M \left(1 - \frac{U_{mn}}{U_{0,m}}\right) \quad (1.1)$$

$$\text{Energy balance} \quad (U_0^2 - U_n^2) = \sum_M (U_{0,m}^2 - U_{mn}^2) \quad (1.2)$$

$$\text{Quadratic summation} \quad \left(1 - \frac{U_n}{U_0}\right)^2 = \sum_M \left(1 - \frac{U_{mn}}{U_{0,m}}\right)^2 \quad (1.3)$$

$$\text{Geometric sum} \quad \frac{U_n}{U_0} = \prod_M \left(\frac{U_{mn}}{U_{0,m}}\right) \quad (1.4)$$

$$\text{Dominating wake/ Maximum deficit} \quad \frac{U_n}{U_0} = \min_M \left(\frac{U_{mn}}{U_{0,m}}\right) \quad (1.5)$$

In the previous equations, Eq. (1.1) - (1.5), U_0 is the free stream horizontal velocity, experienced by the first wind turbine upstream, U_n is the wind speed at wind turbine n , U_{mn} is the wind speed at wind turbine n due to the wake of wind turbine m . The summations/products are

done over all wind turbines M upstream of the wind turbine in question n . A sketch of the locations of the wind speeds is given in Figure 1.1

As the Navier-Stokes equations are non-linear, the linear summation method assumes that the perturbations, i.e. the velocity deficits, are small so these can be linear superposed. The energy balance method is derived from a simple kinetic energy balance between the kinetic energy of a mixed wake and the sum of the kinetic energies for each wake. On the other hand, the quadratic summation method is derived based on the assumption that the kinetic energy deficit of a mixed wake equals the sum of the energy deficits for each wake [16]. The dominating wake takes into account the maximum deficit at the point of interest. This assumes that the closest wind turbine upstream dictates the wake deficit.

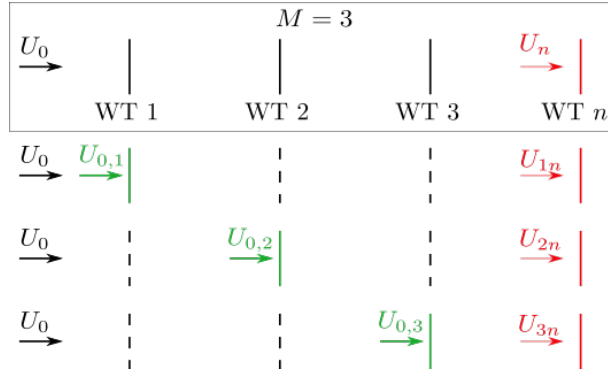


Figure 1.1: Illustration of the local inflow wind speeds, used in the superposition methods.

1.3 Full Farm Models

Apart from superposing single wakes with one of the superposition methods above, also models exist which model the full wind farm. The full field can then be computed based on the Navier-Stokes (NS) equations. The partial differential equations describing the fluid are then transformed to a set of algebraic equations and numerical methods are used to solve these (CFD). Direct Numerical Simulations (DNS) solvers, however, are very computationally costly and only applicable for low Reynolds numbers. Therefore turbulence models, e.g. RANS and LES, are constructed and solved by a numerical solver, e.g. EllipSys3D.

Fuga is a linearized CFD model, developed by Ott et al. (2011) [29]. The model is applicable for wind farms offshore or on homogeneous terrains and is based on the RANS equations for a quasi-steady flow in combination with the continuity equation for an incompressible flow. The flow behind one wind turbine is defined by look-up tables. A logarithmic wind shear profile is assumed with a surface roughness changing with wind speed and wave height. The flow within a full wind farm is calculated making use of the linear superposition method. In the updated version (2011) of the Fuga engineering tool, stability effects and meandering (in post-processing) are implemented [29].

An infinite wind boundary layer model was developed by Frandsen (1992) [8]. Below the rotor, the vertical wind shear profile is logarithmic, in the "rotor layer" the velocity is reduced and above the rotor, the simplified geostrophic drag law is applied. The model is a deep-array model and assumptions are that the wind turbines are evenly spaced and that the change in shear due

to the presence of the wind turbine is concentrated at hub height.

1.4 Problem Analysis & Research Questions

During the development of some (single wake) models, the authors propose a specific wake superposition method to calculate the wake deficit in a wind farm. However, little is known about the validity of the wake superposition approaches and combinations proposed in literature. Due to the computational cost of CFD/LES, the combination of single wakes and superposition methods is a useful tool in engineering applications and therefore it is important to assess the different approaches.

The research objective is to find a combination of a single wake model and a wake superposition method which represents the wind profile behind multiple wind turbines the best by comparing the modelling results with a representative reference for mixed wakes in reality. This reference could be either Large Eddy Simulations (LES) or large-scale measurements data from the BEACon campaign. An intermediate goal of this project is to establish the suitability of these references. For the comparison between the reference data and the superposition of a simple engineering model, one model will be picked.

This research objective can be translated into one main research question:

What is the best wake superposition method in combination with the chosen single wake model to model the wind field in the wake behind wind turbines within a wind farm?

To answer this question, the main research question is split up into different sub-questions to focus on different cases:

- a) What is the best superposition method when the wind speed is around rated wind speed and is there a difference when the wind speed is below rated wind speed?
- b) Which superposition method gives the best result in the wake recovery, i.e. the trend of the wake deficit along a row of wind turbines?
- c) How well is the wake expansion behind multiple turbines approached when multiple wakes are superposed?

The questions above focus on an existing wake model and superposition methods. It assumes indirectly that one of the proposed superposition methods achieves the best results. Therefore, also the following research questions are posed:

Can single LES wakes be superposed to mimic the flow behind multiple wind turbines?

Does an alternative superposition method exist to model the wind field within a wind farm?

1.5 Thesis Outline

Chapter 2 gives an overview of the research methodology and some calculation methods used in this MSc Thesis project. Further, also some general information is given about the large-scale BEACon measurement campaign and Large Eddy Simulations. In literature, some combinations of single wake models and superposition methods are proposed. These are discussed in Chapter 3, together with the choice of an engineering model which will be used in this study. Next, more information about the development and implementation of this engineering model is given in

Chapter 4. It also includes a short sensitivity study of the model. In Chapter 5, the BEACOn and LES data are compared and a decision is made which dataset will serve as the reference dataset. The case studies and an overview of the data generation are presented in Chapter 6. Afterwards, these data sets are used in the comparison with the chosen engineering model in Chapter 7. Chapter 8 discusses if single LES wakes can be superposed to resemble a full LES simulation. Finally, a start of a possible new superposition method, i.e. an optimization method, is discussed in Chapter 9. All chapters which discuss some results end with a short summary, but the main conclusions and recommendations for further research are summarized in Chapter 10.

Chapter 2

Research Methodology

This chapter gives a general overview of the research methodology and discusses some calculation methods used further in the research. General information about the large-scale measurements from the BEACon campaign and Large Eddy Simulations are given as well.

2.1 Overview

In a first step, different proposed combinations in literature of single wakes and superposition methods are examined. Based on these results, a single wake (engineering) model is chosen to use in this MSc Thesis project.

Secondly, the reference dataset is defined. To do this, a comparison is made between the large-scale measurements data from the BEACon campaign and LES results. Once the reference is defined, different datasets are chosen with an eye on the research questions. The inflow wind speeds for the different datasets are both above and below the rated wind speed of the wind turbine to examine the possible change in superposition approach below and above the rated wind speed. More detailed information about the BEACon campaign and LES can be found in Section 2.3 and 2.4 respectively.

Once the datasets are defined, the results are post-processed to be able to compare them with a simple engineering wake model. As a first step, a single wake is calibrated against a single reference wake to reduce the input parameters of the model. This single wake is combined with different superposition methods to examine which method gives the best result for rows of wind turbines and inflow wind speeds above and below rated wind speed. To combine the reference datasets with the engineering model, the datasets are post-processed in different planes, explained in more detail in Section 2.2.1.

In all analyses, the rotor averaged wind speed is looked at. The calculation method is explained in Section 2.2.2, together with the choice of how to define the wake boundary in Section 2.2.3. A quantification system is set up to quantify the differences between a reference dataset and a test result. The focus of this quantification system is based on different measures, e.g. the wake field, the rotor averaged wind speed etc. The measures used and the way these are combined are explained in Section 2.2.4.

After comparing the datasets with the combinations of the engineering model and superposition methods, the focus is on the second main research question: “Can single LES wakes be superposed to mimic the flow behind the multiple wind turbines?”. In this analysis, different single LES wake fields are superposed, making use of different superposition methods to examine if it would be useful to have a database full of single wakes and superpose these, instead of running simulations for a full field with multiple wind turbines.

As it is not clear if one or more of the proposed superposition methods are ‘true’, an optimization method is developed to analyse if the superposition methods can be improved and how many upstream wakes should be taken into account. The optimization method is tested for wind turbine rows with different wind turbine spacings. The calculation methods for the LES superposition and optimization methods are not given in this chapter but in Chapter 8 and Chapter 9 respectively.

2.2 Calculation methods

2.2.1 Data planes

The datasets are post-processed and saved in different planes, defined in a Cartesian grid. The planes are defined as follows:

- Horizontal: A horizontal plane at a predefined height (Figure 2.1a)
- Streamwise: A vertical plane in the streamwise direction through the hub of the first wind turbine (Figure 2.1b)
- Vertical: A vertical plane perpendicular to the streamwise direction at different streamwise positions. The streamwise positions of these planes are both upstream and downstream of the first wind turbine (Figure 2.1c).

The coordinate system is oriented as shown in Figure 2.1d and the domain is indicated with X , Y , and Z .

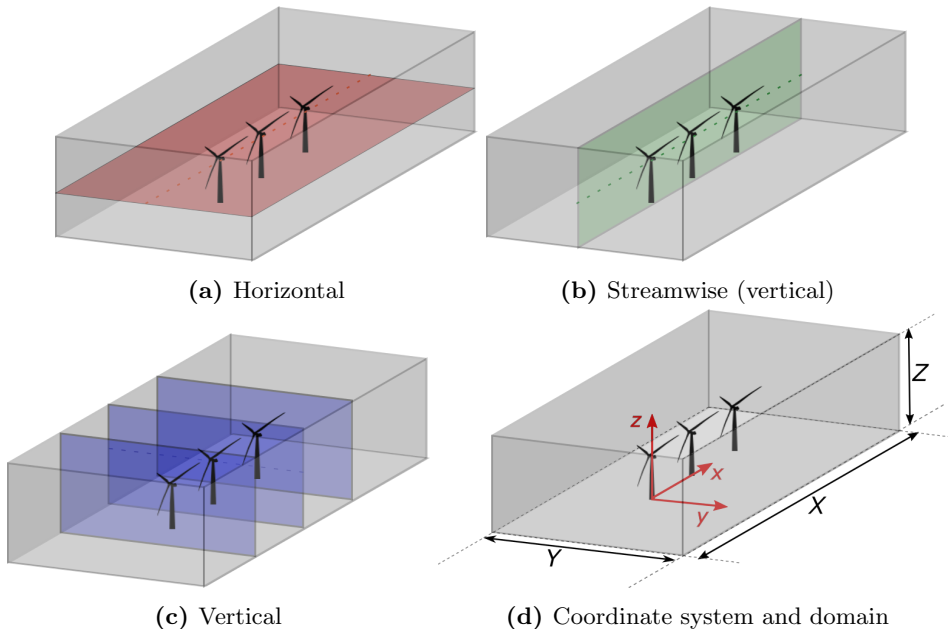


Figure 2.1: Illustration of the different data planes, coordinate system and domain

2.2.2 Rotor averaged wind speed

From an energy yield assessment point of view, the power produced by a wind turbine when standing in the wake of one or multiple wind turbines is important. The rotor averaged wind

speed can be translated into power by making use of the power curve.

If the wind field in a vertical plane downstream of a wind turbine is known, the rotor averaged wind speed can simply be estimated by spatial area averaging all the wind speed data points which lie within the rotor area. The location of the rotor area center is at the same height and cross-stream position as the rotor of the first wind turbine. The drawback of this simple method is that the vertical data plane of interest needs to be available. When this plane is not available, the rotor averaged wind speed can be computed based on the method described below.

If a horizontal data plane at hub height is available, the rotor averaged wind speed can be computed making use of a weighting function. At each downstream position in the horizontal plane at hub height, a horizontal profile can be extracted. An example of such a horizontal profile is shown in Figure 2.2a. The data points closer to the outer part of the rotor area should get a higher weight as they ‘represent’ a higher relative area of the rotor area. The other way around, the data points closer to the center of the rotor area have a lighter weight. The weighting function is linear as the area, dA , of an annulus with an infinitesimal width dr is proportional with the radius r :

$$dA = 2\pi r dr \quad (2.1)$$

The weighting function $w(y)$ can then be expressed as follows:

$$w(y) = \begin{cases} \frac{|y_i|}{C}, & \text{if } |y_i| \leq R \\ 0, & \text{if } |y_i| > R \end{cases} \quad (2.2)$$

in which C is a positive constant to normalize the weighting function so that the sum of all the weights equals one. The weighting function for a rotor diameter of 80 m (with 192 wind speed samples) is shown in Figure 2.2b. The rotor averaged wind speed U_R is then the result of the integral of the product of the weighting function and the horizontal velocity profile:

$$U_R = \sum_{i=1}^N U(y_i) w(y_i) \quad (2.3)$$

with N the total number of samples. A limitation of this method is that the wind speed field should be axisymmetric within the rotor area. As multiple cases used further in this study have a uniform inflow profile and no veer, the method can be used.

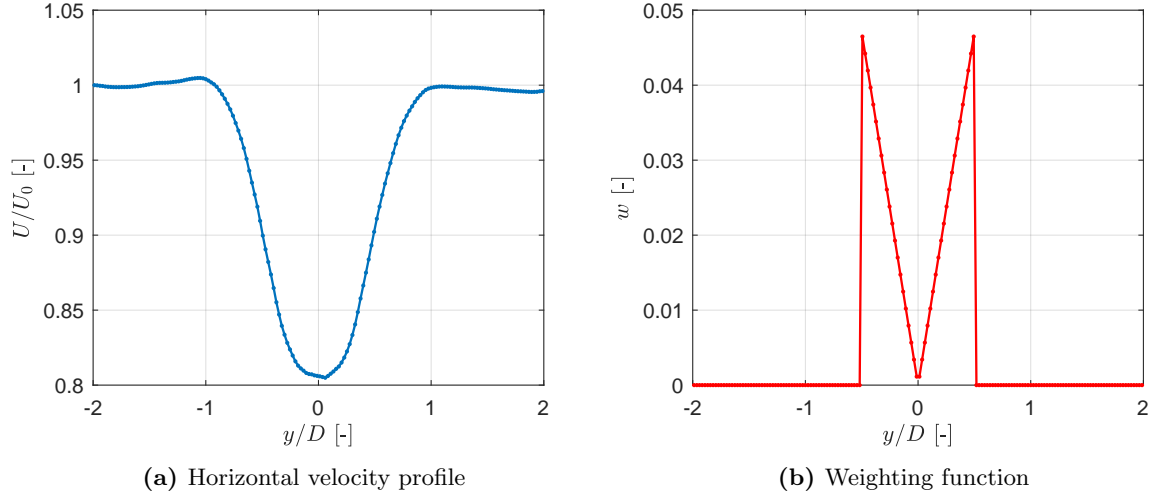


Figure 2.2: Example of (a) a horizontal velocity profile and (b) a weighting function for a wind turbine with a rotor diameter of 80 m.

To test the method described above, the spatially averaged rotor wind speed and weighting function averaged rotor wind speed are computed based on LES results with a uniform inflow of 14 m.s^{-1} . The results are shown in Figure 2.3. The relative error between the two results is of the order of 10^{-3} . Details of these LES simulation results can be found in Section 6.2, Case A1.

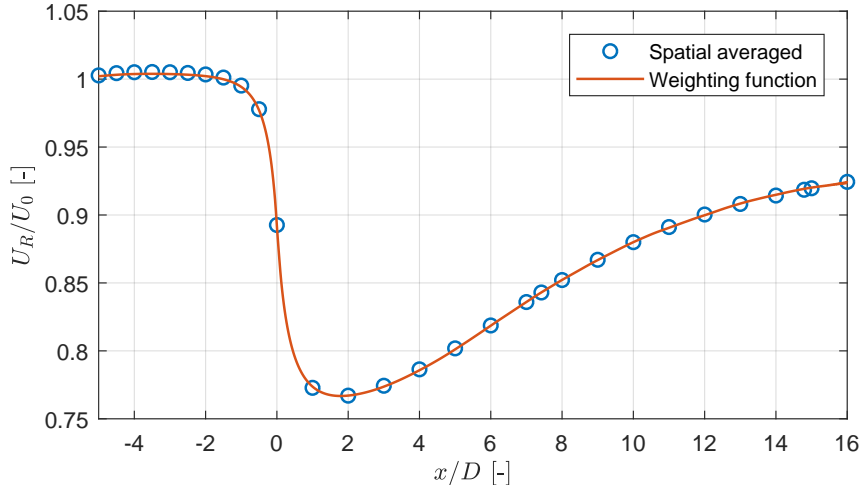


Figure 2.3: Rotor averaged wind speed, calculated as spatial average and with the weighting function.

If the wind turbines are not aligned with the wind direction and/or do not have the same hub height, a decision should be made on the location of the rotor area. It can be decided to change the rotor area based on the downstream location. If the location is behind e.g. the second wind turbine, the rotor area center can be located at the position of the hub of the second wind turbine.

2.2.3 Wake boundary

To define the wake boundary, an arbitrary wind speed value is chosen. This value should lie close to the undisturbed inflow wind speed U_0 . Therefore, the wake boundary wind speed U_{WB} equals $0.98U_0$. The location of the wake boundary is then found for every downstream location where the wind speed is closest to U_{WB} . The wake boundary is found using this method for every dataset unless mentioned otherwise.

2.2.4 Quantification system

To quantify the differences between the reference and a test result, e.g. the difference between LES simulations results as a reference and the engineering model as a test result, a quantification system is used. This system is based on different measures. Those measures are the following:

- a. The full wind speed field in a horizontal plane¹. The domain of the wind speed field is restricted to the wake field that needs to be compared. In general, the limits of the cross-stream direction should not be too big so that the influence of the undisturbed wind field outside the wake is minimized. (Figure 2.4a)

$$Q_a = \frac{U_{field}}{U_0}$$

- b. The rotor averaged wind speed (Figure 2.4b)

$$Q_b = \frac{U_R}{U_0} \quad (2.4)$$

- c. The rotor averaged wind speed at the wind turbine locations. (Figure 2.4b)

$$Q_c = \frac{U_{R,WT}}{U_0} \quad (2.5)$$

- d. The power production, possibly based on the power curve depending on the data source.

$$Q_d = \frac{P(U_{R,WT})}{P_{rated}}$$

- e. Derivative of the rotor averaged wind speed. This is an indication of the wind speed recovery in the wake. (Figure 2.4b)

$$Q_e = \frac{\partial(U_R/U_0)}{\partial(x/D)} \cdot \frac{1}{C} \quad (2.6)$$

C is a scaling constant and will be explained further. The calculation of the derivative is done making use of a central differencing scheme (CDS):

$$Q_e = \frac{U_{R,i+\frac{1}{2}} - U_{R,i-\frac{1}{2}}}{x_{i+\frac{1}{2}} - x_{i-\frac{1}{2}}} \cdot \frac{D}{U_0} \cdot \frac{1}{C} \quad (2.7)$$

The comparison is only made in the regions where the derivative of the reference is positive. This is to ignore the regions with a decreasing wind speed, i.e. in the induction zone and the very near wake.

The order of magnitude of the derivative is $\mathcal{O}(10^{-4})$, while the order of magnitude of the other measures is $\mathcal{O}(10^0)$ as they are normalized. Therefore, the scaling constant C equals the maximum value of the derivative of the reference dataset.

¹Vizualised with contour plots, making use of the Matlab function `contourf`.

If different results of the same model (e.g. Park) with different input parameters are compared and it is known that the first wake is identical for all test cases, it is better to restrict the domain and only compare the test cases with the reference downstream of e.g. the second wind turbine. Hence, the focus is on the differences between the test cases.

In what follows is ‘the reference’ the reference dataset that will be approached as close as possible. The ‘test case’ is the engineering model or dataset which is tested against ”the reference”. The root mean square error (RMSE) is computed between the measure Q_j of the reference and the test case.

$$\text{RMSE}_{Q,j} = \sqrt{E \left[(Q_{j,\text{reference}} - Q_{j,\text{test}})^2 \right]} \quad (2.8)$$

$$= \sqrt{\frac{\sum_{i=1}^N \left[(Q_{j,\text{reference}} - Q_{j,\text{test}})^2 \right]}{N}} \quad (2.9)$$

with N the number of samples for each measure. For measure Q_a , N equals the number of data points within the horizontal domain. N equals the number of data points of the rotor averaged wind speed for Q_b . For measure Q_c and Q_d , N equals the number of wind turbines and finally, for measure Q_{en} N equals the number of points with a positive derivative of the rotor averaged wind speed. The lower the value of the RMSE, the better the test case scores on the measure looked at.

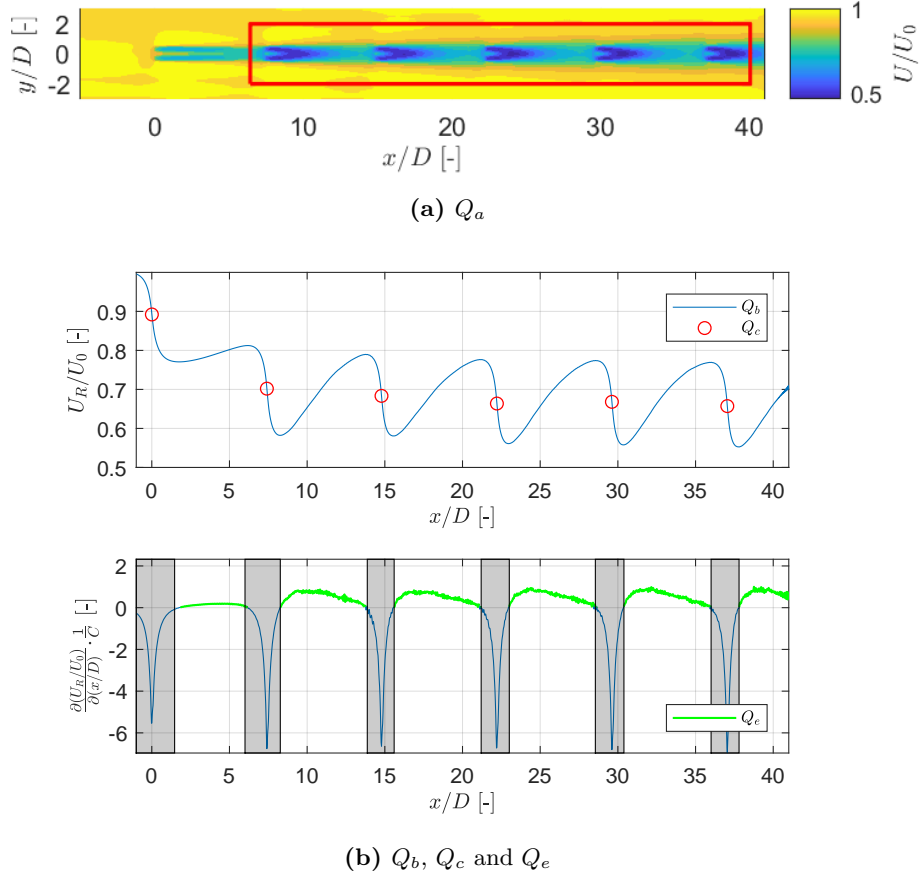


Figure 2.4: Illustration of the different quantification measures.

When comparing different test cases, e.g. different superposition methods and/or different engineering models, to the same reference, the RMSE of each measure can be compared. This can give a clear conclusion of which test case performs the best if this test case has the lowest RMSE for all or most of the measures. But if different test cases are compared and one of the test cases performs well on some measures but less on others and the other test case the other way around, it might not be clear which one is actually the best. In this case, a weight can be given to each RMSE and afterwards all measures are summed. To express that the best test case has the highest end score S , the RMSE is subtracted from one.

$$S = \sum_i (w_{Q,i} (1 - \text{RMSE}_{Q,i})) \quad (2.10)$$

The sum of the weights w_Q itself equals one, but there exist different possibilities to distribute the weights over the measures. Depending on the interest or use of the results, different weight combinations can be used. Figure 2.5 shows some fictitious examples. If, for example, the goal is to assess the power production, a higher weight will be given to the rotor average wind speed (measure Q_c and Q_d , "weights 1" in Figure 2.5b). But if on the other hand, the full wind field is the goal of a study, a higher weight might be given to measure Q_a ("weights 2" in Figure 2.5b). Both weight combinations give a different result for which test case performs the best. The focus of a study can be on other characteristics or parameters, so measures can be added, but in this study, the focus is on the five measures described above.

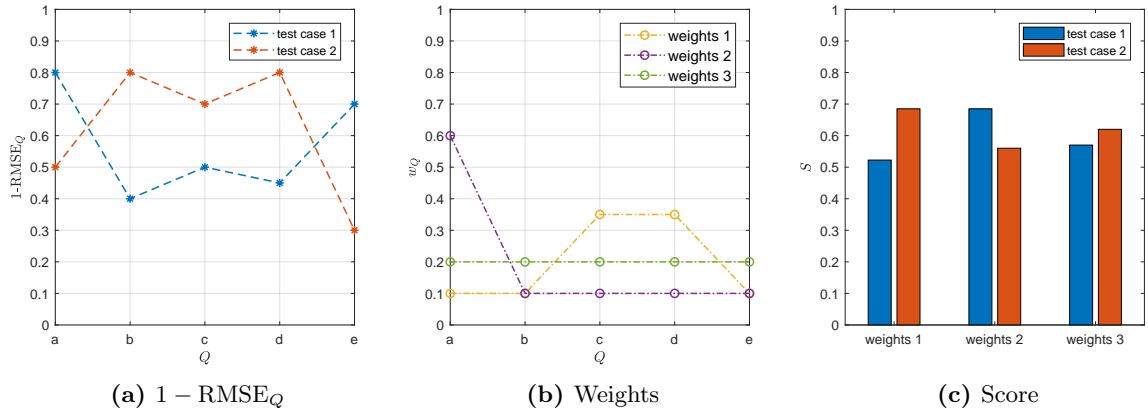


Figure 2.5: Illustration of the quantification method.

2.3 Radar - BEACon

2.3.1 BEACon measurement campaign

With the BEACon project, a research project by Ørsted (formerly DONG Energy) in collaboration with Texas Tech University and SmartWind Technologies, measurements are performed at the Westermost Rough offshore wind farm, making use of a dual-Doppler radar system. The radar system consists of two Doppler scanning radar systems and is located on the east coast of the UK, 8 km from the Westermost Rough wind farm. The lay-out is shown in Figure 2.7a [27]. The green areas shown in the figure are the dual-Doppler lobes, in which the uncertainty of the horizontal wind speed and wind direction is low when combining the data of both radars. Plan Position Indicator (PPI) scans are performed at 13 different elevation tilts. Each single Doppler sector covers approximately 530 km^2 , so the resulting dual-Doppler domain covers about 115

km^2 . The scan speed is constant at $30^\circ/\text{s}$. Approximately one minute is needed to scan each 3D volume.

The radial wind speeds of the dual-Doppler system are interpolated onto a 3D Cartesian grid, shared between the two radars. Figure 2.6 shows the radial velocities of each single Doppler radar and the dual-Doppler velocities. The structure of the wakes can be seen in great detail. For the analysis of wakes and to isolate the wind speed deficit, the inflow profile needs to be extracted from the measured wind speed. Therefore, the inflow in the cross-stream direction at each height is averaged to get an averaged vertical wind speed profile.

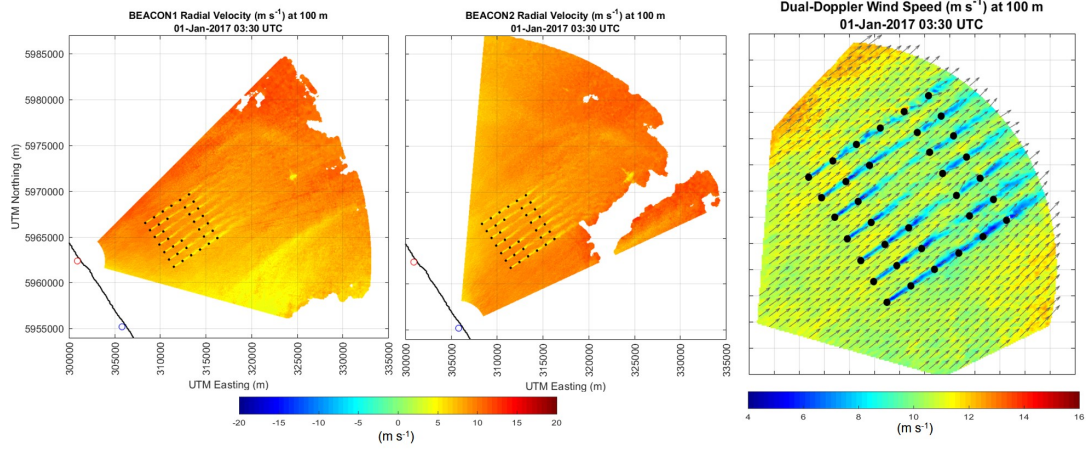


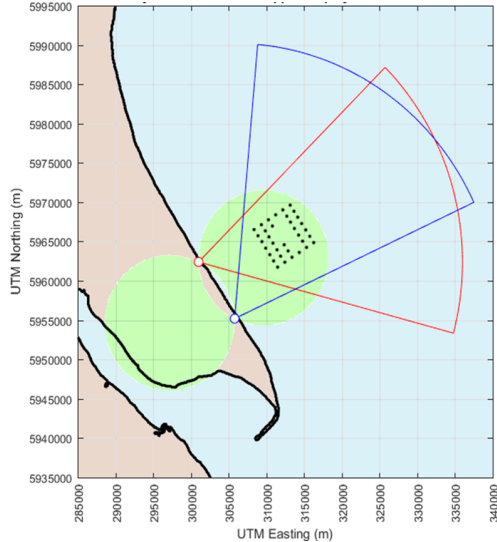
Figure 2.6: Example of radial velocity measured by the two single Doppler radar systems (left and middle) and the corresponding Cartesian velocity (right) (reproduced from Nygaard et al. [27]).

2.3.2 Westermost Rough offshore wind farm

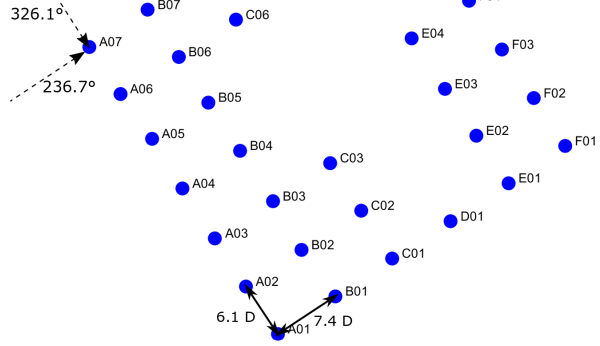
The lay-out of the Westermost Rough offshore wind farm can be seen in Figure 2.7b. The distance between the wind turbines in the 236.7° -direction is $7.4D$ and in the 326.1° -direction is $6.1D$. The wind farm consists of 35 Siemens SWT-6.0-154 wind turbines [2]. The relevant data about the wind farm and wind turbines are summarized in Table 2.1 [2, 1, 36]. More detailed information about the wind turbine generator is given in Section 5.1.

Table 2.1: Westermost Rough offshore wind farm data [2, 1, 36].

Parameter	Value
Number of wind turbines	35
Rated power	210 MW
Mean wind speed (10-year, at 100 m)	9.2 m.s^{-1}
Annual mean speed (at 100 m)	8.4 m.s^{-1}
Area	35 km^2
Distance from shore	8-11.2 km



(a) BEACon measurement set-up



(b) Lay-out of the Westermost Rough Offshore Wind.

Figure 2.7: Schematic overview of (a) the BEACon measurement set-up [27] and (b) the lay-out of the Westermost Rough offshore wind farm with indications of wind turbine spacings and row directions (based on Ørsted data).

2.4 Large Eddy Simulation

2.4.1 Navier-Stokes equations

The flow field within a wind farm is assumed to be incompressible and can therefore be described by the incompressible Navier-Stokes (NS) equations:

$$\frac{\partial u_j}{\partial x_j} = 0 \quad (2.11)$$

$$\frac{\partial u_i}{\partial t} + u_j \frac{\partial u_i}{\partial x_j} = -\frac{1}{\rho} \frac{\partial p}{\partial x_i} + \frac{\partial}{\partial x_j} (2\nu S_{ij}) + f_i \quad (2.12)$$

with S_{ij} , the stress-strain tensor, defined as follows:

$$S_{ij} = \frac{1}{2} \left(\frac{\partial u_i}{\partial x_j} + \frac{\partial u_j}{\partial x_i} \right) \quad (2.13)$$

This set of equations is not easily solved because of the non-linear convective term. The range of scales for which the model needs to be resolved depends on the Reynolds number, which is generally high for wind farm applications and therefore it is not feasible to perform Direct Numerical Simulations (DNS). Turbulence models are constructed to model the Navier-Stokes equations by making use of the Reynolds decomposition [32] and Large Eddy Simulations (LES). The large turbulence scales are resolved in time and space in combination with a small scale model [35]. The LES is performed by the EllipSys3D solver in this work and explained in more detail below.

2.4.2 LES

LES is used to model the turbulence characteristics by decomposing the flow into small and large scales. The time dependent Navier-Stokes equations are filtered in space to filter out the

eddies below a certain size. The resulting equations only involve the large scales and the smaller scales are modelled using a eddy-viscosity based sub-grid scale model [12, 43]. This is based on the assumption that the smallest eddies in the flow have universal characteristics and do not depend on the flow geometry [35].

The filtered velocity \tilde{u} is computed by the convolution of the velocity $u(x, t)$ and the filter function $G_{\Delta x}(\vec{x})$. As a result, eddies smaller than a grid size Δx are filtered out. The sub-grid scale field is then defined as the difference between the actual and the filtered flow:

$$u' = u - \tilde{u} \quad (2.14)$$

The filter operation is applied to the Navier-Stokes equations (Eq. (2.12)) and results in

$$\frac{\partial \tilde{u}_i}{\partial t} + \frac{\partial}{\partial x_j} (\tilde{u}_i \tilde{u}_j) = -\frac{1}{\rho} \frac{\partial \tilde{p}}{\partial x_j} + \frac{\partial}{\partial x_j} (2\nu S_{ij} + T_{ij}) + \tilde{f}_j \quad (2.15)$$

T_{ij} is the sub-grid stress tensor and represents the effect of the small scales on the large scales. Using the Boussinesq hypothesis, the sub-grid stress tensor can be written as

$$T_{ij} = 2\nu_{SGS} \tilde{S}_{ij} \quad (2.16)$$

The most widely used sub-grid stress viscosity ν_{SGS} is defined by Smagorinsky et al. [38] as $\nu_{SGS} = C_s^2 \Delta^2 |\tilde{S}|$, with C_s the Smagorinsky constant, $|\tilde{S}| = \sqrt{2\tilde{S}_{ij}\tilde{S}_{ij}}$ and $\Delta = \sqrt[3]{\Delta x \Delta y \Delta z}$. Another vorticity based mixed scale model, used in the current work, is developed by Ta Phuoc et al. [42] and explained in the work of Troldborg [43] to define ν_{SGS} .

2.4.3 EllipSys3D solver

The EllipSys3D solver, developed by Michelsen [25] and Sørensen [41], solves the discretized Navier-Stokes equations in curvilinear coordinates using a block structured finite volume approach, formulated in a non-staggered grid arrangement [43]. To solve the NS equations in time, an iterative time-stepping (including sub-iterations and pressure correction equation) method is used. The convective terms are solved making use of the third order QUICK [23] and fourth order CDS scheme to avoid non-physical numerical fluctuations.

2.4.4 Actuator line and turbine modelling

The body forces, \tilde{f}_j in Eq. (2.15), are the loadings on the rotating blades and are distributed radially along lines representing the blades of the wind turbine, i.e. the actuator line model is used [40]. The airfoil data is tabulated and used to determine the local forces on the blade, depending on the local inflow conditions. The 2D airfoil data is corrected to take into account 3D effects. The body forces are calculated by a full coupling with Flex5, a full aeroelastic code [5, 39].

2.4.5 Inflow wind profile and turbulence

The atmospheric flow is characterized by the orography, roughness (changes) and the atmospheric stability. The vertical inflow velocity profile can be modelled making use of different approaches, eg. the logarithmic law (whether or not including stability) [30] or the power law [13, 17]. To apply an arbitrary vertical wind shear profile, the prescribed boundary layer method (PBL) is applied, which uses body forces [43]. If a specific wind profile is not given, a shear force is applied at the ground and the simulation is run (without wind turbines) until the flow

is fully developed. Once the flow is in balance, the wind turbines are added to the simulation. The shear force is chosen in relation to the surface roughness to extract the inflow profile. Atmospheric turbulence is generated by imposing small body forces into the flow, which are applied in a vertical plane upstream of the first wind turbine [5]. The turbulent fluctuations are generated using the Mann model [24], which is based on a linearisation of the incompressible Navier-Stokes equations.

2.4.6 Post-processing

To be able to correctly time average the LES data, the initial transient should be ignored. The approach used to calculate the time instant at which the transient leaves the domain, t^* , is as follows:

$$t^* = \frac{\Delta x_N}{U_0} \quad (2.17)$$

with U_0 the mean inflow velocity at hub height and Δx_N the distance from the start of the domain to the last wind turbine. As the wind speed decreases within the wake, t^* needs to be increased by a factor of 1.4 to 2. The sampling time δt equals 0.5 s (or 1 s for a long domain, due to computer memory reasons). Afterwards, the total 20 min average is computed.

When the LES simulation results are compared to the BEACon dataset, the LES results are interpolated onto the BEACon grid, i.e. a grid spacing of 25 m and the domain as described in Section 5.1.

When the rotor averaged wind speed U_R is computed, as described in Section 2.2.2, the 10 min averages of these rotor averaged wind speed are also computed within the total period by shifting the averaging window by 1 min to get a larger number of samples [5]. The results show that the standard deviation of these 10 min U_R averages is very small. However, these 10 min averages are not statistically independent.

Chapter 3

Wake Superposition Methods

In some cases, wake superposition methods are proposed in agreement with specific single wake models. This chapter gives a brief overview of the proposed combinations. Afterwards, a number of studies, which compare different models for wind turbine rows are discussed. To end, a decision is made which wake model is used in this MSc Thesis project.

3.1 Single Wake Models and Superposition Methods

In the Park model, implemented in WAsP [26], quadratic superposition is used. However, the revised WAsP Park model by Rathmann [33] proposed linear superposition as the velocity deficits are assumed to be small.

For the Larsen model, two different approaches are used to calculate the (uniform) inflow wind speed: geometric averaging (linear approach) and the momentum balance (non-linear approach) [19]. For both approaches, the uniform inflow wind speed at a wind turbine within a multiple wake is calculated making use of the linear superposition method. Larsen proposed also a simplified approximation of the linear approach if the wind speed is below rated wind speed.

Larsen et al. [22] carried out a validation of the Dynamic Wake Meandering model in which the superposition method changes if the wind speed is below or above rated. Below rated wind speed, the most dominant wake among all wake contributions dictates the wind speed at a given location. Above rated wind speed, a linear superposition of all wakes is used.

As the Fuga model is a linearized CFD model [29], the flow behind one wind turbine is defined by look-up tables and the wake superposition is performed by linear summing all velocity deficits, as already mentioned in Section 1.3.

3.2 Literature Review

The aim of this MSc Thesis project is to focus on the velocity deficit, while it could also be possible to focus on turbulence intensity, power output (the velocity deficit is reflected in the power deficit), loads, etc. In this section, a selection of wake (superposition) model reviews for offshore wind farms is discussed. It has to be noted that sometimes it is not clear which implementation of a model is used exactly. The inflow wind speeds used in the studies are below rated wind speed.

In the study of Gaumond [10] is shown that the wind direction sector taken around the examined wind direction is of importance. The power output for a row of wind turbines, calculated with the Jensen (WAsP) [16, 26], Larsen [19] and Fuga [29] model, is compared to measurements of the Horns Rev and Lillgrund wind farms and in both cases all models underpredict the power

prediction for narrow wind direction sectors (of 3° to 5°). For wide sectors, all models give accurate predictions. The results for the Horns Rev wind farm are shown in Figure 3.1. When looking to the figure on the right, it is clear that the combination of the Jensen wake model and quadratic superposition method is not good as the trend of the power deficit is off compared to the SCADA data.

Göçmen et al. [12] compared different models with SCADA data from the Lillgrund wind farm as well. The Jensen wake model is used with $k = 0.04$ and quadratic wake summation. For the Larsen model, the linear superposition method is applied. As one or two wind turbines are missing (depending on the wind direction), wake recovery is expected. Some results are shown in Figure 3.2. For the Larsen and Jensen model post-processing for the wind direction uncertainty (indicated with GauAve) is performed as well, which gives better results. For both spacings, the EllipSys3D RANS simulation gives the best trend in the power deficit. For the large wind turbine spacing, the Fuga model gives results which are close to the SCADA data, but for a smaller spacing, the wake recovery noticed in the SCADA data, is less explicit, while it is visible for the Jensen model results.

The model developed by Bastankhah and Porté-Agel [7] is compared to the Jensen model ($k = 0.05$) [14, 16], Frandsen model [9], wind tunnel measurement data of a miniature WT and LES data. The velocity deficit is only calculated for a single wake. Figure 3.3 shows that the Jensen model predicts the maximum velocity deficit well for large distances downwind. The Bastankhah model and LES results are in good agreement for all distances behind the wind turbine.

3.3 Choice of Engineering Model

For the research carried out in this study, i.e. comparing the wake field within a wind farm with the wind field computed based on the superposition of single wakes, a particular model is chosen. As the Jensen/Park model predicts the normalized velocity well at large downstream distances in the study of Bastankhah and Porté-Agel [7] and also the wake recovery for a wind turbine row is predicted well, the Park model will be used. Although the trend of the Jensen/-Park model power deficit is not in agreement with the SCADA data in the study of Gaumond [10], this disagreement might also lie in the combination of the model and superposition method.

The Park model is a very simple model and not computationally costly. Different variants of the model exist which use even different superposition methods. The Park model is used in industry and is available in a commercial software package (WAsP). Therefore, it is worth examining how well this model predicts the wind field.

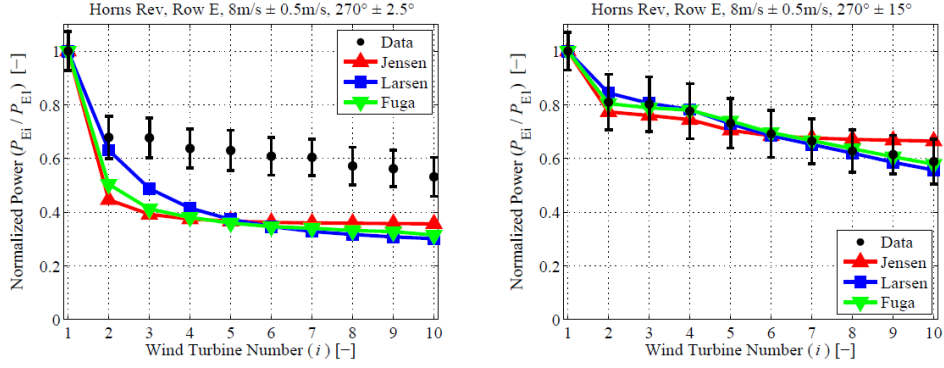


Figure 3.1: Normalized power in an interior row at the Horns Rev wind farm for the wind direction sector $270^\circ \pm 2.5^\circ$ (left) and for the wind direction sector $270^\circ \pm 15^\circ$ (right) (reproduced from Gaumond et al. [10]).

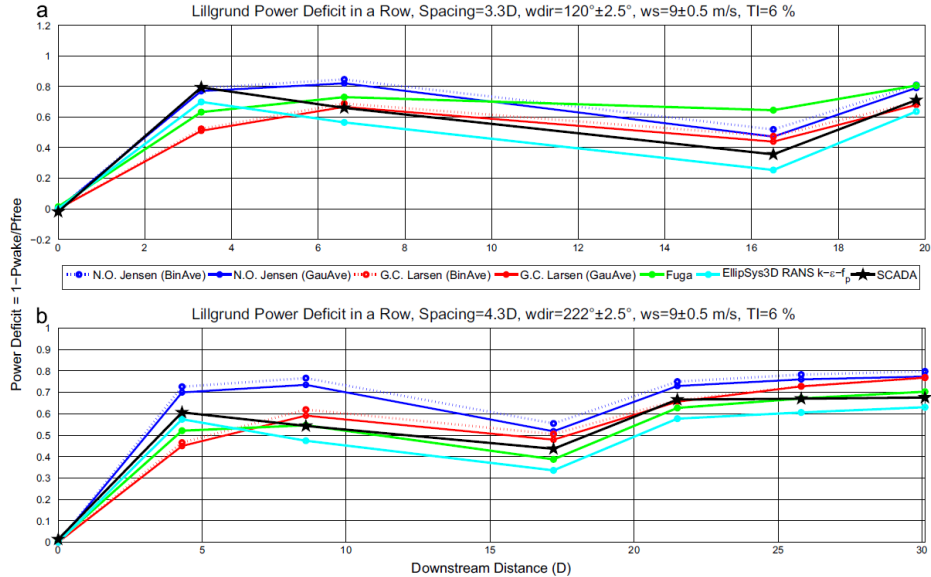


Figure 3.2: Lillgrund power deficit in a row with (a) 3.3D spacing, 2 missing wind turbines and (b) 4.3D spacing, 1 missing turbine. The data are located at the position of a wind turbine (reproduced from Göçmen et al. [12]).

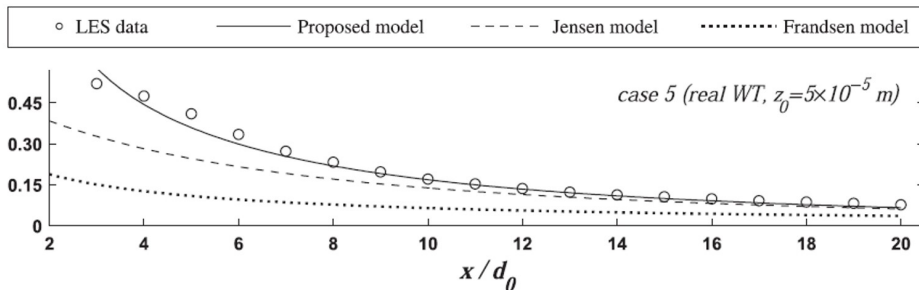


Figure 3.3: Normalized velocity deficit at hub height as a function of the normalized distance downwind of a wind turbine for the Jensen, Frandsen, Bastankhah (proposed) model and LES result (reproduced from Bastankhah and Porté-Agel [7]).

Chapter 4

Engineering Models

The single wake models and engineering models are introduced in Section 1.1 and Section 1.2 respectively. The chosen engineering model, i.e. the Jensen/Park model, will be used in the comparison against the reference dataset, defined in Chapter 5. In this section, the development and implementation are discussed in detail. To end, a short sensitivity study is carried out.

4.1 Development of the Park Model

4.1.1 Jensen wake model

A simple engineering model for the wake deficit in the far wake, developed by Jensen [14] and Katić et al. [16], assumes an axial symmetric flow, no rotation and no turbulence. Inside the wake, the velocity is constant in the radial direction, i.e. a top-hat profile, as given in Eq. (4.1).

$$\frac{\Delta U}{U_0} = \left(1 - \sqrt{1 - C_T}\right) \left(\frac{D + 2kx}{D}\right)^2 \quad (4.1)$$

x is the downstream distance, D the rotor diameter, C_T the thrust coefficient corresponding to the inflow wind speed and k the wake decay coefficient. $D + 2kx$ is the wake width and ΔU equals $U_0 - U$. The value for the wake decay coefficient $k = \frac{0.5}{\ln(H/z_0)}$ is suggested by Frandsen [8], with H the hub height and z_0 the surface roughness. The effect of the ground on the velocity in the wake is calculated by placing an ‘underground mirror’ wind turbine.

4.1.2 Park 1 model

The Park model, implemented in WAsP [26], combines multiple wakes by implementing the quadratic superposition method (Eq. (1.3)) and making use of Eq. (4.2) for the single wakes.

$$\frac{\Delta U_{mn}}{U_{0,m}}(dx) = \left(1 - \frac{U_m}{U_{0,m}} \sqrt{1 - C_T(U_m)}\right) \left(\frac{D_m}{D_m + 2kx_{mn}}\right)^2 \quad (4.2)$$

$$x_{mn} = x_n + dx - x_m \quad (4.3)$$

The term $\sqrt{1 - C_T(U_m)}$ is corrected by the (normalized) inflow velocity of wind turbine m . Figure 4.1 shows a situation sketch of the inflow wind speeds with an indication of the wind speeds $U_{0,m}$ and U_m , the locations x_m , x_n , dx and the rotor diameter D_m .

‘Underground mirror’ wind turbines are still implemented and the wake decay coefficient k is by default 0.05 or 0.075 for offshore and onshore applications respectively but can be adjusted. In large wind farms or for multiple wakes, k is often set to 0.04 [10]. Further, this model will

be referred to as the ‘Park 1’ model.

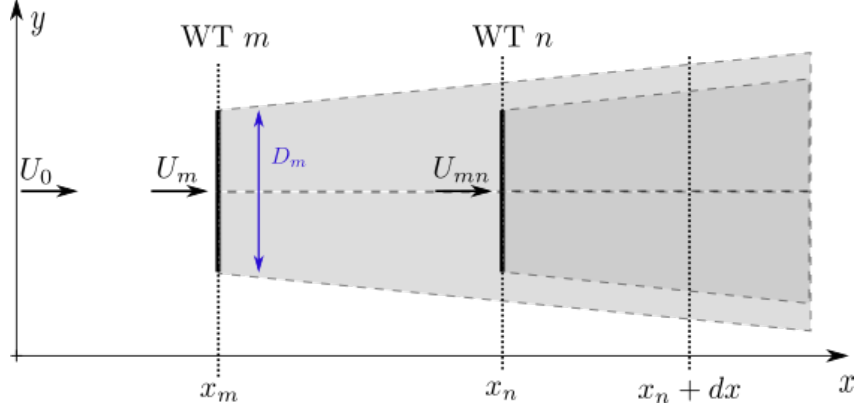


Figure 4.1: Situation sketch of the Park model with an indication of the wind speeds U_0 , U_m and U_{mn} , the locations x_m , x_n , dx and the rotor diameter D_m (top view).

4.1.3 Modified Park model (Peña, 2013)

Peña et al. [31] developed a modified version of the Park model. The modified version does not include the ‘mirror underground’ wind turbines to take into account the ground effect. A suggestion for the wake decay coefficient is made, based on the Monin-Obukhov similarity theory, to take into account the atmospheric stability:

$$k = \frac{\kappa}{\ln(H/z_0) - \psi(H/L)} \quad (4.4)$$

with κ the von Kármán constant, H the hub height, L the Obukhov length and z_0 the surface roughness. k can also be expressed as a function of the turbulence intensity TI:

$$k = 0.4 \text{ TI} \quad (4.5)$$

4.1.4 Park 2 model: revised WAsP Park model

The WAsP Park model is revised by Rathmann et al. [33]. A top-hat speed deficit profile is still used, but the formulation for the wake speed deficit is adopted. The wake interaction with the surface is disregarded by not considering the ‘mirror underground’ reflection model, used in the original Park model [16]. The wake velocity deficit at or downstream of a wind turbine n is expressed as:

$$\frac{\Delta U_{mn}}{U_{0,m}}(dx) = \left(1 - \sqrt{1 - C_T(U_m)}\right) \left(\frac{D_m}{D_m + 2kx_{mn}}\right)^2 \frac{A_{overlap,mn}}{A_n} \quad (4.6)$$

$$x_{mn} = x_n + dx - x_m \quad (4.7)$$

with $U_{0,m}$ the incident wind speed at turbine m . $A_{overlap,mn}$ is the part of the partial wake of wind turbine m overlapping the rotor of wind turbine n , illustrated in Figure 4.2. When multiple wakes are overlapping, the assumption is made that the speed deficits are considered to be small perturbations and so linear wake superposition is imposed (compared to quadratic summation in the original Park model [14]). After calibrating the model with wind farm data of Horns Rev I, Nysted and Lillgrund, the wake expansion factor k is found to be 0.06 for offshore

situations. Further, this model will be referred to as the ‘Park 2’ model.

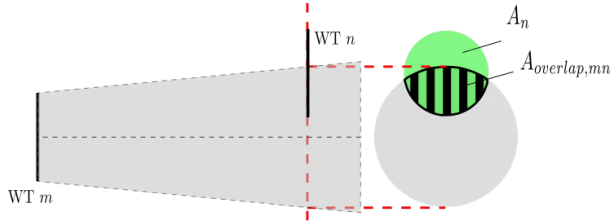


Figure 4.2: Illustration of the overlapping area, used in the Park model revised by Rathmann et al. [33].

4.2 Implementation of the Park Model

In this section, the implementation of the Park model is given in more detail. The different options which can be included (yaw misalignment, correction factor, wake reflection) and the different superposition methods (linear, quadratic or maximum deficit) are discussed as well. As the Park model has a lot of input parameters, a sensitivity study is carried out in Section 4.3. Flow charts of the implementation of the Park model are given in Figure 4.6 (general) and Figure 4.7 (more details), and include the elements discussed below.

The total wake deficit behind turbine n is influenced by all upstream wind turbines m , i.e. the total wake deficit is a function of all partial wake deficits:

$$\frac{\Delta U_n}{U_0} = f(\Delta U_{mn}) \quad \text{with } m = 1, 2, \dots, n \quad (4.8)$$

The partial wake deficit at a distance dx behind the wind turbine n is calculated as follows:

$$\frac{\Delta U_{mn}}{U_{0,m}}(dx) = \left(1 - \sqrt{1 - C_T(U_m)}\right) \left(\frac{D_m}{D_m + 2kx_{mn}}\right)^2 \frac{A_{overlap,mn}}{A_n} \quad (4.9)$$

$$x_{mn} = x_n + dx - x_m \quad (4.10)$$

with x_m and x_n the downstream location of turbine m and n respectively and D_m the rotor diameter of turbine m as earlier indicated in Figure 4.1.

The term $D_m + 2kx_{mn}$ gives the wake width at the position x_{mn} behind turbine m , which is dependent on the wake decay coefficient k . In case the wake boundary of the Park method result is compared with another dataset, this expression will be used for the wake boundary instead of the methodology described in Section 2.2.3.

4.2.1 Yaw misalignment

Due to yaw misalignment, the wake centerline will deflect. The wake deflection implemented in the Park model is based on the study of Jiménez et al. [15] and Gebraad et al. [11]. A relation is found between the wake centerline lateral offset Δy_{yaw} , the thrust coefficient C_T in non-yawed conditions, the distance to the wind turbine dx_m , the rotor diameter D and the yaw

misalignment angle $\Delta\gamma$.

$$\Delta y_{yaw,m}(dx_m) = \frac{\xi_{init} \left(15 \left(\frac{\beta}{D_m} dx_m + 1 \right)^4 + \xi_{init}^2 \right)}{\frac{15\beta}{D_m} \left(\frac{\beta}{D_i} dx_m + 1 \right)^5} - \frac{\xi_{init} D_m (15 + \xi_{init}^2)}{15\beta} \quad (4.11)$$

with

$$\xi_{init} = \frac{1}{2} \cos^2(\Delta\gamma_m) \sin(\Delta\gamma_m) C_{T,m} \quad (4.12)$$

ξ_{init} is the initial skew angle of the wake. The factor β ranges between 0.09 and 0.125, based on a comparison between the yaw misalignment and LES calculations [15]. Figure 4.3 shows the centerline offset as a function of the distance to the wind turbine for $D = 154$ and $C_T = 0.74$.

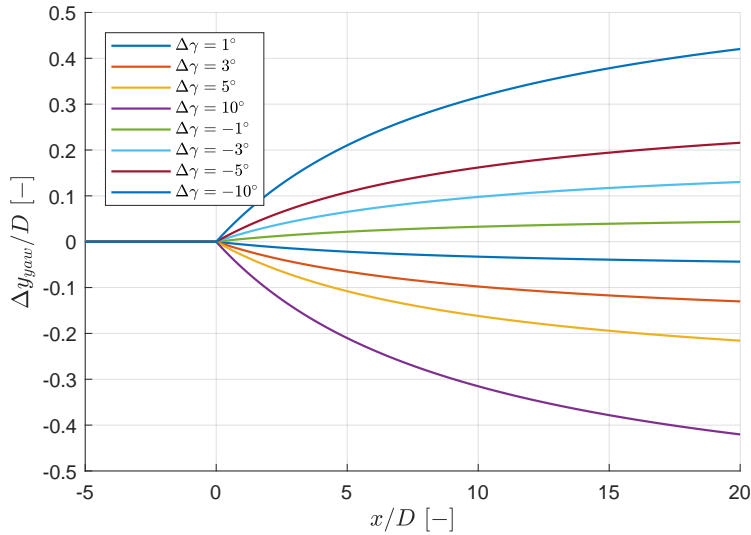


Figure 4.3: Normalized wake centerline lateral offset Δy_{yaw} as a function of the distance to the wind turbine for different yaw angles $\Delta\gamma$ for a C_T value of 0.75 and $\beta = 0.1$.

4.2.2 Correction factor

The correction factor to account for the decreased wind speed at a downstream wind turbine is applied in front of the term $\sqrt{1 - C_T(U_m)}$ in Eq. (4.9), which then becomes:

$$\frac{\Delta U_{mn}}{U_{0,m}}(dx) = \left(1 - \frac{U_m}{U_{0,m}} \sqrt{1 - C_T(U_m)} \right) \left(\frac{D_m}{D_m + 2kx_{mn}} \right)^2 \frac{A_{overlap,mn}}{A_n} \quad (4.13)$$

$$x_{mn} = x_n + dx - x_m \quad (4.14)$$

with x_m and x_n the positions in the streamwise direction of the wind turbines m and n respectively.

4.2.3 Wake reflection

As already described in Section 4.1, ‘underground mirror’ wind turbines can be added to take into account the effect of the ground. Figure 4.4 illustrates the principle of the ‘underground mirror’ wind turbine which results in an added wake deficit. The existing wind turbines are

mirrored with respect to the ground causing fictitious underground wind turbines. This could also be understood as the reflection of the wake of the (above ground) wind turbine. The added wake only has an influence if the point of interest lies in the wake of the ‘underground mirror’ wind turbine. The points which are influenced by the reflected wake are within the shaded blue area in Figure 4.4.

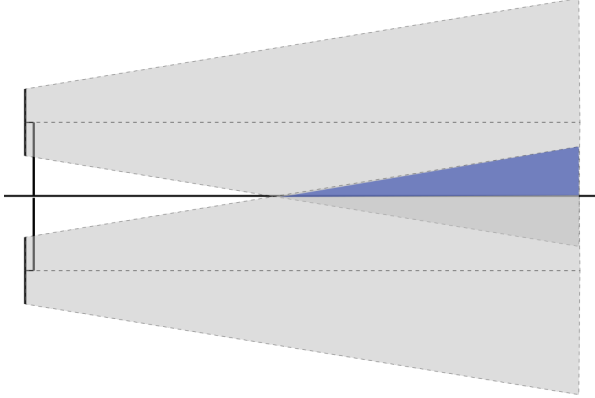


Figure 4.4: Illustration of the ‘underground mirror’ wind turbine technique or wake reflection (side view). The region in which wake reflection has an influence is shaded in blue.

4.2.4 Superposition methods

The superposition methods implemented in the Park model are linear superposition (Eq. (1.1)), quadratic superposition (Eq. (1.3)) and maximum wake deficit/domination wake (Eq. (1.5)). These methods are chosen as those are most commonly used in literature.

4.2.5 Park wake example

Figure 4.5a gives an example of a horizontal wind speed field at hub height of a wind field with a wind turbine row including three wind turbines, aligned with the wind direction and no yaw misalignment. In this example, quadratic wake superposition with wake reflection and correction factor is used. The horizontal profiles $4D$, $6D$ and $8D$ downstream of the first wind turbine are given in Figure 4.5b.

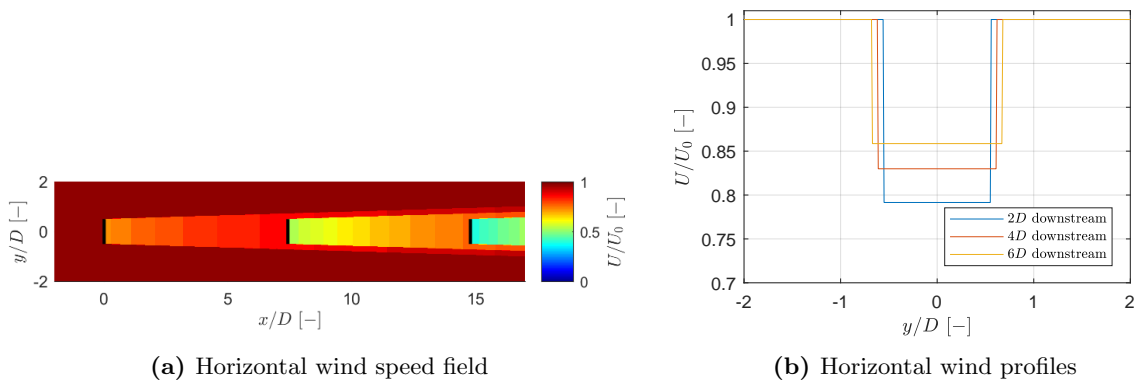


Figure 4.5: Example of (a) a horizontal wind speed field with three wind turbines and (b) a horizontal wind profiles at $4D$, $6D$ and $8D$ downstream of the first wind turbine.

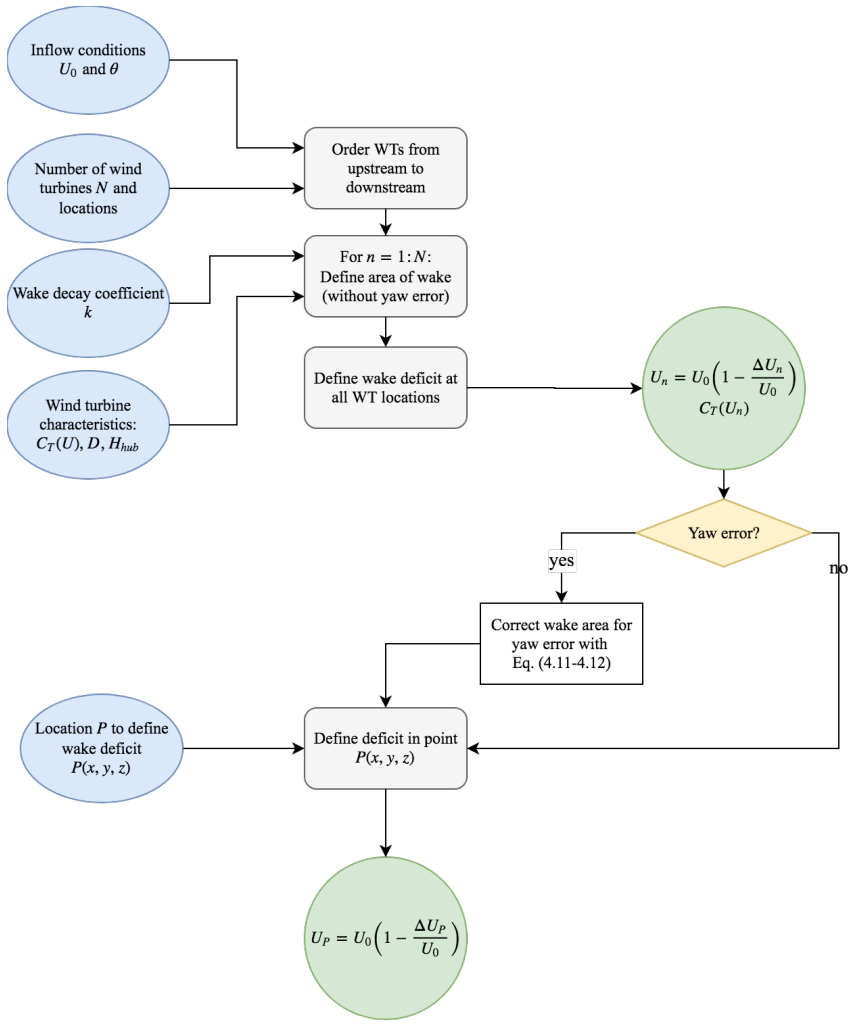


Figure 4.6: General flow chart of the Park model.

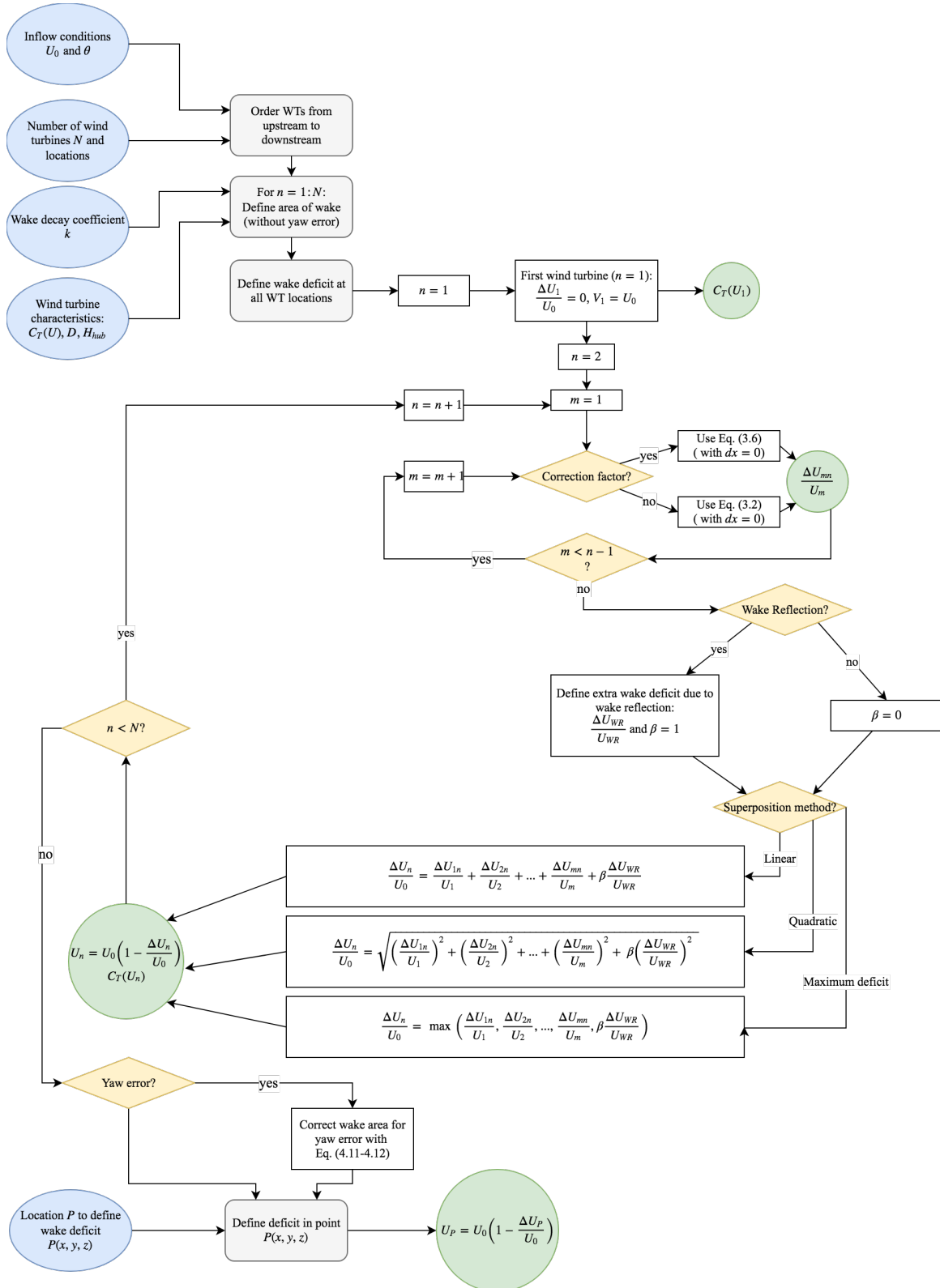


Figure 4.7: Flow chart of the Park model, with a detailed description of calculating the wake deficit at the wind turbine locations.

4.3 Sensitivity Study of the Park Model

To examine the influence of the different parameters used in the Park model, a sensitivity study is carried out. The influence of the superposition method and correction factor are examined here. The difference in results between Park 1 and Park 2 are shown as well.

The sensitivity study is split up into different cases, each focusing on one or two parameters. The C_T -curves used in the sensitivity study are shown in Figure 4.8. The fictitious wind farm used in the Park model calculations is shown in Figure 4.9, unless mentioned otherwise. S_x is the (constant) wind turbine spacing in the downstream direction.

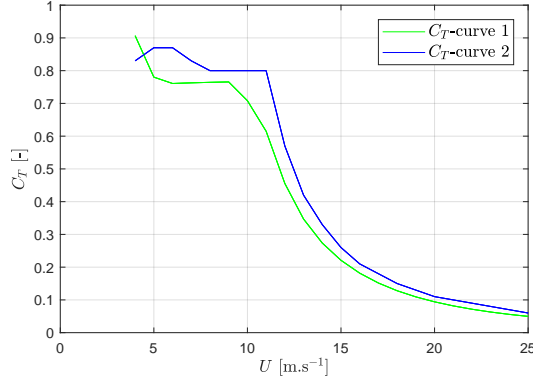


Figure 4.8: C_T -curves of the wind turbines in the sensitivity study.

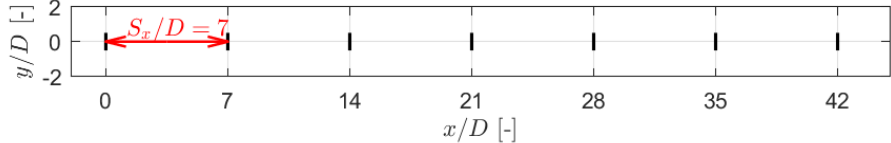


Figure 4.9: Wind farm lay-out used in the sensitivity study of the Park model.

4.3.1 Influence of superposition method

In the first case, the superposition method and whether or not wake reflection is included is examined. The wake coefficient k and wind turbine distance S_x are fixed to a value of 0.04 and $7D$ respectively. The other parameters are summarized in Table 4.1. The wind speed at the wind turbine positions is calculated making use of three different superposition methods: linear superposition, quadratic superposition and maximum deficit. All cases are calculated with and without wake reflection. The wake deficit for these different cases are shown in Figure 4.10.

It is clear that the velocity deficit is the smallest for the maximum deficit approach as contributions of the wake deficit of different wind turbines are not summed up. Therefore, it also does not make a difference whether or not wake reflection is implemented.

The wake deficit is the largest when the linear superposition method is used. If wake reflection is implemented, the wake deficit is larger as an extra deficit is taken into account. Wake reflection does not have an influence for the second wind turbine as the reflected wake of the first wind turbine does not influence the rotor area of the second wind turbine yet for a spacing of $7D$ and k equal to 0.04. The difference in the normalized wake deficit at the seventh wind

turbine between the linear superposition method including wake reflection and the maximum deficit method is 0.6.

Apart from the difference in the value of the wake deficit, the trend of the wake deficit differs as well. The quadratic and maximum deficit method converge after four to five wind turbines, but the wake deficit computed with the linear superposition method is still increasing at the seventh wind turbine.

Table 4.1: Input parameters for sensitivity study of superposition method and wake reflection.

U_0 [m.s $^{-1}$]	k [-]	S_x [m]	Superposition	Correction Factor	Wake reflection	C_T
10	0.04	$7D$	Variable	True	False/True	curve 1

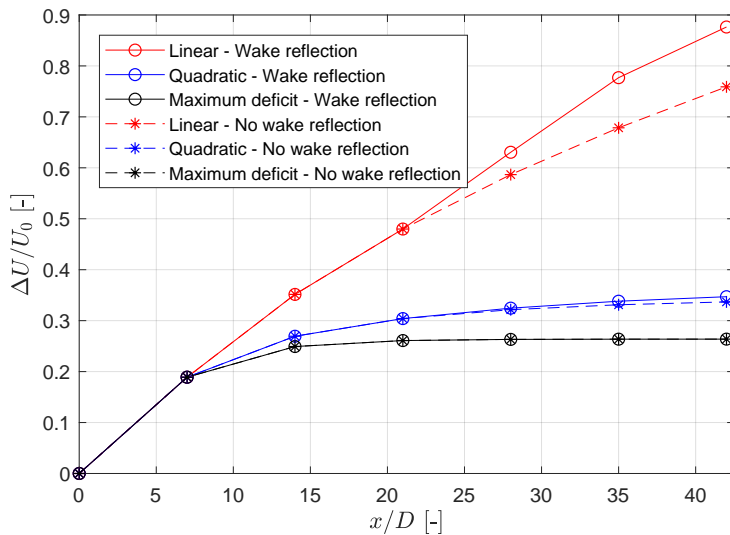


Figure 4.10: Wake deficit at each wind turbine for different superposition methods in combination with including wake reflection or not.

4.3.2 Influence of correction factor

The sensitivity study carried out, in this case, is similar to the previous one, only now, the influence of the correction factor is examined as well. See Table 4.2 for the input parameters. If the correction factor is implemented, the wake deficit is higher, as can be seen in Figure 4.11. With wake reflection implemented, the wake deficit difference is up to 0.26, 0.08 and 0.05 for the linear, quadratic and maximum deficit superposition method respectively at the seventh wind turbine ($x = 42D$). When wake reflection is not implemented, the difference is slightly lower.

Table 4.2: Input parameters for sensitivity study of superposition method, wake reflection and correction factor.

U_0 [m.s $^{-1}$]	k [-]	S_x [m]	Superposition	Correction Factor	Wake reflection	C_T
10	0.04	$7D$	Variable	False/True	False/True	curve 1

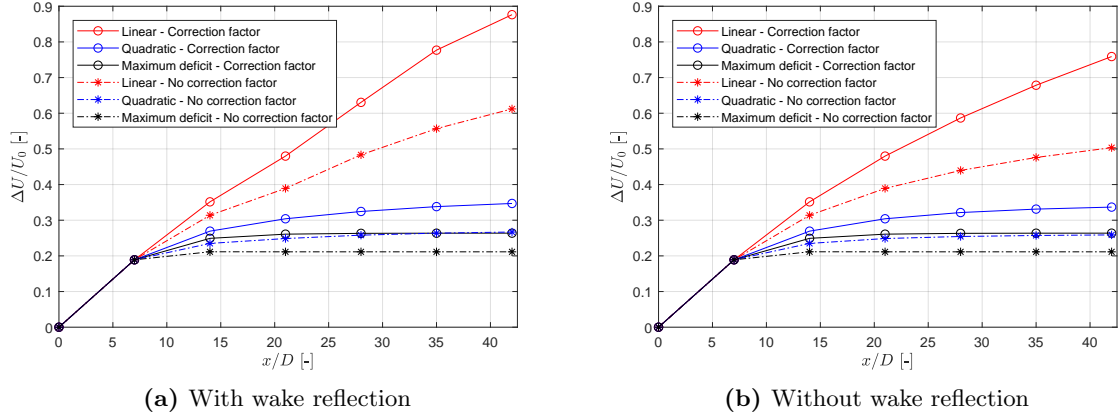


Figure 4.11: Wake deficit at each wind turbine (a) with wake reflection and (b) without wake reflection. In both cases the results are shown with and without the implementation of the correction factor.

4.3.3 Difference between Park 1 and Park 2

Currently, two different models are implemented in WAsP: Park 1 and Park 2. The difference in implementation is also summarized in Table 4.3. To compare the difference in wake deficit for both implementations, the inflow wind speed, turbine distance and C_T -curve are the same in both cases. The result is shown in Figure 4.12. The biggest difference in wake deficit is 0.05 at the third wind turbine. Based on the known ‘deep-array effect’ [5], for which the power output of long rows converges, it is expected that also the wake deficit converges for long rows of wind turbines. It can be seen that the wake deficit for Park 1 indeed converges, but the wake deficit for Park 2 seems to keep increasing.

Table 4.3: Input parameters for sensitivity study of the Park1 and Park 2 model.

	U_0 [m.s ⁻¹]	k [-]	S_x [m]	Superposition	Correction factor	Wake reflection	C_T
Park 1	10	0.04	7D	Quadratic	True	True	curve 1
Park 2	10	0.06	7D	Linear	False	False	curve 1

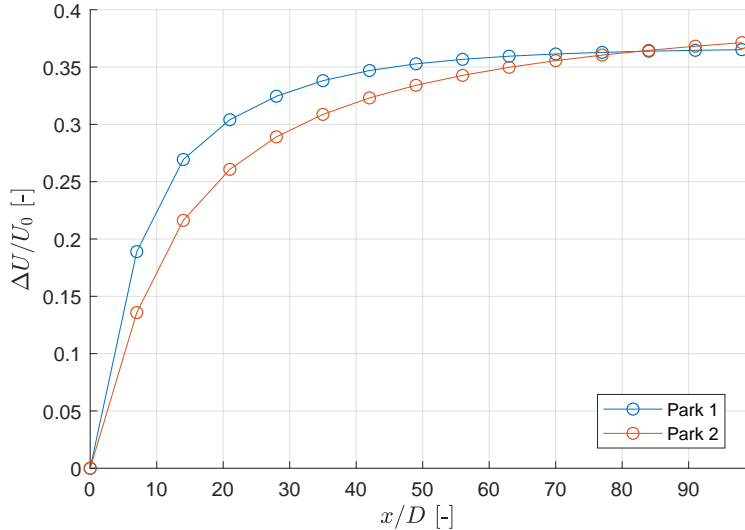


Figure 4.12: Wake deficit at the wind turbines for the Park 1 and Park 2 model, implemented in WAsP.

The sensitivity study of the wake decay coefficient k is given in Appendix A.1 as the k coefficient will be defined in the calibration of a single Park wake. Afterwards, this result is used in the comparison between a reference dataset and the Park model including different superposition methods. The sensitivity study of k is combined with the wind turbine spacing. As the C_T -curve of the wind turbine is known when comparing to a reference set, the sensitivity study of the thrust coefficient is shown in Appendix A.2 to show, amongst others, what the difference is when a slightly different C_T -curve is used in the Park model.

4.3.4 Summary

The sensitivity study shows that the wake deficit is highly dependent on the chosen superposition method. The linear superposition gives the highest wake deficit, while the maximum deficit method results in the lowest wake deficit. When wake reflection is included, the wake deficit increases. The increase in wake deficit is the largest for the linear superposition method and keeps increasing for downstream wind turbines. In the same way, the correction factor has the biggest influence on the linear superposition method. When the correction factor is implemented, the wake deficit increases, but the increase is limited for the quadratic and maximum deficit superposition method. The wake deficits of the latter methods reach also more quickly a converged level.

The difference between the Park 1 and Park 2 model is the highest for the third wind turbine and decreases afterwards. The wake deficit of the Park 1 model, making use of quadratic superposition, converges for long rows of wind turbines. The wake deficit of the Park 2 model, which makes use of linear superposition, keeps increasing.

Chapter 5

Defining the Reference

To define the reference dataset(s), data from the BEACon measurement campaign and LES data are compared. In this chapter, the inflow conditions of the BEACon dataset and the input parameters for the LES simulations are discussed. The differences between the resulting datasets are discussed and interpreted. To end, the power production of the LES wind turbines are examined.

5.1 Test case

As already mentioned in Section 2.3.2, the wind turbines installed at the Westermost Rough (WMR) wind farm are Siemens SWT-6.0-154 wind turbines. The wind turbine used in the LES simulation, which mimics the inflow conditions and set-up of the WMR wind farm, is a down-scaled version of the DTU 10MW wind turbine [6]. The characteristics of both wind turbines are given in Table 5.1. The power and C_T - curve of the scaled DTU 10MW wind turbine are shown in Figure 5.1.

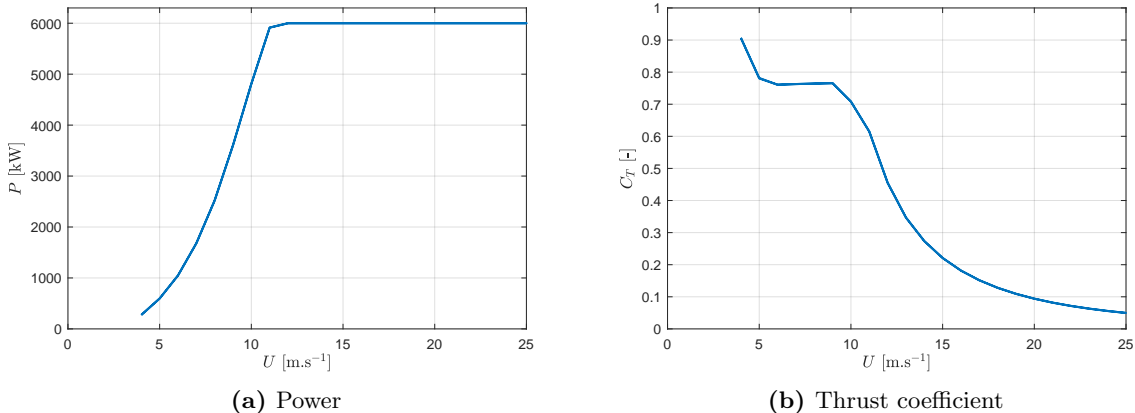


Figure 5.1: (a) Power curve and (b) thrust coefficient curve of the scaled DTU 10MW wind turbine.

Table 5.1: Wind turbine characteristics of the Siemens SWT-6.0-154 [1, 36, 37] and scaled DTU 10MW wind turbines .

	Siemens SWT-6.0-154	Scaled DTU 10MW
Rated power	6 MW	6 MW
Hub height	106 m	106 m
Rotor diameter	154 m	154 m
Rated wind speed	12-14 m.s ⁻¹	12 m.s ⁻¹

A case is selected in which the mean inflow wind speed is around rated wind speed and the mean wind direction is aligned with a row of wind turbines. The date of the selected data is on the 7th of January 2017, from 14:50 to 15:00. The mean wind speed at hub height equals 12 m.s^{-1} and the mean wind direction is 236.8° . In this way the wind direction is aligned with the wind turbines A01, B01 and C01 (as in Figure 2.7). The spacing between the wind turbines in the LES simulations is identical as the spacing between the wind turbines in the WMR wind farm.

The mean inflow conditions, i.e. wind speed and wind direction, are defined $5D$ upstream of the first wind turbine and averaged at each height in a vertical plane (as in Figure 2.1c). The vertical inflow profiles of the BEACon data cases are shown in Figure 5.2. In the LES, turbulence is imposed in planes at $4.95D$ upstream of the first wind turbine. Therefore, the inflow profiles are computed at $4D$ upstream of the first wind turbine. Due to the locations of the saved vertical planes for these LES results, the inflow profile at $1D$ upstream is shown.

The boundary conditions for the LES are:

- Bottom: no-slip condition
- Top: far field, i.e. constant velocity
- Sides: cyclic, i.e. the flow that leaves the domain on the left side, enters again on the right side and vice versa
- Front and back: inflow and outflow boundaries

As can be seen in Figure 5.2a, the LES ran with a too low inflow wind speed. However, the shear of the mean wind speed profile is similar to the one of the BEACon dataset. The mean wind speed at hub height of the LES data is 11.8 m.s^{-1} , compared to a wind speed of 12 m.s^{-1} for the BEACon data at hub height. This results in a C_T value of 0.48 and 0.44 for LES and BEACon respectively. The standard deviation of the LES results is indicated by the blue shaded area. The mean wind direction profile of the BEACon dataset and LES results are shown in Figure 5.2b, which shows that the veer is similar as well.

The turbulence intensity is unknown at the time of the BEACon dataset. The turbulence intensity of the LES is approximately 9.7%, defined $3D$ upstream of the first wind turbine. Apart from missing information about the turbulence intensity, no information is available about the atmospheric stability at the time of the BEACon measurements.

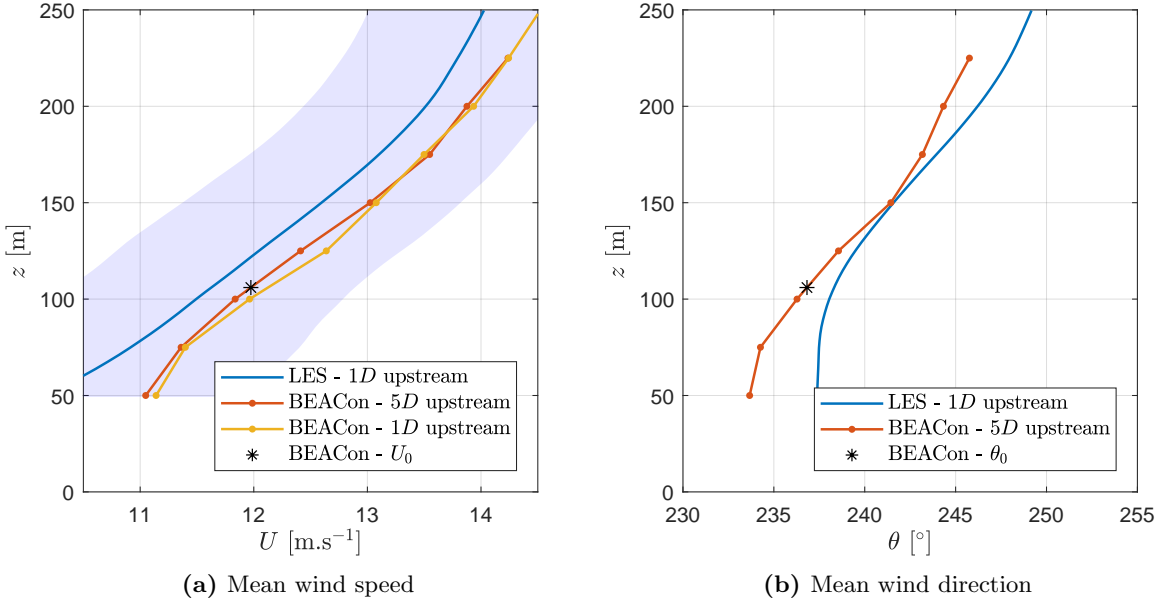


Figure 5.2: (a) Mean vertical wind speed inflow profile with an indication of the mean wind speed at hub height for the BEACon dataset and (b) mean wind direction profiles with indication of the mean wind direction at hub height for the BEACon dataset.

The possible yaw misalignment of the wind turbines at the WMR wind farm at the time of the BEACon dataset is estimated to set similar conditions for the LES. As the yaw angle γ of the wind turbines of the BEACon wind turbines and the mean wind direction θ are known, the yaw misalignment can easily be computed for every wind turbine n :

$$\Delta\gamma_n = \theta - \gamma_n$$

This results in a yaw misalignment of -0.6° , 2.3° and 3.3° for wind turbine A01, B01 and C01 respectively. (For positive yaw misalignment, the rotor is turned counter-clockwise, looking down from above.) Comparing these values with the centerline deficit in Figure 4.3, gives wake deflections under $0.15D$ up to $20D$ downstream.

The data will be represented so that the x -axes is aligned with the mean wind direction. The BEACon domain ranges from 800 m ($=5.2D$) upstream of the first wind turbine to 2500 m ($=16.2D$) downstream of the first wind turbine. The cross-stream domain ranges from -350 m to 350 m ($=2.3D$). Some vertical data planes are available, ranging from a height of 50 m to 250 m. The grid spacing is 25 m ($=0.16D$) in all directions. The LES results are post-processed and averaged to the same grid as the BEACon data since the grid spacing of the original LES results equals $0.02D$.

5.2 Wind Field

In this section, the wind fields of the BEACon dataset and LES results are compared. Figure 5.3 shows the wind field in a horizontal plane at a height of 100 m and Figure 5.4 shows the velocity at a streamwise line through the wind turbine at a height of 100 m. The horizontal profiles in the cross-stream direction at a height of 100 m are shown in Figure 5.5. Six profiles are shown: at $4D$, $5D$ and $6D$ behind the first and second wind turbine. Apart from the fact

that the LES is run for a slightly too low inflow wind speed, there is a clear difference between the two wind fields. The most remarkable differences are:

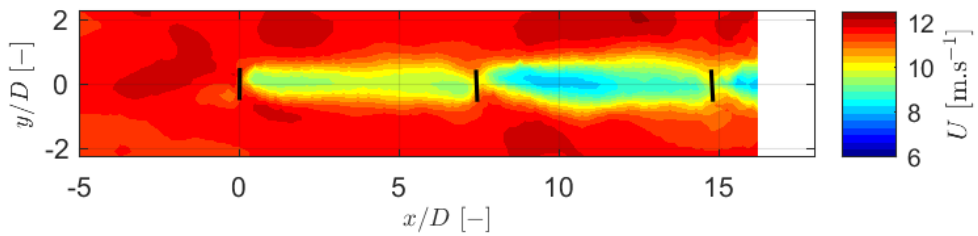
- The velocity deficit in the near wake of the BEACon data is lower than the one from the LES data. There is a small difference in C_T value for both cases (0.48 and 0.44 for LES and BEACon respectively), but the difference between the minimum wind speeds cannot be explained by this difference.
- The wake recovery of the BEACon data is very small. The wake recovery of the LES results is much larger. This is expressed both in the velocity at the streamwise line as in the comparison between the different horizontal profiles.
- In the induction zone, the wind speed is expected to decrease. This is true for the LES results, but the wind speed is increasing for the BEACon data.

Despite the differences, the shape of the horizontal profiles of both results is as expected. They both have a trend similar to a Gaussian profile [39].

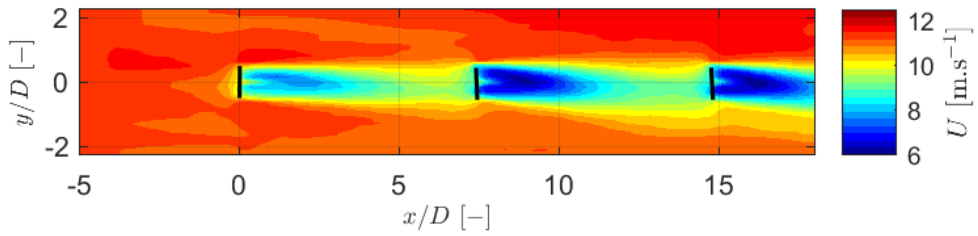
The results of the LES behave more as expected but there are still uncertainties regarding the input parameters for the LES, based on the knowledge of the BEACon data sets. The turbulence intensity has a big influence on the wake recovery. The higher the turbulence intensity, the faster the wake recovers. This shows that the turbulence of the LES might have been chosen too high. Apart from the turbulence intensity, also the scanning process by the Dual-Doppler system and the post-processing are very specific processes.

The fact that the wind turbine is close to the shore and the wind is coming from the direction of land might change the results as well. In the work of Nygaard et al. [28] is shown that the comparison of the BEACon data with wake models is complicated due to the coastal gradients. Therefore, the local inflow wind speed is corrected, but the coastal gradients influence also the wake recovery. This influence on the wake recovery might also be one of the reasons why the BEACon measurement data behave differently than the LES results.

Further research is needed to see if the scanning process and post-processing ‘change’ the wake velocities and how the proximity of the coast influences the wake recovery. Due to these uncertainties is chosen to define the LES simulation results as the benchmark for testing wake superposition methods.



(a) BEACon



(b) LES

Figure 5.3: Wind field in a horizontal plane at a height of 100 m for (a) the BEACon data and (b) LES results.

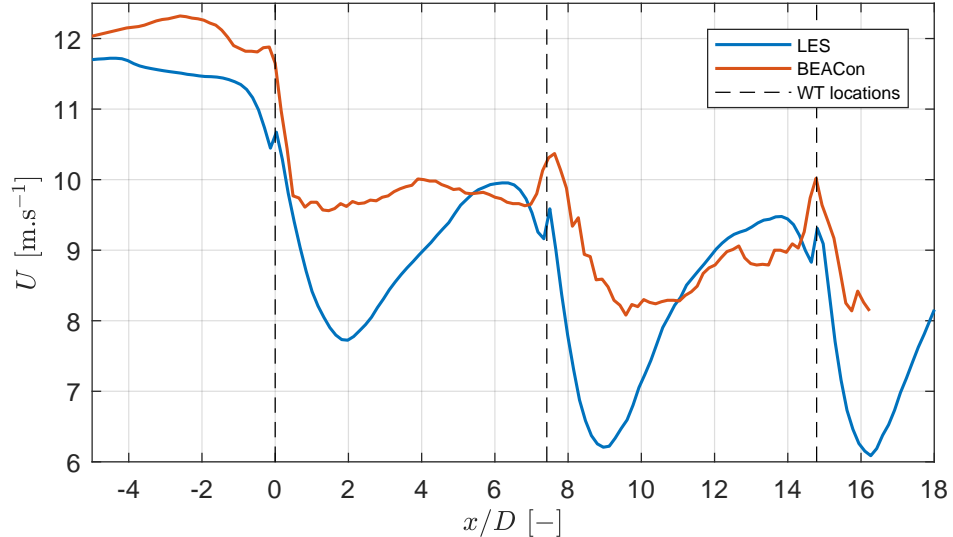


Figure 5.4: Streamwise wind speed at a streamwise line through the first wind turbine at a height of 100 m.

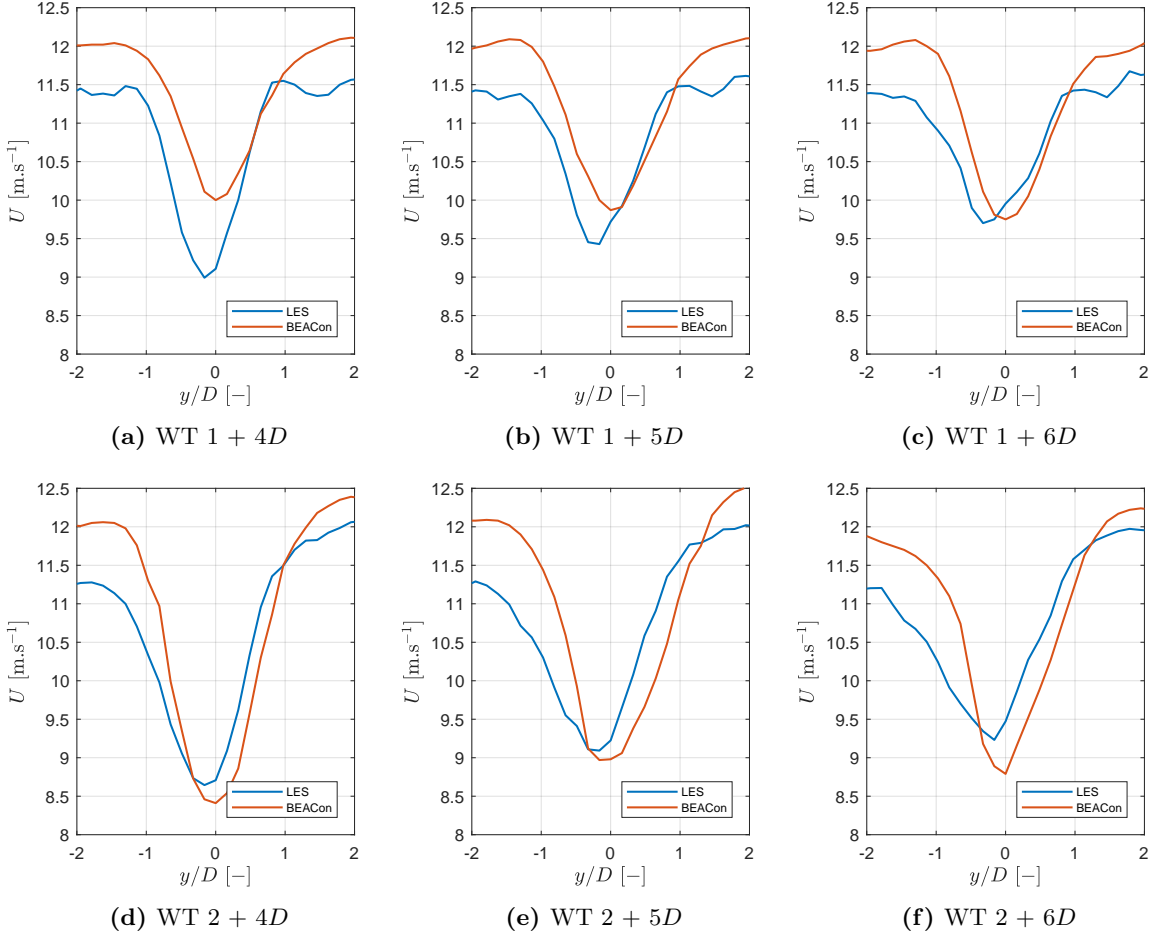


Figure 5.5: Horizontal profiles of the BEACon and LES datasets. The horizontal profiles shown are at a height of 100 m and 4D, 5D or 6D downstream of the first or second wind turbine.

5.3 Power Production

The wind speed at hub height, $1R$ upstream of the wind turbine U_{hub} , and the electrical power of the different wind turbines of the LES are shown in Figure 5.6. The wind speed is decreasing for the downstream wind turbines, compared to the first upstream wind turbine. The rated power is 6 MW, but for the second and third wind turbine, the electrical power is above rated for long periods. This is not desired and might be due to the controller performance of the scaled DTU 10MW wind turbine, used in the LES. As the LES results are chosen as the reference data to test the superposition methods against, another wind turbine model will be used instead. This wind turbine model is the NM80 wind turbine and does not show this particular behaviour for wind speeds just below rated wind speed.

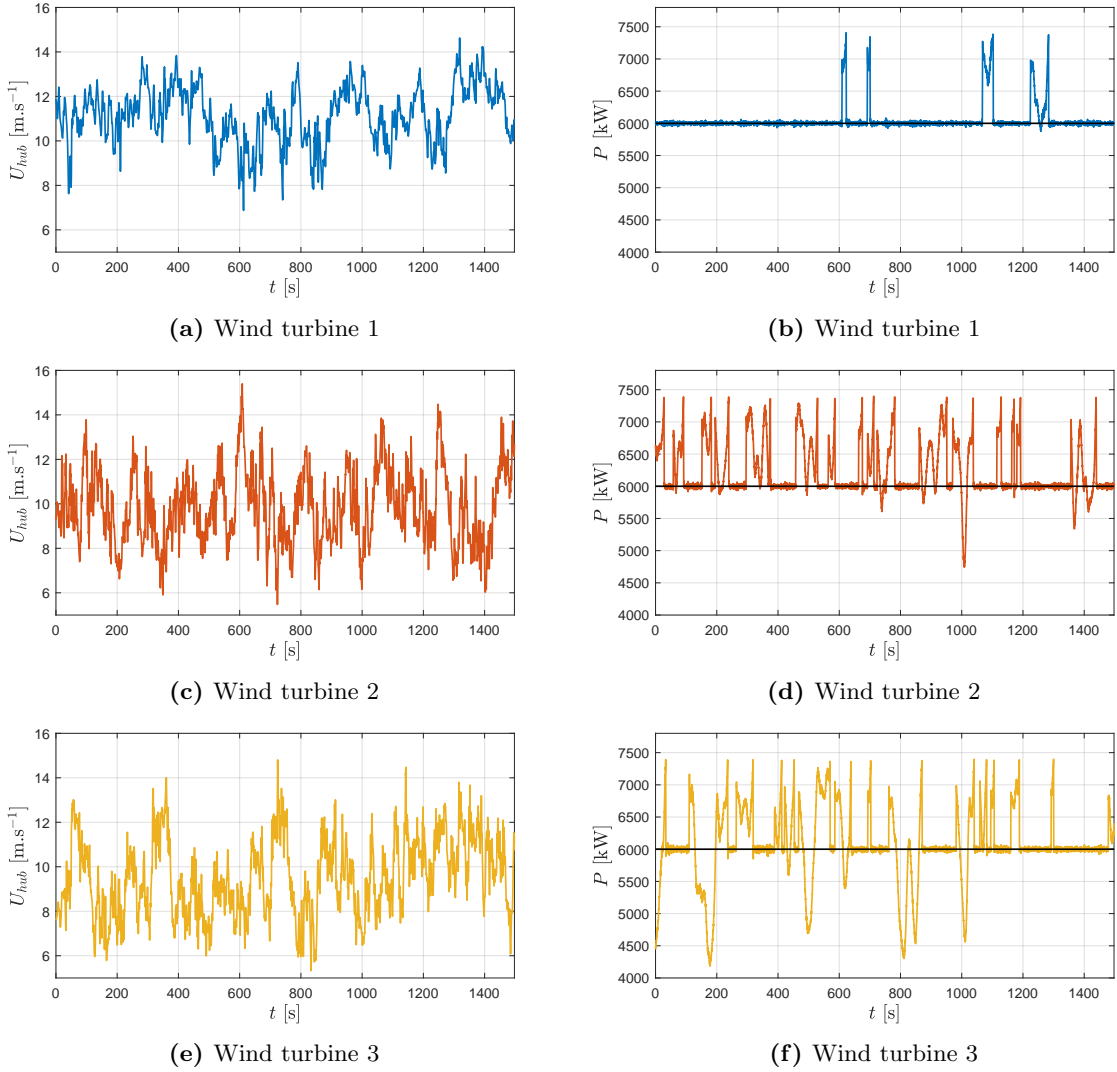


Figure 5.6: Wind speed $1R$ upstream of the hub (left) and electrical power (right) as a function of time for the three wind turbines of the LES results.

5.4 Summary

Because the LES results are more in line with the expectations, based on the known input parameters, i.e. wind speed and wind direction, LES results are chosen as the reference cases to test the different superposition methods against. However, the power output of the scaled DTU 10MW wind turbine does not behave optimally. Therefore, another wind turbine is used to perform other LES simulations, i.e. the NM80 wind turbine. To focus on the superposition principles and to simplify the cases, the LES simulations will be performed with no shear wind speed inflow profiles, low veer wind direction inflow profiles and low turbulence intensity.

Chapter 6

Case Studies & Data

In this section, the different cases which will be used in the analysis of the superposition methods are discussed.

6.1 Case Studies

As already discussed in Chapter 5, LES results will be used as a reference to examine the different superposition methods. To assess the different superposition methods, LES are performed with different inflow conditions and different wind turbine spacings. Long rows of wind turbines are preferred, but due to the computational cost of LES, the domain is limited.

Apart from comparing LES results to the Park model, the superposition of single LES wakes is performed as well to assess if, in this way, full LES wakes, i.e. LES results with multiple wind turbines, can be approached. For the LES superposition, multiple single wakes are needed with different inflow conditions.

To minimize the number of LES runs, the inflow conditions for the simulations are combined so that they can be used both for the comparison with the Park model and the LES superposition. The Park models are run with the same inflow conditions, number of wind turbines, wind turbine spacing and domain as the LES data. The wake decay coefficient k will be calibrated against a single wake, but the other input parameters, discussed in Section 4.2, are varied.

As the scaled DTU 10MW wind turbine did not perform well, another wind turbine model is chosen. Section 6.2 gives an overview of the wind turbine and the inflow conditions (wind speed and turbulence intensity). The cases are categorized as a function of the inflow wind speed. The number of wind turbines and spacing, turbulence intensity, domain and grid spacing are summarized as well.

6.2 Data Generation

The wind turbines characteristics of the wind turbine used in the LES simulations are given in Section 6.2.1. The inflow conditions and the determination of them are discussed in Section 6.2.2. Section 6.2.3 gives an overview of all the cases which will be used in the comparison with the Park model and for the LES superposition. The grid spacing and domain and the data planes available are summarized in Section 6.2.4 and Section 6.2.5 respectively.

6.2.1 Wind turbine

Because the scaled DTU 10MW did not perform as expected, the NM80 wind turbine generator [3] is used in the LES. This wind turbine does not have a hub height, i.e. the wind turbine rotor

is floating. This is due to the no shear inflow wind profile. The characteristics are summarized in Table 6.1 and Figure 6.1 shows the power and C_T -curve.

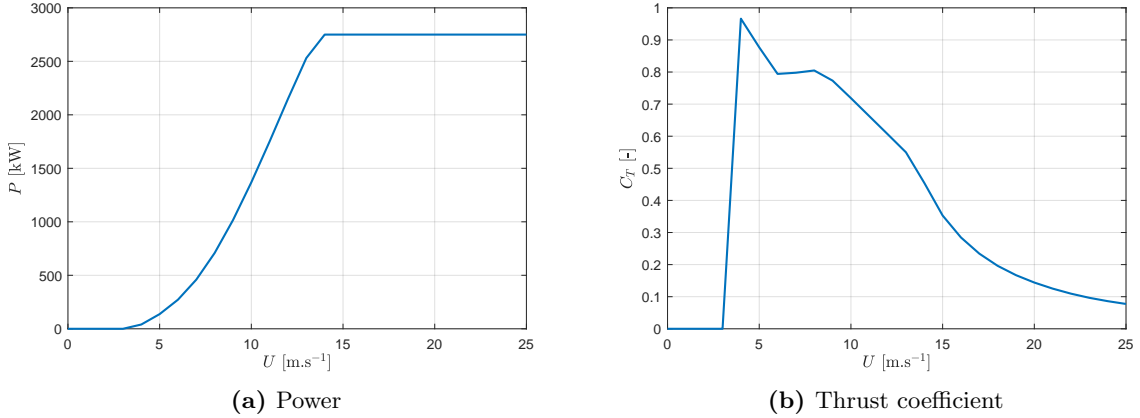


Figure 6.1: (a) Power curve and (b) thrust coefficient curve of the NM80 wind turbine.

Table 6.1: Wind turbine characteristics [3]

	NM80
Rated power	2.75 MW
Hub height	-
Rotor diameter	80 m
Rated wind speed	14 m.s^{-1}

6.2.2 Inflow conditions & boundary conditions

The set-up of the LES is based on the research questions to answer what the best superposition method is in combination with the Park model around rated wind speed and if it is possible to superpose single LES wakes. Therefore, three different inflow wind speeds are chosen: the rated wind speed, a wind speed just below rated wind speed and a wind speed below rated wind speed and in the region with a constant C_T -value.

The rated wind speed is 14 m.s^{-1} and the wind speeds below rated are defined following the steps below. The wind turbine spacing equals $7.4D$.

1. Single wake 1: LES of a single wake with an inflow wind speed of 14 m.s^{-1} and turbulence intensity of 3.6 %.
 - (a) Estimate the mean wind speed at the location of the hub of the second wind turbine in ‘single wake 1’. This equals 11.2 m.s^{-1} . (Figure 6.2a)
 - (b) Define the turbulence intensity at the location of the hub of the second wind turbine in ‘single wake 1’. This equals 8.6 %. (Figure 6.2a)
2. Single wake 2: LES of a single wake with an inflow wind speed of 11.2 m.s^{-1} and (low) turbulence intensity of 3.6 %.
 - (a) Estimate the mean wind speed at the location of the hub of the second wind turbine in ‘single wake 2’. This equals 8.6 m.s^{-1} .
 - (b) Check if this wind speed lies in the region with constant C_T . As this is not the case, another single wake simulation is performed.

3. Single wake 3: LES of a single wake with an inflow wind speed of 8.6 m.s^{-1} and turbulence intensity of 3.6 %.

- (a) Check if this wind speed lies in the region with constant C_T . This is true, so there is no need to run another simulation with a lower inflow wind speed.

The definition of the mean wind speed and turbulence intensity at the location of the second wind turbine in ‘single wake 1’ are illustrated in Figure 6.2. The turbulence intensity defined in step 1b (8.6 %) is used to calculate an extra single wake with an inflow wind speed of 11.2 m.s^{-1} and an increased turbulence intensity.

The inflow wind speeds defined above form the basis to run the other LES. These simulations have a different number of wind turbines and different spacing between the wind turbines and are summarized in Section 6.2.3.

As boundary conditions, the far field condition (constant velocity) is applied on all sides, except the front and back side for which inflow and outflow are applied.

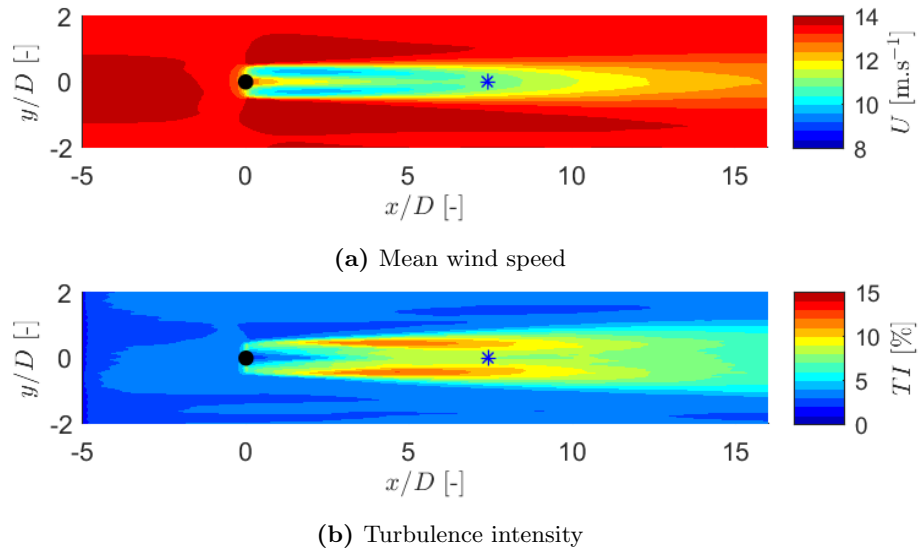


Figure 6.2: Illustration of the calculation of the mean wind speed and turbulence intensity at the location of the second wind turbine in ‘single wake 1’. The first and second wind turbine are indicated in black and blue respectively.

6.2.3 Cases

The parameters of all the LES cases are summarized in this section. The mean inflow velocity, number of wind turbines, spacing S_x and turbulence intensity are summarized in Table 6.2. The spacing is expressed as a function of the rotor diameter D , which equals 80 m. The naming of the cases is as follows: all cases with the same inflow wind speed are given the same letter, followed by a number to differentiate in number of wind turbines, spacing and/or turbulence intensity. The wind speed inflow profiles are uniform, i.e. no shear, which is also the reason that no physical hub height is assigned to the rotor.

Table 6.2: Overview of LES datasets.

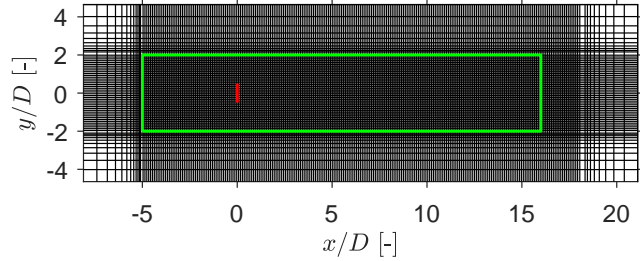
Case	U_0 [m.s $^{-1}$]	# WT	S_x/D [-]	TI [%]	Remarks
A1	14	1	-	3.6	
A2	14	3	7.4	3.6	
A3	14	4	4.9	3.6	
A4	14	5	3.7	3.6	
A5	14	6	7.4	3.6	Long domain (see Section 6.2.4)
A6	14	13	3.3	3.6	Long domain (see Section 6.2.4)
B1	11.2	1	-	3.6	
B2	11.2	1	-	8.6	Increased turbulence intensity
B3	11.2	3	7.4	3.6	
C1	8.6	1	-	3.6	

6.2.4 Grid spacing and domain

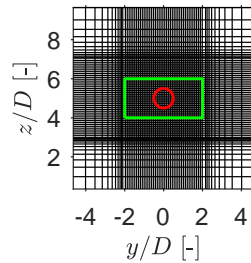
In the LES, the grid spacing increases towards the boundaries of the domain, i.e. fine grid around the wind turbines and a coarse grid at the edges. Due to the larger grid spacing at the end of the LES domain, the data at the end of the domain needs to be disregarded, i.e. the last $5D$ is disregarded. Figure 6.3a and Figure 6.3b show the horizontal and vertical grid respectively. The domain of the data, that will be used in the calculations and discussions, is indicated in green. This domain is further referred to as ‘the domain’. The first wind turbine and rotor are indicated in red.

The domain of the LES data is defined by X , Y and Z , as indicated in Figure 2.1.

X ranges from $-5D$ to $16D$ for the short domain and from $-5D$ to $41D$ for the long domain (for Case A5 and A6). The domain in the cross-stream and vertical direction are equal for all cases. Y ranges from $-2D$ to $2D$ and Z ranges from $4D$ to $6D$. The grid spacings in the fine grid, ΔX , ΔY and ΔZ , equal $0.02D$ for all datasets.



(a) Horizontal LES grid



(b) Vertical LES grid

Figure 6.3: Illustration of the LES grids for (a) a horizontal plane and (b) a vertical plane. The location of the first wind turbine and wind turbine rotor are indicated in red. The domain used in the calculations is indicated in green.

6.2.5 LES data planes

The data planes, as shown in Section 2.2.1, of the LES data are located as given in Table 6.3. For Case A5 and A6, which have a bigger domain in the streamwise direction (X), more vertical data planes are extracted.

Table 6.3: Locations of the data planes of the LES simulations

Plane	Case	Location
Horizontal	All cases	Plane at hub height
Streamwise	All cases	Plane through the hub
Vertical	Case A5 and A6	Upstream of the 1 st WT: at $-5D$ to $-0.5D$ in steps of $0.5D$ At WT positions (of Case A5): at $0D$ to $37D$, in steps of $7.4D$ Downstream of the 1 st WT: at $1D$ to $42D$, in steps of $1D$
	Other cases	Upstream of the 1 st WT: at $-5D$ to $-0.5D$ in steps of $0.5D$ At WT positions: at $0D$, $7.4D$ and $14.8D$ Downstream of the 1 st WT: at $1D$ to $19D$, in steps of $1D$

Chapter 7

Comparison LES & Engineering Models

In this section, the Park model will be compared with the LES results of the simulation cases discussed in Section 6.2. As a first step, a single Park wake will be calibrated to a single LES wake. Afterwards, different superposition methods (linear, quadratic and maximum deficit) are performed on the single wake and these results will be compared to the full LES results.

7.1 Calibration of Single Park Wake

The Park model has different input parameters: the wake decay coefficient k , the correction factor, whether or not to include wake reflection and the superposition method (see Section 4.2). The superposition method is of no importance for a single wake and the correction factor equals always one for the first wake. To lower the number of variables during the comparison of a full LES wake, i.e. an LES with multiple wind turbines, a single Park wake is calibrated to match a single LES wake as good as possible.

As the wind turbine rotor in the LES is floating, wake reflection is not considered as there is no reflecting ground. The inflow wind speed of both wakes is identical, and therefore also the thrust coefficient. The choice for k is based on the comparison of wake width and the rotor averaged wind speed. The wake coefficients that are tested lie in the calibration range of 0.02 to 0.06.

Figure 7.1a shows the wind field in a horizontal plane at hub height of the single LES wake for an inflow wind speed U_0 of 14 m.s^{-1} , corresponding to $C_T = 0.45$. The wake shown in Figure 7.1b is an example of a Park wake with $k = 0.04$ and the same inflow wind speed as the single LES wake. The other wakes for different values of k can be found in Appendix B.1, Figure B.1.

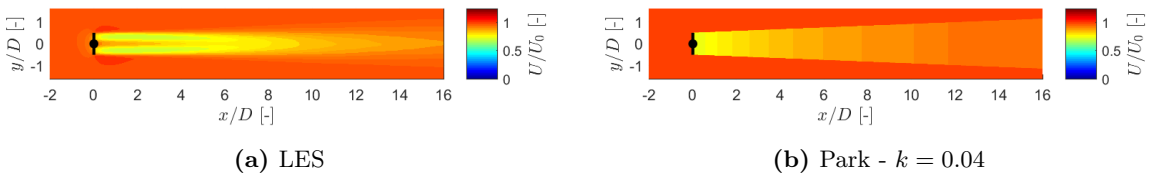


Figure 7.1: Wind field in a horizontal plane at hub height of a single wake with $U_0 = 14 \text{ m.s}^{-1}$ of (a) LES simulation (b) Park model with $k = 0.04$.

The wake boundary is defined by the location where the wind speed reaches $0.98U_0$ for the LES wake. The wake boundary of the Park single wake is taken as the analytical wake boundary ($U = U_0$), as described in Section 4.2. The result is shown for different values of k in Figure 7.2.

The differences between the boundary of the single LES wake and the Park wakes, ΔWB , are shown in Figure 7.3. The boundary of the LES wake in the upper and lower part of the wake is slightly different. Therefore, for every streamwise location the mean is taken of the difference between the LES and Park wake for the upper and lower part of the wake:

$$\Delta WB = \frac{(y_{top,Park} - y_{top,LES}) + (y_{bottom,Park} - y_{bottom,LES})}{2} \quad (7.1)$$

For both $k = 0.03$ and $k = 0.04$ the difference stays under $0.1D$ (up to $14D$ downstream for $k = 0.04$).

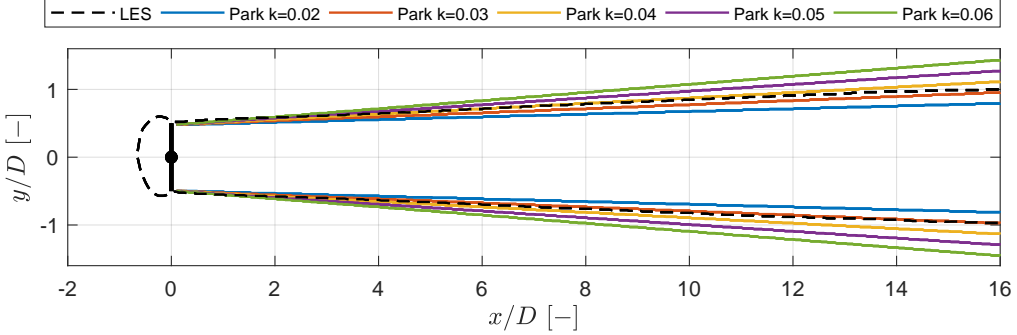


Figure 7.2: Wake boundary of the single LES wake ($U = 0.98U_0$) and different single Park wakes ($U = U_0$).

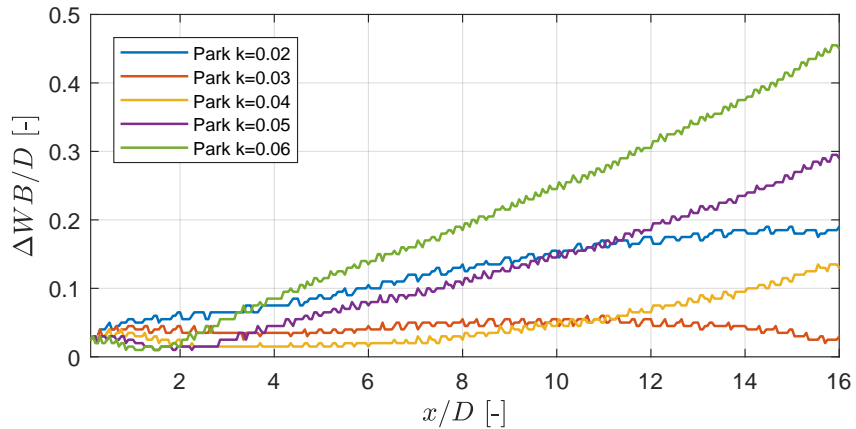


Figure 7.3: Absolute difference between the wake boundary of the single LES wake and the different single Park wakes.

Figure 7.4 shows the centerline wind speed¹, U_C , of both the single LES wake and the different single Park wakes. As already could be seen in Figure 7.1a, the minimum velocity in the LES wake is not the same as the centerline wake deficit. As the deficit of the Park model is a top-hat profile, the centerline deficit of the Park model might underestimate the wake deficit, while the outer parts of the Park wake might overestimate the wake deficit. This is shown in Figure 7.5, where the horizontal profiles at hub height are shown. The double peaks in the horizontal wind profiles, or also seen as streaks/lobes in Figure 7.1a, are due to the tip vortices and the presence of the hub. The tip vortices break down to small turbulent scales as the

¹Centerline wind speed: wind speed at hub height, at a downstream line behind the first wind turbine

wake develops. If the wake reaches a fully turbulent state, the horizontal profile is Gaussian [39].

Because of the observations of the centerline wind speed and horizontal wind profiles, the comparison is made between the rotor averaged wind speed of the LES wake and the Park wakes. The rotor averaged wind speed of the LES simulation is calculated as described in Section 2.2.2 because the wake is axisymmetric, as can be seen in Figure 7.6.

Figure 7.7 shows the rotor averaged wind speed, U_R , of the LES simulation and the different Park wakes. The focus is on the far wake, i.e. further than $4D$ downstream. The rotor averaged wind speed of the single Park wakes for $k = 0.04$ to $k = 0.06$ underestimate the wake deficit. The single Park wake for $k = 0.02$ underestimates the rotor averaged wake velocity for the (very) far wake, but for $k = 0.03$ the Park wake and the LES wake are close.

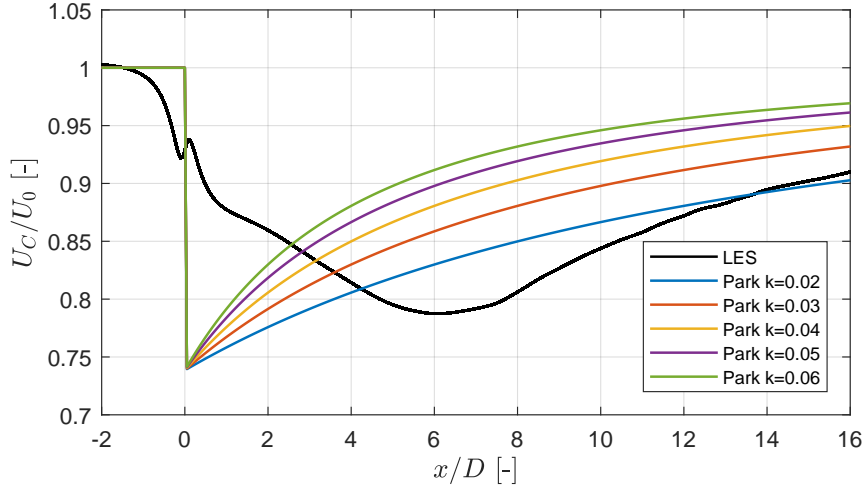


Figure 7.4: Centerline wind speed U_C of the single LES wake (Case A1) and the different single Park wakes.

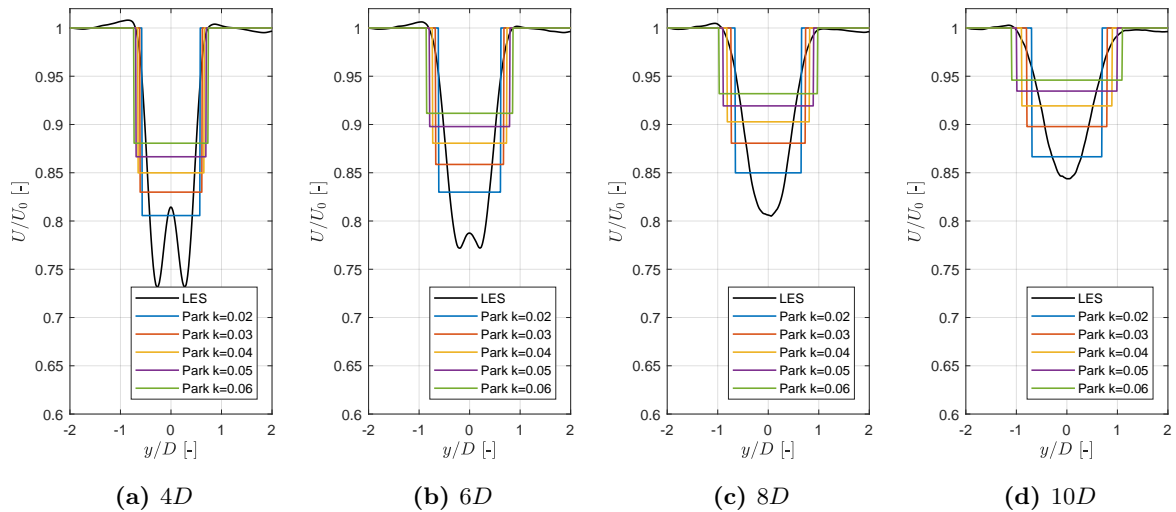


Figure 7.5: Horizontal profiles of the single LES wake (Case A1) and different Park wakes at hub height and $4D$, $6D$, $8D$ or $10D$ downstream of the wind turbine.

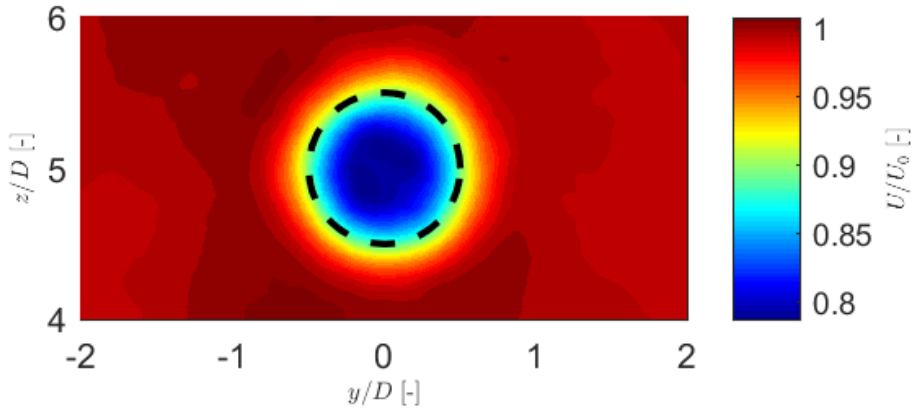


Figure 7.6: Vertical plane $7D$ downstream of the single LES wake (Case A1). The rotor area is indicated in black.

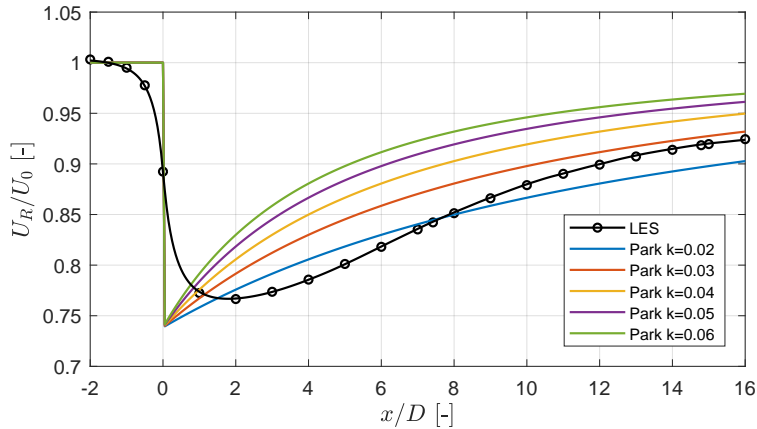


Figure 7.7: Rotor averaged wind speed U_R of the LES simulation and single Park wakes for an inflow wind speed of 14 m.s^{-1} (Case A1).

Based on the wake boundary and the rotor averaged wind speed, $k = 0.03$ is chosen to be used for the single Park wake. The wake boundary difference between the single LES wake and the single Park wake is below $0.1D$ up to $16D$ (i.e. the end of the domain). Also for $k = 0.03$ the rotor averaged wind speed for both cases match well in the far wake. The wake decay coefficient of $k = 0.03$ will be used in the Park model for the calculation of the wind field with multiple wind turbines and an inflow wind speed of 14 m.s^{-1} .

With the inflow wind speed U_0 equal to 11.2 m.s^{-1} , the Park wake is calibrated to $k = 0.04$, following the same procedure. The rotor averaged wind speed is shown in Figure 7.8. All other plots which are also shown for the case with $U_0 = 14 \text{ m.s}^{-1}$, are shown in Appendix B.2 as a reference.

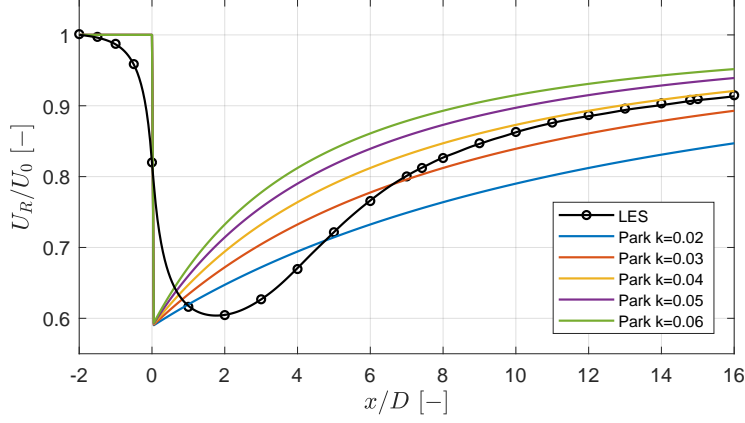


Figure 7.8: Rotor averaged wind speed U_R of the LES simulation and single Park wakes for an inflow wind speed of 11.2 m.s^{-1} (Case B1).

7.2 Park Superposition

The wake decay coefficient k , defined in the previous section, is used in the Park model computation of the full wind field with multiple wind turbines. By fixing the wake coefficient k , six different superposition results remain: three superposition methods and with/without correction factor. The superposition methods considered are the linear ('lin'), quadratic ('quadr') and maximum deficit ('max') superposition methods. Wake reflection is not taken into account as the LES wind turbine does not have a reflecting ground.

7.2.1 Inflow wind speed at rated wind speed

First, cases with an inflow velocity at hub height equal to the rated wind speed are looked at. Case A3, A4 and A5 include respectively four, five and six wind turbines with spacings of $4.9D$, $3.7D$ and $7.4D$, as described in Section 6.2.3. The different spacings make it possible to look into the question if the optimal superposition method changes if the wind turbines are placed close to each other ($3.7D$) or further apart ($7.4D$).

The LES and Park (with quadratic superposition and correction factor) of Case A4 are shown in Figure 7.9a and 7.9b respectively. The other LES and Park wind fields for Case A3 and A6 are given in Appendix C.1.

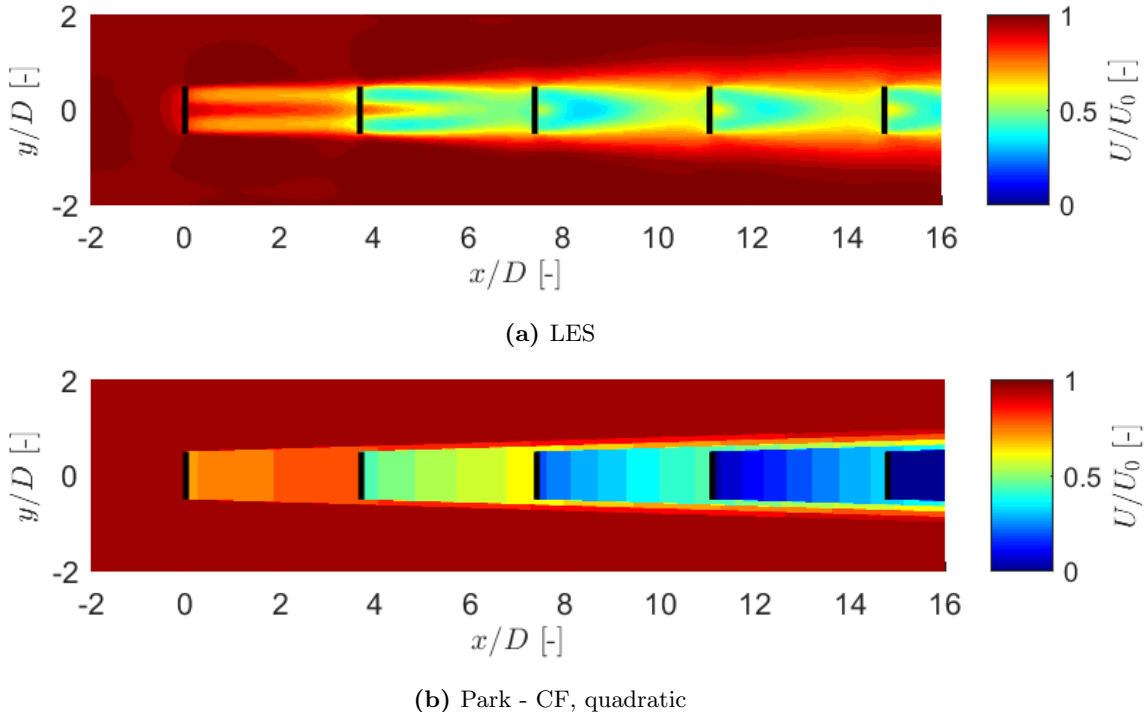


Figure 7.9: Horizontal wind field at hub height of the LES simulation and Park model for Case A4, with the Park model ran with the quadratic superposition method and correction factor (CF).

Wake boundary

Since the k parameter is equal to 0.03 for all superposition method calculations, the wake width or wake boundary is the same as well. The boundary for the LES wake is put to $0.98U_0$. The wake boundaries for Case A3, A4 and A5 are shown in Figure 7.10. The main difference in all cases between the LES wake width and the Park wake width is the induction zone. This zone is present in all LES results: very clearly upstream of the first wind turbine, but an increase in the wake width can also be seen upstream of the other wind turbines.

The wake boundaries for Case A3 and A4 match well behind the first wind turbine, but the difference increases downstream. The closer the spacing, the larger the difference downstream. i.e. the difference is higher for Case A4 than for Case A3. For a large wind turbine spacing (Case A6), the wake boundary of the LES simulation and the Park model are very close and have the same trend.

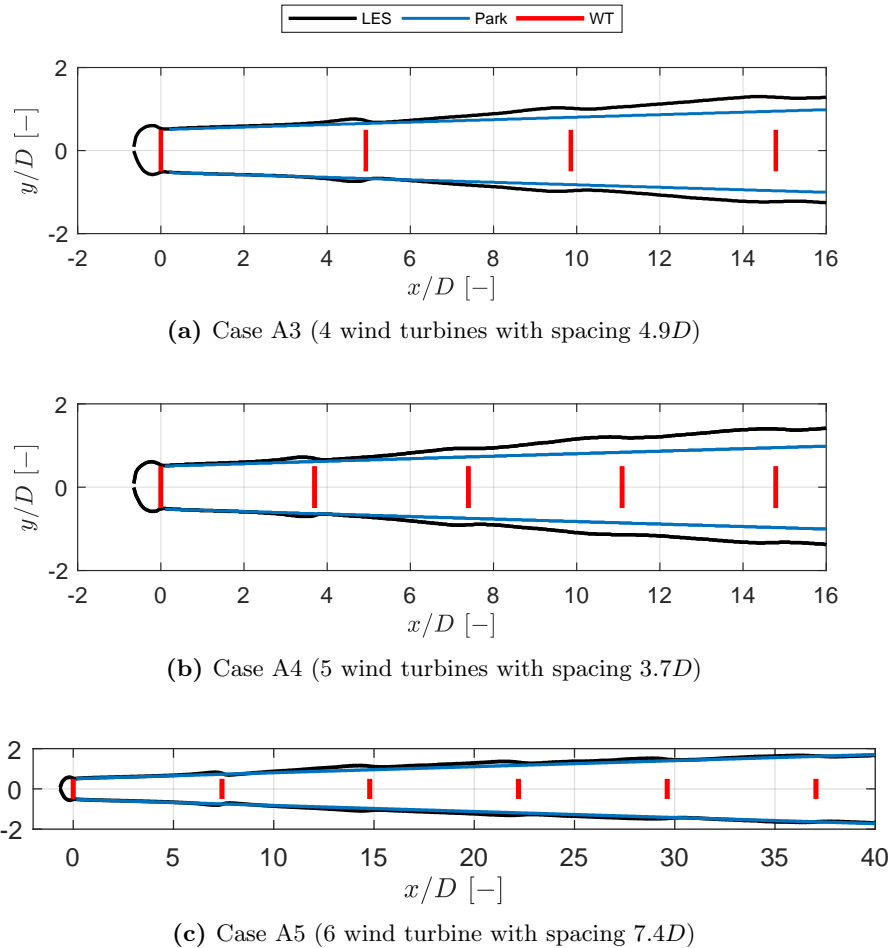


Figure 7.10: Wake boundary of the LES simulation and Park model for Case A3, A4 and A5.

Rotor averaged wind speed

Due to the ‘lobes’ in the horizontal wind speed profiles at hub height of the LES wakes and the top-hat profile of the Park wakes, the centerline velocity comparison between those two does not give meaningful results. From the second wake on, the lobes are less explicit due to the mixing of the wakes because of the induced turbulence by the downstream wind turbines. Due to the top-hat profile of the Park model is the focus on the rotor average wind speed.

Figure 7.11, 7.12 and 7.13 show the rotor averaged wind speed of the LES simulations and Park model of Case A3, A4 and A5. In the first wake, there is no difference between the six Park combinations as there is no superposition of wakes and no correction factor applies. In the second wake, all six Park combinations are close to the rotor averaged wind speed of the LES simulations. For Case A3 and A4, the quadratic and maximum deficit method with correction factor (CF) and linear method without correction factor are closest to the LES results. The quadratic and maximum deficit method without correction factor overpredict the rotor averaged wind speed. The linear superposition method with correction factor underpredicts the LES results in the second wake. For Case A5, the results are slightly different. In this case, all results based on the Park model lie in the vicinity of the LES rotor averaged wind speed. Only the linear superposition method with correction factor gives a low rotor averaged wind speed

compared to the LES results.

From the third wake on, the six superposition methods differentiate more. For Case A3 and A4, the quadratic and maximum deficit method without correction factor give the best results for the third wake. The former method underpredicts the rotor averaged wind speed, while the latter overpredicts the LES results. Looking to the fourth wake of Case A4, the maximum deficit method without correction factor predicts the LES rotor averaged wind speed well.

For Case A5, with six wind turbines and a large wind turbine spacing, the observations are slightly different. In the third wake, the results of the quadratic and maximum deficit method without correction factor are also close to the LES results. This observation also holds for the fourth and fifth wake. The maximum deficit method without correction factor predicts the far wake the best, while the quadratic superposition method without correction factor is closest to the near wake. The linear wake superposition methods, both with and without correction factor, and the quadratic and maximum deficit method with correction factor, all underpredict the rotor averaged wind speed. For the linear superposition methods, the wake deficit becomes so high that the velocity becomes negative, which is, of course, physical not possible.

The spacing between the wind turbines in Case A6 is small. The rotor averaged wind speed is shown in Figure 7.14. The results for the second and third wake are similar to the cases discussed above. From the fourth wake one, the wake deficit is strongly overpredicted for the linear and quadratic superposition method so that for the linear (both with and without correction factor) and the quadratic (with correction factor) method, the wind speed even becomes negative. Clearly, the maximum deficit method without correction factor approaches the rotor averaged wind speed of the LES simulation the best.

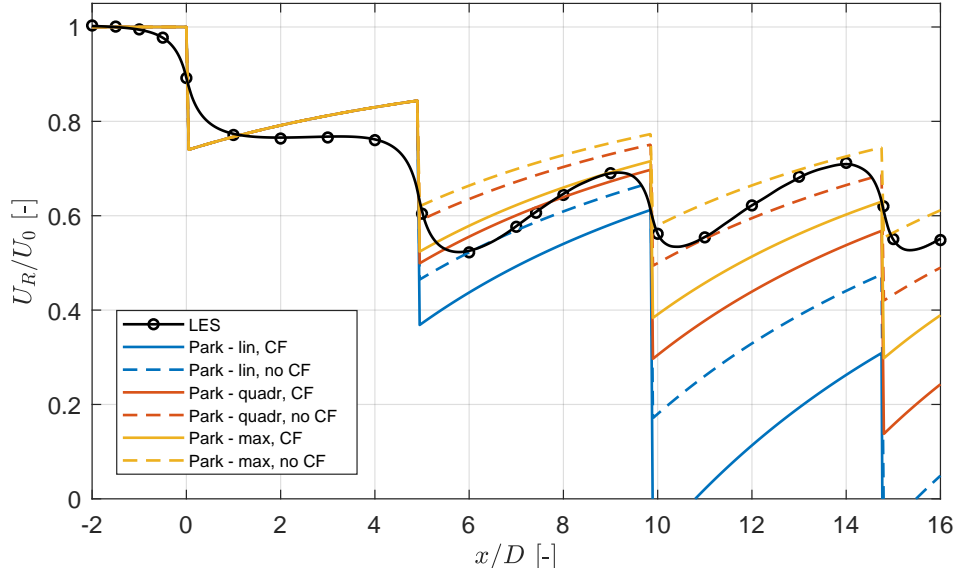


Figure 7.11: Rotor averaged wind speed U_R for Case A3 with four wind turbines and an inflow wind speed of 14 m.s^{-1} . The wake coefficient k of the Park model equals 0.03.

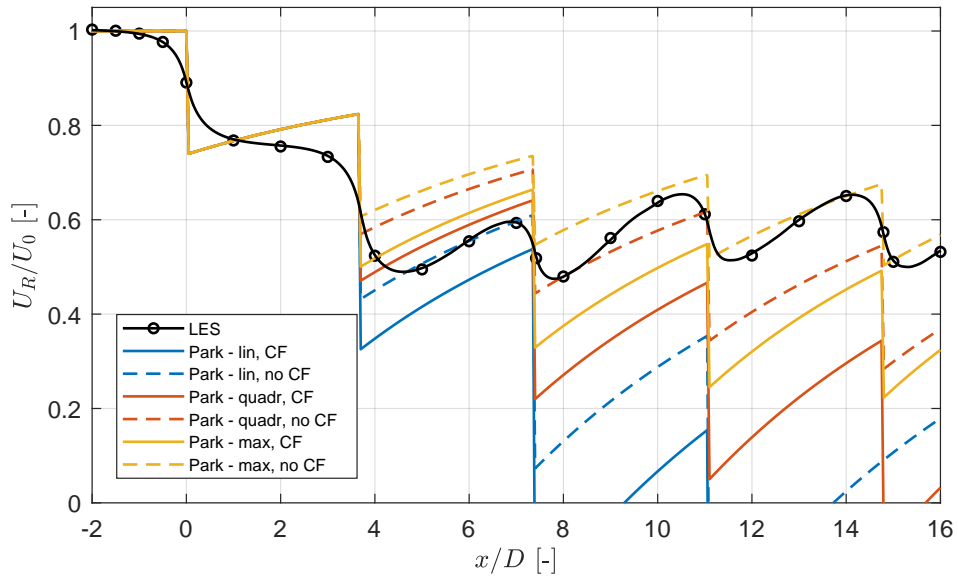


Figure 7.12: Rotor averaged wind speed U_R for Case A4 with five wind turbines and an inflow wind speed of 14 m.s^{-1} . The wake coefficient k of the Park model equals 0.03.

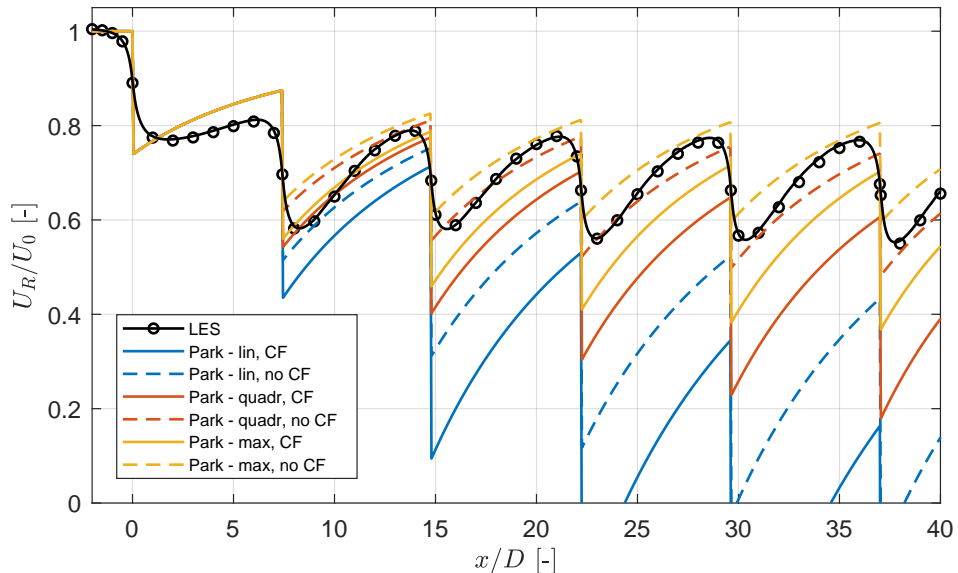


Figure 7.13: Rotor averaged wind speed U_R for Case A5 with six wind turbines and an inflow wind speed of 14 m.s^{-1} . The wake coefficient k of the Park model equals 0.03.

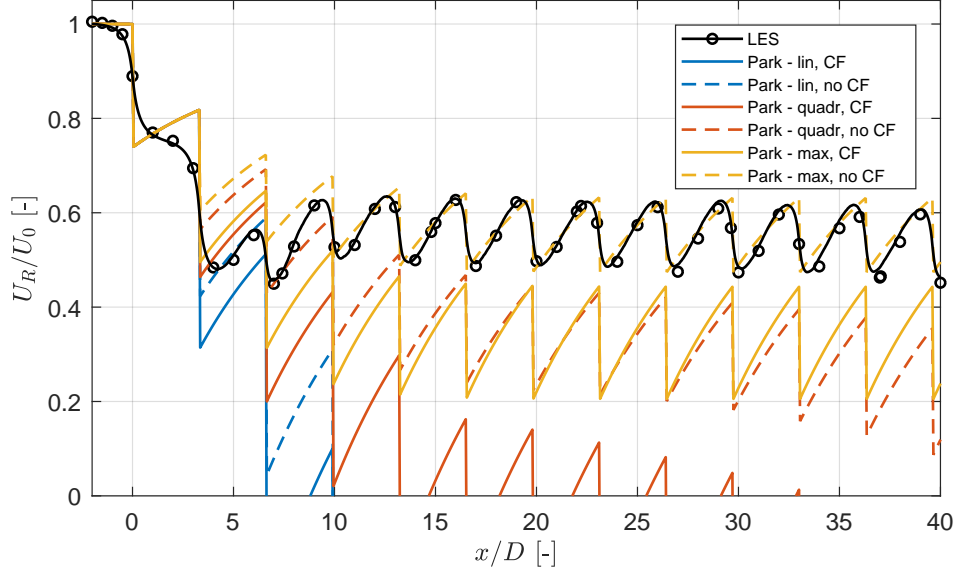


Figure 7.14: Rotor averaged wind speed U_R for Case A6 with 13 wind turbines and an inflow wind speed of 14 m.s^{-1} . The wake coefficient k of the Park model equals 0.03.

Wind speed at the wind turbines

From a yield assessment point of view, the interest is on the rotor averaged wind speed at the wind turbines, $U_{R,WT}$. Figure 7.15a shows the rotor averaged wind speed just upstream of the wind turbines for Case A6. This wind speed in the Park model is actually the highest wind speed in each wake as the Park model does not include an induction zone. Even though the maximum deficit method without correction factor predicts the trend of the rotor averaged wind speed the best, the rotor averaged wind speed at the wind turbines is overpredicted. From the fourth wind turbine on, the quadratic superposition method with correction factor is closer to the LES rotor average wind speed, but the trend of both is not the same.

The mean value of the rotor averaged wind speed just upstream and just downstream of the wind turbine locations, $\overline{U_{R,WT}}$, is calculated as well and shown in Figure 7.15b. It is clear that the quadratic and maximum deficit method without correction factor are the closest and have the same trend as the LES rotor average wind speed. The quadratic and maximum deficit superposition method over- and underpredict the LES wind speed respectively with 7% at the sixth wind turbine.

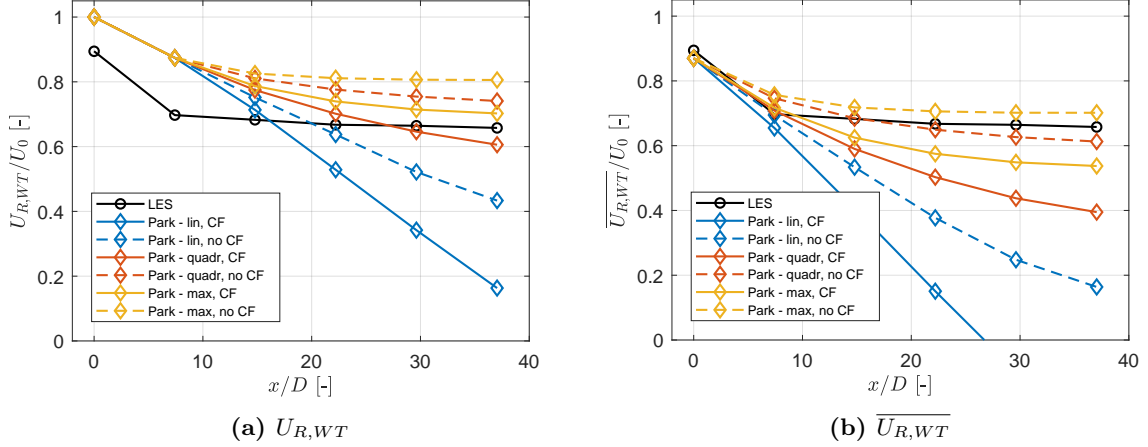


Figure 7.15: (a) Rotor averaged wind speed $U_{R,WT}$ just upstream of the wind turbine locations and (b) averaged rotor averaged wind speed $\overline{U}_{R,WT}$ for Case A5.

The result for $\overline{U}_{R,WT}$ of Case A4 is shown in Figure 7.16a. In this case, the maximum deficit method without correction factor gives the best results for the fourth and fifth wind turbine. This is expected as this method also gives the best result when comparing the full rotor averaged wind speed (Figure 7.12). It overestimates the LES rotor average wind speed at the fifth wind turbine with 3.5%. However, it should be noted that the increase in the wind speed at the fourth wind turbine is not expected.

In case A6, the trend of the maximum deficit method without correction factor is closest to the trend of the LES simulations. Therefore, it is also expected that $\overline{U}_{R,WT}$ for this method is in line with the rotor averaged wind speed at the wind turbines of the LES simulations. This is indeed true, as shown in Figure 7.16b.

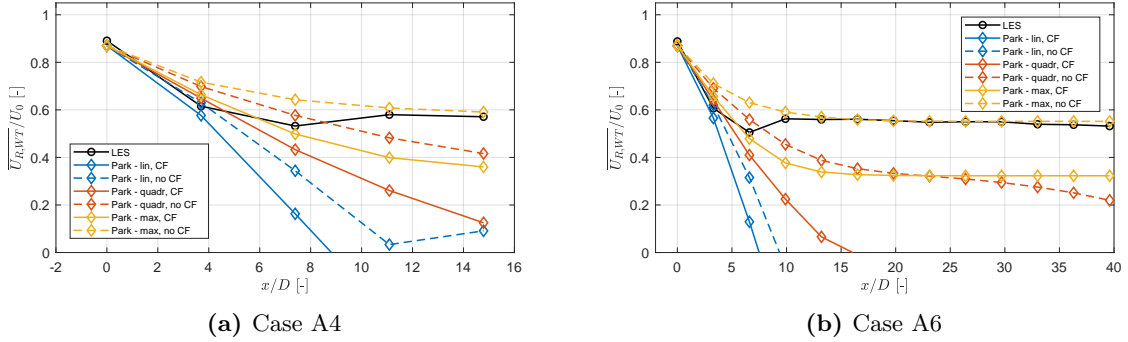


Figure 7.16: Rotor averaged wind speed $\overline{U}_{R,WT}$ at the wind turbine locations for (a) Case A4 and (b) Case A6.

Power

In industry, the Park model is used for the energy yield assessment. Usually, the wind speed just upstream of the wind turbines is used to assess the power. Figure 7.17 shows the power of all wind turbines for the LES results and Park results of Case A6. The power of the Park results is computed making use of the power curve and the wind speed just upstream of the wind turbines. The Power of the LES simulation is computed making use of the time series,

achieved by the coupling with Flex5 (see Section 2.4). Again, the maximum deficit method without correction factor has a very similar trend as the power of the LES. The largest difference occurs at the fourth wind turbine with an underestimation of 165 kW or 8 %.

The power of Case A3 and A4 are shown in Appendix C.1. As for Case A5, the conclusions can be compared to the trends of the rotor averaged wind speed. For Case A3 can be seen that the LES power converges faster than the Park results. The difference in power for Case A4 is larger due to the (unexpected) increase in wind speed at the fourth wind turbine. This does not occur in the Park results.

Figure 7.18 shows the power for Case A6. Although the rotor averaged wind speed of the maximum deficit method without correction factor matches well with the LES results, the difference in the power is big. The difference is up to 520 kW or 35 %.

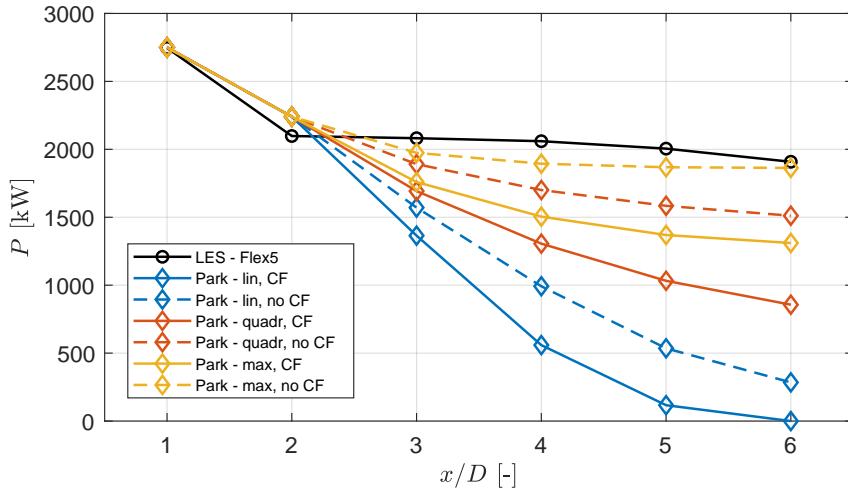


Figure 7.17: Power of the LES results and Park models for Case A5.

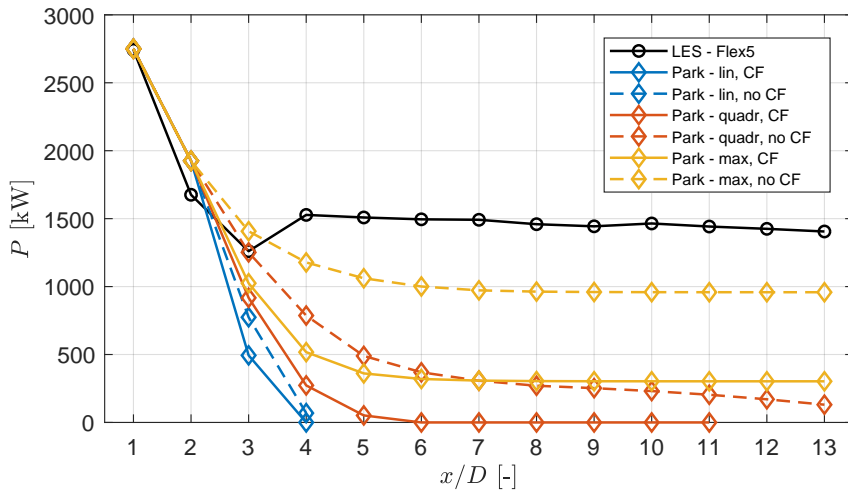


Figure 7.18: Power of the LES results and Park models for Case A6.

Wake recovery

The wake recovery, expressed as the change of rotor averaged wind speed along the streamwise direction, is calculated as discussed in Section 7.3 (Eq. (2.7)). An example of the wake recovery for Case A5 is shown in Figure 7.19. The wake recovery of the LES data is most in line with the wake recovery of the quadratic and maximum deficit superposition methods.

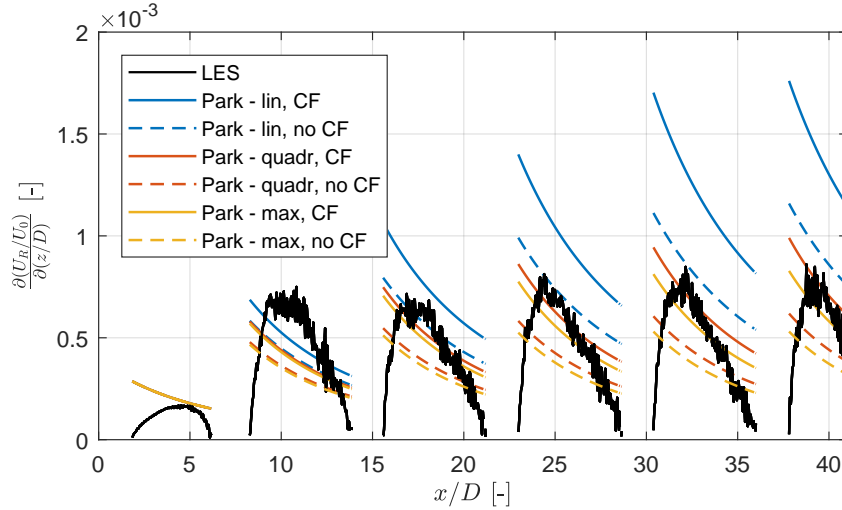


Figure 7.19: Wake recovery for Case A5.

7.2.2 Inflow wind speed below rated wind speed

During the single wake calibration, performed in Section 7.1, for a single wake with an inflow wind speed of 11.2 m.s^{-1} , which is below the rated wind speed, the wake decay coefficient k is chosen equal to 0.04. Again, as there is no reflecting ground, wake reflection is not considered. The spacing between the wind turbines in Case B3 is $7.4D$, which is the same as the spacing for Case A5 in the previous section, but only three wind turbines are present. Figure 7.20 shows the horizontal wind field at hub height of the LES results and the Park model with quadratic superposition and correction factor. The other wake fields are shown in Appendix C.2.1.

The rotor averaged wind speed is shown in Figure 7.21. As the domain is only big enough to capture two full wakes and a part of the third wake, it is very difficult to draw conclusions regarding the superposition method. As in Case A5, with an inflow wind speed at rated wind speed, it seems that the quadratic and maximum deficit superposition methods fit the best with the LES rotor averaged wind speed. The linear superposition method overpredicts the wake deficit. Figure 7.22a gives the rotor averaged wind speed at the wind turbines, $U_{R,WT}$. The rotor averaged wind speed of the Park models with different superposition approaches is higher than the rotor averaged wind speed of the LES results, as expected. When the rotor averaged wind speed of the Park model is averaged over the wind turbine, the results are closer, as shown in Figure 7.22b. However, it seems that the rotor averaged wind speed of the LES results converges already at the third wind turbine, while the results of the Park model still keep decreasing. The decrease, however, is small for the maximum deficit method without correction factor.

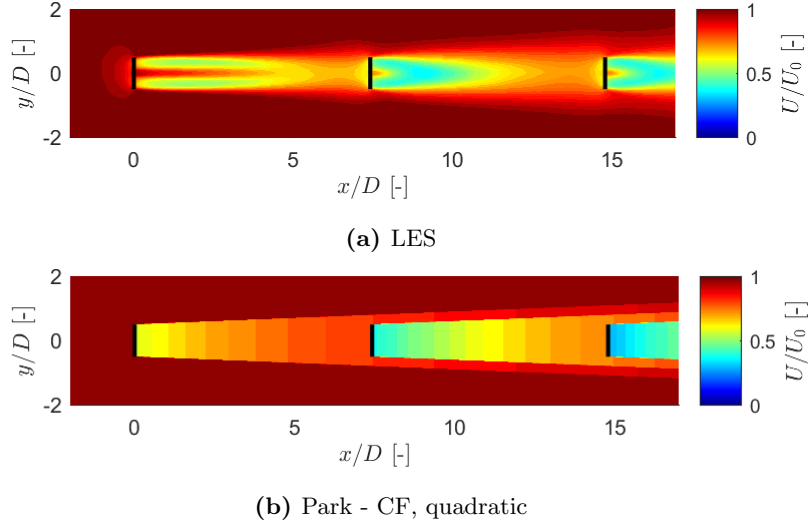


Figure 7.20: Horizontal wind field at hub height of the LES simulation and Park model for Case B3, with the Park model ran with the quadratic superposition method and correction factor (CF).

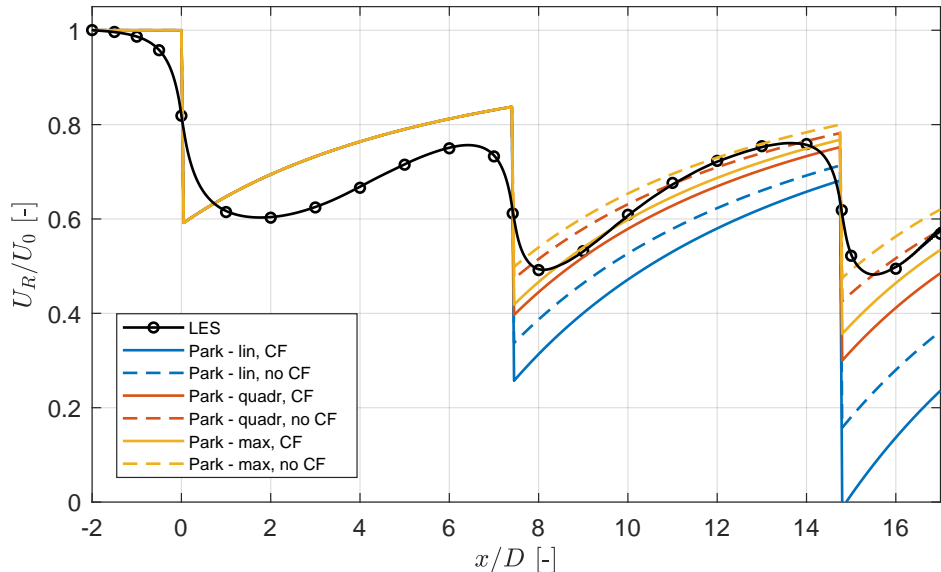


Figure 7.21: Rotor averaged wind speed for Case B3 (3 wind turbines).

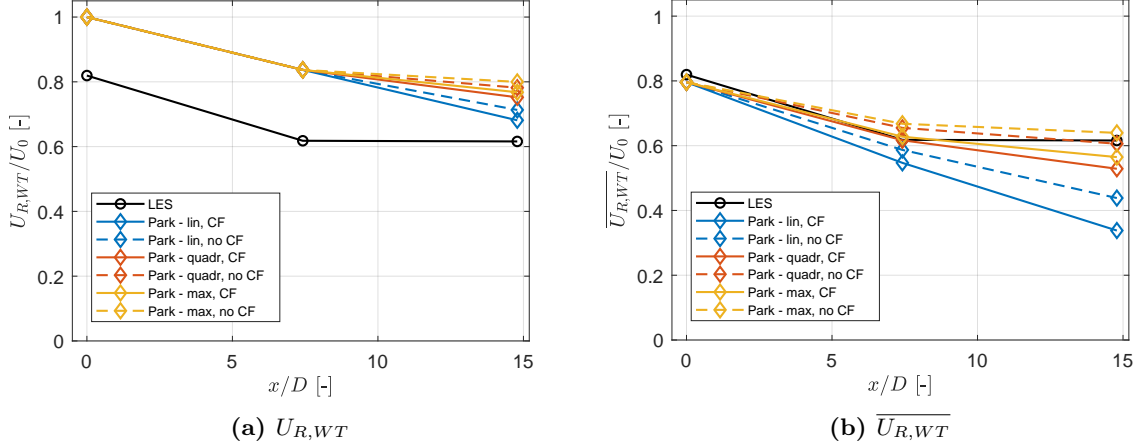


Figure 7.22: (a) Rotor averaged wind speed at the wind turbine locations $U_{R,WT}$ and (b) averaged rotor averaged wind speed $\overline{U}_{R,WT}$ for Case B3.

7.3 Quantification

In this section, the focus is on Case A5 and A6 as the domain is long and six and thirteen wind turbines are available respectively. The quantification measures used, explained in Section 2.2.4, are the wind wake field (Q_a), the rotor averaged wind speed (Q_b), the rotor averaged wind speed at the wind turbine locations (Q_c), the power (Q_d) and the wake recovery (Q_e). The measures are based on the RMSE. Three different weights sets are looked at. These weights sets are arbitrary and depend on the purpose of the study.

The first set of weights gives an equal weight (of 0.2) to all measures. The second set focusses on the rotor averaged wind speed and gives a weight of 0.3 to Q_b and 0.7 to Q_c . The last set gives the full weight of 1 to the measure of the power Q_d . The weights are shown in Figure 7.23. The domain of the wake field and rotor averaged wind speed are limited to take only into account the results from the second wind turbine on. If negative wind speeds² occur in the results of a superposition method, these wind speeds are put to zero to make sure they are taken into account.

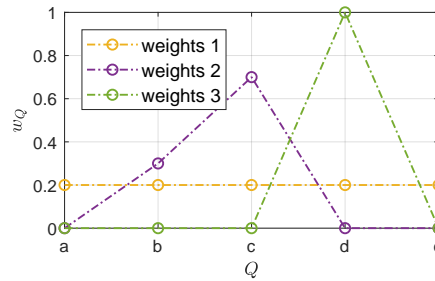


Figure 7.23: The different weight sets used in the quantification of the Park model.

Figure 7.24 shows the results for Case A5 and Case A6. As $(1 - \text{RMSE}_Q)$ is plotted, the superposition methods with the highest values perform better. Afterwards, these measures are combined with the different weights sets to compute the total score, making use of Eq. (2.10).

²Appearing in the numerical superposition results as “Not a number”

It is clear that the linear superposition method has the lowest scores for all weights sets for Case A5. The score of the other superposition methods, however, depends on the weights set used, but in general, the quadratic and maximum deficit method without correction factor perform well, which is also concluded in the previous paragraph.

For Case A6, the first three superposition methods perform poorly compared to the others. This is mainly because the wind speeds become negative, as also can be seen in the wake field (Appendix C.1.5). In general, whichever weights set is used, the maximum deficit without correction factor outperforms the other superposition methods.

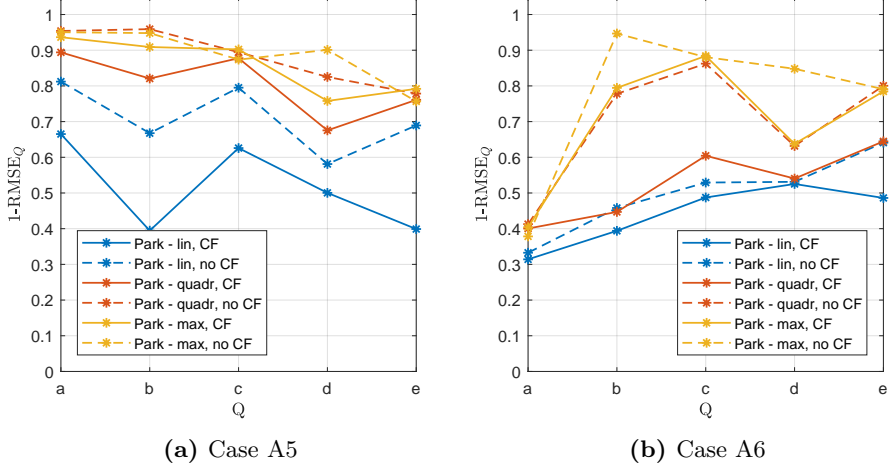


Figure 7.24: The measures Q_i for all superposition methods, shown as $(1 - \text{RMSE}_Q)$.

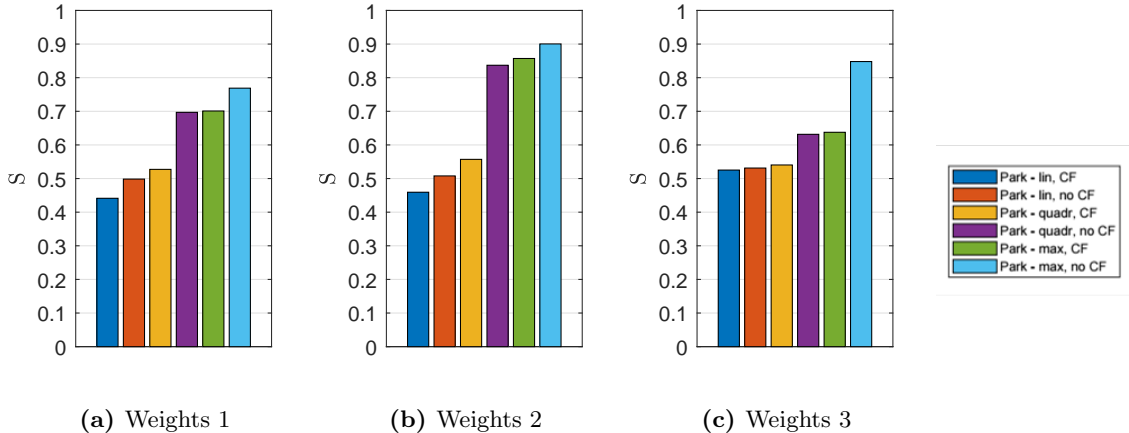


Figure 7.25: The total scores for Case A6 making use of three different weights sets.

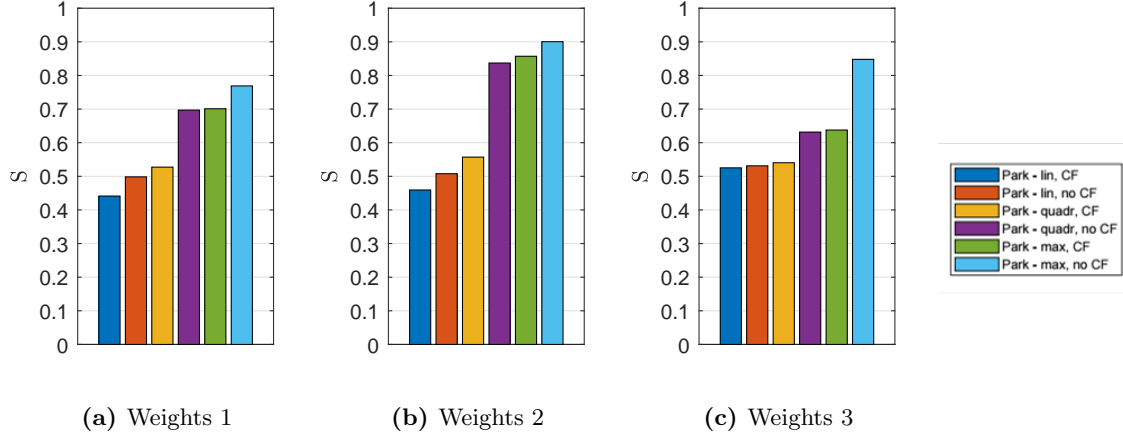


Figure 7.26: The total scores for Case A6 making use of three different weights sets.

7.4 Summary

To compare LES results with the Park engineering model, the wake decay coefficient k is calibrated based on a single wake. The coefficient is dependent on the inflow conditions, i.e the inflow wind speed which is reflected in the C_T -value. The focus of the study is on the rotor averaged wind speed due to the streaks/lobes in the horizontal wind speed field/profile, originating from the tip vortices.

Based on the cases studied in this chapter, the best superposition method in combination with the Park model is the maximum deficit method without correction factor for small wind turbine spacings. When the wind turbine spacing is larger, the result is less clear as both the quadratic and maximum deficit method without correction factor give good results. This is also expressed in the scores obtained with the quantification system.

As no induction zone is included in the Park model, the mean of the wind speed just upstream and downstream of the rotor, $\overline{U_{R,WT}}$, gives the best estimate to compare with the rotor averaged wind speed at the wind turbine locations of the LES results. Although this might give a good estimate of the rotor averaged wind speed, the match with the power is not always as good, for example for small wind turbine spacings. The wake width of a wake behind a row of wind turbines, aligned with the wind direction, is approximated well for small wind turbine spacings but is generally underestimated by the Park models.

Recommendations for further research are given in Chapter 10.

Chapter 8

Superposition of single LES wakes

“Would it be possible to have a database, consisting of LES simulations of single wakes with different inflow conditions, and superpose these single wakes to match LES results with multiple wind turbines?” That is the main question of this chapter. The validation is based on the wake deficit and the wake width. The different superposition methods used in this study are linear superposition (‘lin’), quadratic superposition (‘quadr’) and maximum deficit (‘max’).

8.1 Single wakes

The single wakes available are the ones described earlier in Chapter 6, i.e. Case A1, B1, B2 and C1, and shown in Figure 8.1. The single wakes have a mean inflow wind speed U_0 of 14 m.s⁻¹, 11.2 m.s⁻¹, 11.2 m.s⁻¹ and 8.6 m.s⁻¹ respectively. The turbulence intensity of Case B2 is 8.6% and 3.6% for the other cases. The choice of the inflow wind speeds is explained in Section 6.2.2. The C_T -curve of the NM80 wind turbine is constant between approximately 6 m.s⁻¹ and 9 m.s⁻¹ (Figure 5.1). Therefore the single wake with inflow wind speed of 8.6 m.s⁻¹ (Case C1) can be scaled to other inflow wind speeds within the constant C_T range. The normalised velocity (U/U_0) will stay the same but can be scaled with another mean inflow wind speed U_0 .

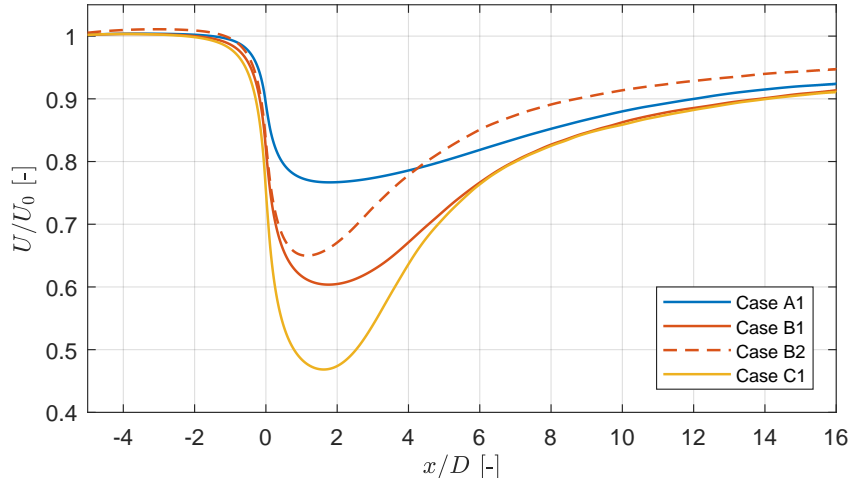


Figure 8.1: Rotor averaged wind speed of single wakes A1, B1, B2 and C1.

8.2 Methodology for LES superposition

To compute the wind field of a wind farm with multiple wind turbines, the single LES wakes are superposed. The result is compared with an LES result with multiple wind turbines, further referred to as the ‘full wake’. In a first step, the single wakes are chosen. The first single LES wake has the same inflow wind speed and turbulence intensity as the full LES wake reference case. The second single LES wake is based on the wind speed and turbulence intensity at the location of the second wind turbine, in the first single wake. The turbulence intensity is increased due to the turbulence induced by the wind turbine. The third single wake is chosen based on the location of the third wind turbine in the second single LES wake and so on. When the inflow wind speed of the single LES wake reaches the region of constant C_T value, the normalised same wake can be used for the other downstream wakes.

8.2.1 Induction zone

Once the single wakes are defined, they are moved to the locations of the wind turbines. The single wake takes also into account the induction zone upstream of the rotor. The length of the induction zone is computed based on the work of Andersen et al. [5]. The distance from the local maximum velocity upstream of every wind turbine defines the beginning of the induction zone. The wake recovery is no longer dominant due to the adverse pressure gradient upstream of the wind turbine. The induction zone length Δx_I is found to be $1D$ and $1.6D$ for a wind turbine spacing of $6D$ and $10D$ respectively (for the DTU EllipSys3D - Actuator Line model), based on the time-averaged streamwise velocity at hub height. The reason that the induction zone is larger for larger spacings is due to the fact that the wake recovery is stronger for larger spacings and therefore is the wake deficit less dominant upstream of the next wind turbine.

A long row of wind turbines is needed to estimate the induction zone length as generally, the average streamwise velocity reaches a converged level from the fourth wind turbine on [5]. Case A5 and A6 include 6 and 13 wind turbines with a spacing of $7.4D$ and $3.3D$ respectively. The results for the induction zone are compared with the results of Andersen et al. [5] and shown in Figure 8.2. The induction zone length is calculated both based on the mean centerline velocity at hub height U_C and the rotor averaged wind speed U_R . The result based on the centerline velocity of Case A6 is in good agreement with the extrapolation of the results of Andersen et al. It has to be noted that the value for $S_x = 7.4D$ is based on only two values as only a simulation with six wind turbines is available (Case A5). If the induction zone length is computed based on the rotor averaged wind speed, the length seems to be shorter, but more research is needed to confirm this.

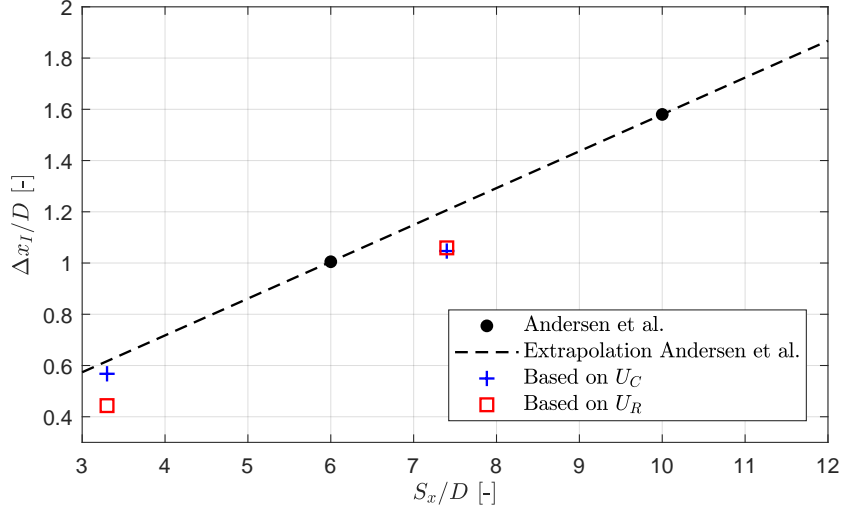


Figure 8.2: Induction zone length Δx_I for different wind turbine spacings. The results of the study of Andersen et al. [5] are shown together with the induction zone length based on the streamwise velocity at hub height U_C and the rotor averaged wind speed U_R of Case A5 and A6.

8.2.2 LES Superposition

Figure 8.3 shows an example of some single wakes moved to the locations of the wind turbines for a spacing of $7.4D$. The figures on the left side show the wind fields and the figures on the right side show the normalised wind fields at hub height. The start of the induction zone is indicated with a dashed line. The domain of the single LES wake is not long enough to cover the whole domain of the full LES wake. The single wakes are not extrapolated, but the wake deficit is put to zero when the domain ends and is therefore underestimated.

Three different superposition methods are used: linear, quadratic and maximum deficit superposition. The methods are the same as explained in Chapter 3, i.e. the normalised wake deficits are superposed.

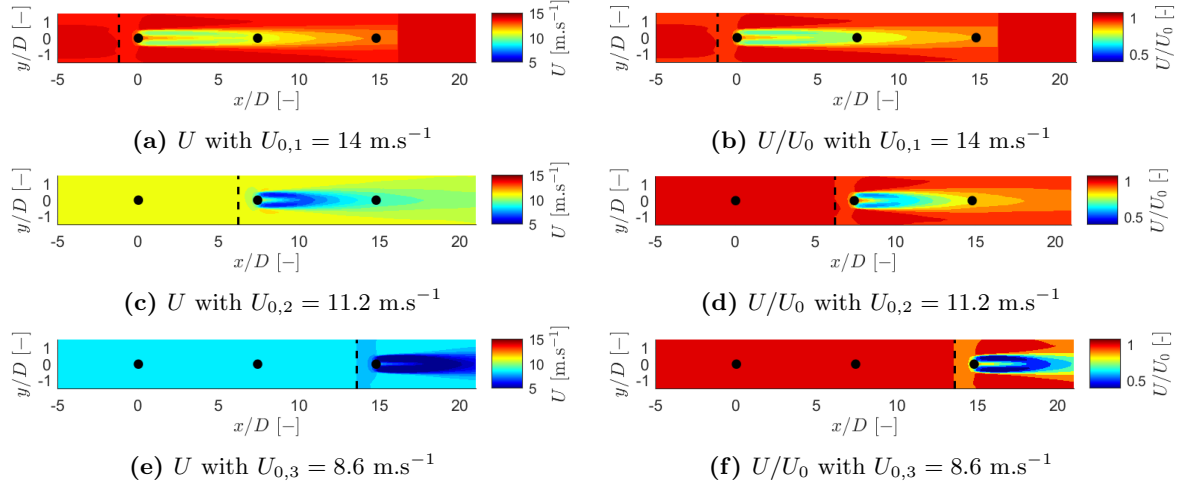


Figure 8.3: Illustration of the single wakes at the location of the different wind turbines. The mean wind speed field and normalised mean wind speed field are shown on the left and right side respectively, for an inflow wind speed of (a)(b) $U_0 = 14 \text{ m.s}^{-1}$, (c)(d) $U_0 = 11.2 \text{ m.s}^{-1}$ and (e)(f) $U_0 = 8.6 \text{ m.s}^{-1}$. The wind turbines and the start of the induction zone are indicated with a black dot and dashed line.

8.3 Results

The focus of the LES superposition is on the cases with long rows of wind turbines, both with a large and small spacing. The first results looked at are the ones for Case A5 with six wind turbines, a spacing of $7.4D$ and an inflow wind speed of 14 m.s^{-1} . The second case is Case A6 with 13 wind turbines, a spacing of $3.3D$ and the same inflow wind speed.

8.3.1 Case A5: 6 wind turbines

The wakes chosen for this case are the following:

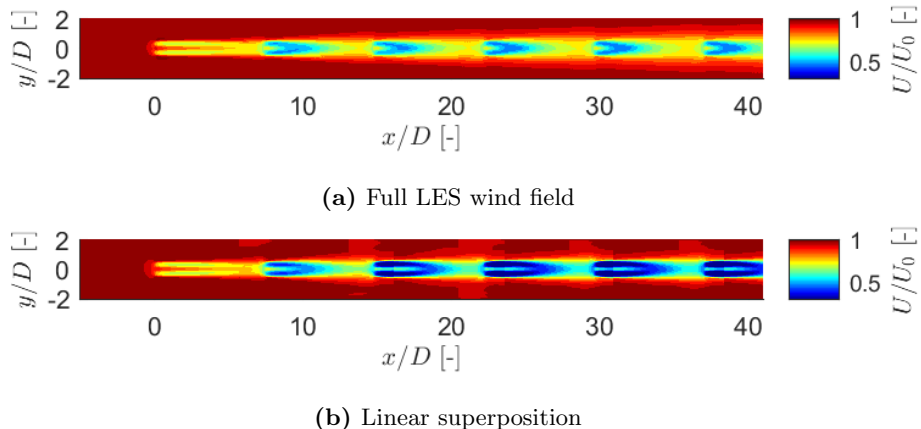
- Wake 1: $U_0 = 14 \text{ m.s}^{-1}$ and $\text{TI}=3.6\%$ (Case A1, normalised with $U_0 = 14 \text{ m.s}^{-1}$)
- Wake 2: $U_0 = 11.2 \text{ m.s}^{-1}$ and $\text{TI}=8.6\%$ (Case B2, normalised with $U_0 = 11.2 \text{ m.s}^{-1}$)
- Wake 3-6: $U_0 = 8.6 \text{ m.s}^{-1}$ and $\text{TI}=3.6\%$ (Case C1, normalised with $U_0 = 8.6 \text{ m.s}^{-1}$)

For the third to sixth wake, it would be better to use a wake with an increased turbulence intensity. However, this wake is at this moment not available. Therefore is chosen for the single wake of Case C1. Another option is to use a normalised single wake with $U_0 = 11.2 \text{ m.s}^{-1}$ and $\text{TI}=8.6\%$ (Case B2) for the third to sixth wake. Those results are discussed later.

The horizontal wind speed fields at hub height are shown in Figure 8.4. It is clear that the linear superposition method overpredicts the velocity deficit, i.e. the wind speed is lower compared to the full LES wake. To make clear where in the domain the differences between the full wake (U_{full}) and the superposed wake fields (U_{SP}) are the biggest, the difference between the fields is calculated:

$$\Delta \left(\frac{U}{U_0} \right) = \frac{U_{full}}{U_0} - \frac{U_{SP}}{U_0} \quad (8.1)$$

These results are shown in Figure 8.5. Again, it is clear that the field calculated with the linear superposition method underpredicts the wind speed field the most. The solutions for the quadratic and maximum deficit method seem to be similar and give a small overprediction of the wind speed for the second wake, but larger differences from the third wake on.



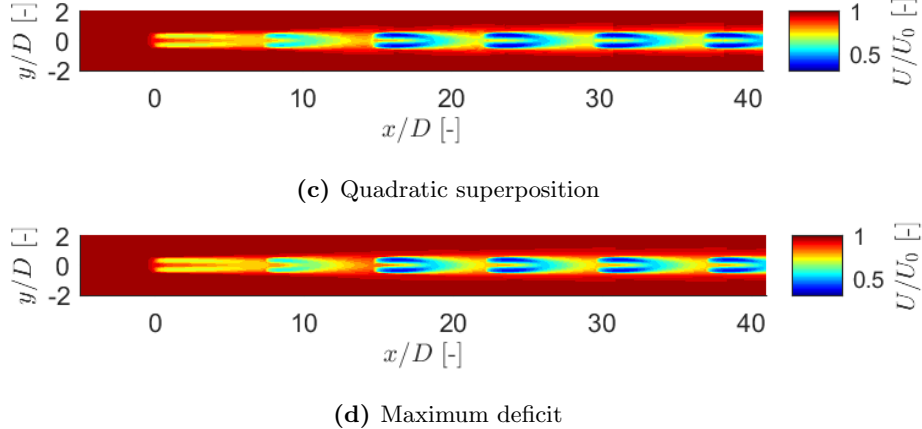


Figure 8.4: Horizontal wind speed fields at hub height of (a) the full LES wake, followed by the superposed LES wakes, making use of (b) linear, (c) quadratic and (d) maximum deficit superposition. The LES superposition is carried out making use of the single LES wakes of Case A1, B2 and C1.

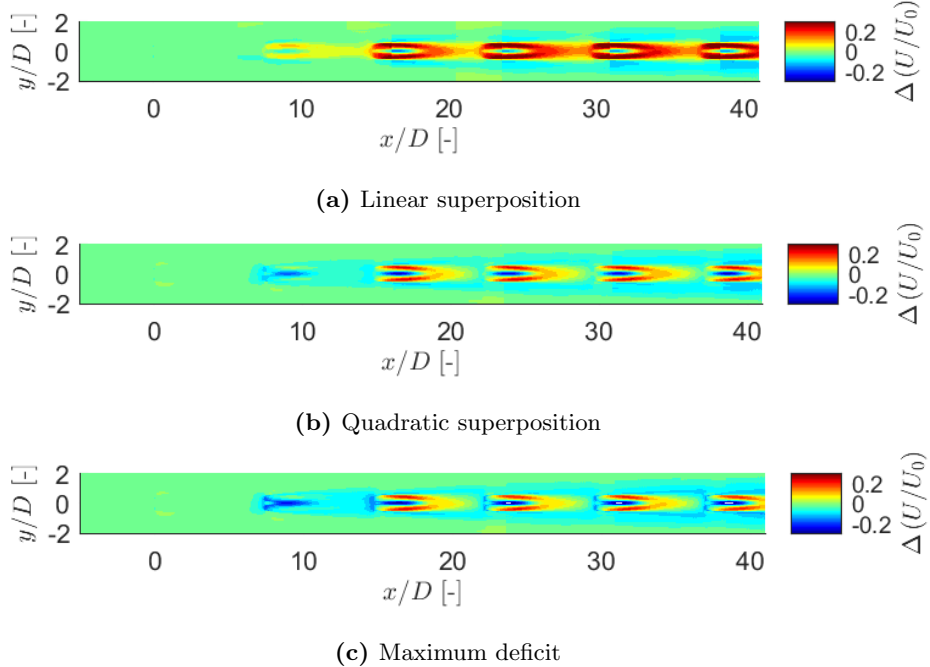


Figure 8.5: Difference in the horizontal wind speed fields at hub height of the full LES wake results and the superposed LES wakes, making use of (a) linear, (b) quadratic and (c) maximum deficit superposition. The LES superposition is carried out making use of the single LES wakes of Case A1, B2 and C1.

The horizontal profiles are given in Figure 8.6. The first row gives the horizontal profiles at $3D$, $4D$, $5D$ and $6D$ downstream of the first wind turbine. The second row gives the horizontal profiles downstream of the second wind turbine etc. It shows that for the first wake all methods give the same result as the full LES wake. For the second wake, the results are in agreement with the full LES wake, but from the third wake on, the differences are larger. From the second wind turbine on, the horizontal profile of the full wake looks Gaussian. Close to the wind turbines, the streaks/lobes, observed in the single wakes, are still present in the superposed fields, while it is not observed in the full LES simulations due to the extra imposed turbulence by the wind turbines. The horizontal wind speed profiles downstream of the fourth, fifth and sixth wind

turbine are shown in Appendix D.1.

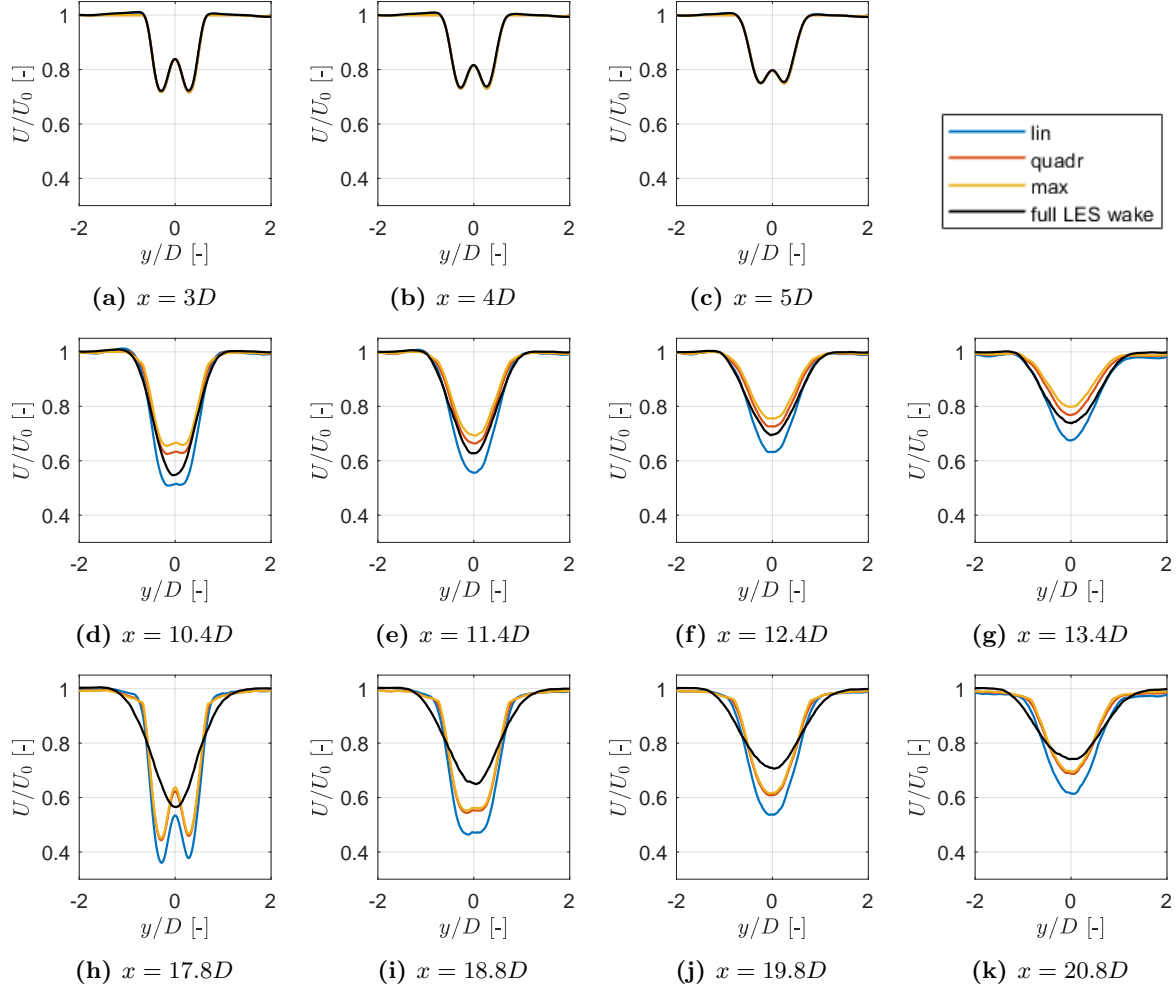


Figure 8.6: Horizontal profiles at hub height of the original LES simulation with six wind turbines (Case A5) and the fields constructed out of single LES wakes. The LES superposition is carried out making use of the single LES wakes of Case A1, B2 and C1.

Figure 8.7 shows the rotor averaged wind speed, computed based on the horizontal profiles and the weighting function, described in Section 2.2.2. The trend of the rotor averaged wind speed in the second wake is similar to the trend of the full LES simulation. This changes from the third wake on. This can possibly be explained by the low turbulence intensity of the third to sixth single wake. The jumps in the rotor averaged wind speeds, most clearly visible in the results of the linear superposition method, are due to not extrapolating the single wake fields. Therefore, the wake deficit is underestimated after the domain of the single wake ends.

The rotor averaged wind speed at the wind turbine locations is shown in Figure 8.8. The rotor averaged wind speed at the second wind turbine is the same for the full LES simulation and the linear superposition method. This shows that the linear superposition method gives a better estimate for the induction zone. For the sixth wind turbine downstream, the linear superposition method gives an underestimation of 25% for the rotor averaged wind speed. The quadratic superposition method gives results closest to the full LES simulation, but the difference in rotor averaged wind speed is still up to 5% at the sixth wind turbine.

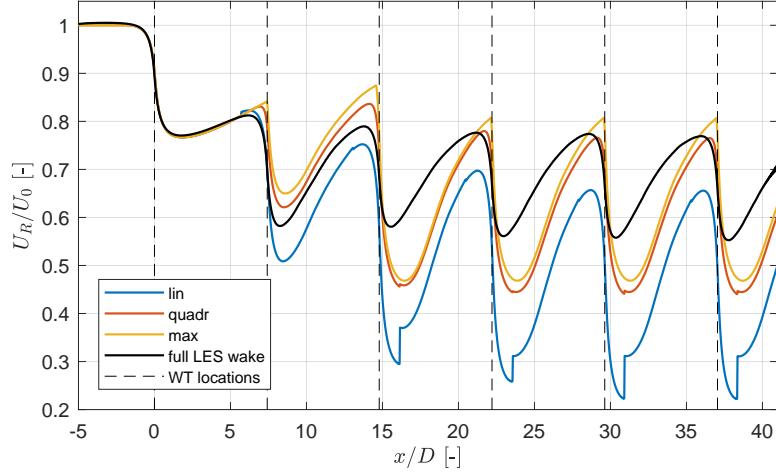


Figure 8.7: Rotor averaged wind speed of the full LES wake (Case A5) and the wakes constructed out of single LES wakes. The LES superposition is carried out making use of the single LES wakes of Case A1, B2 and C1.

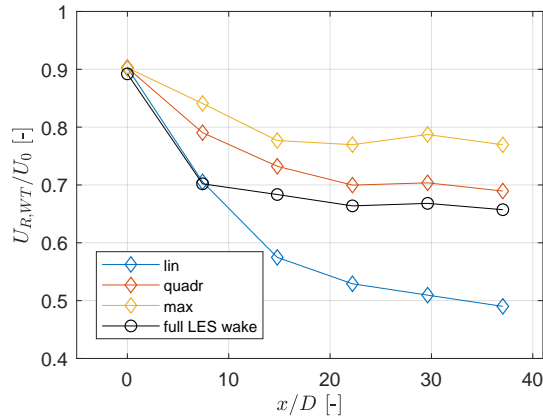


Figure 8.8: Rotor averaged wind speed at the wind turbine locations $U_{R,WT}$ of the full LES wake (Case A5) and the superposed wake fields. The LES superposition is carried out making use of the single LES wakes of Case A1, B2 and C1.

The wake boundary of the full LES wake and the superposed wake field are shown in Figure 8.9. The wake width of the full LES wake field is larger than the ones from the superposed fields, but the wake boundary of all superposed fields are similar. The smaller wake width can be explained by the fact that at the location of the next wind turbine (each $7.4D$), the wake width of the single wake is still limited. So every time a wake is superposed, the small width of the wake is preserved.

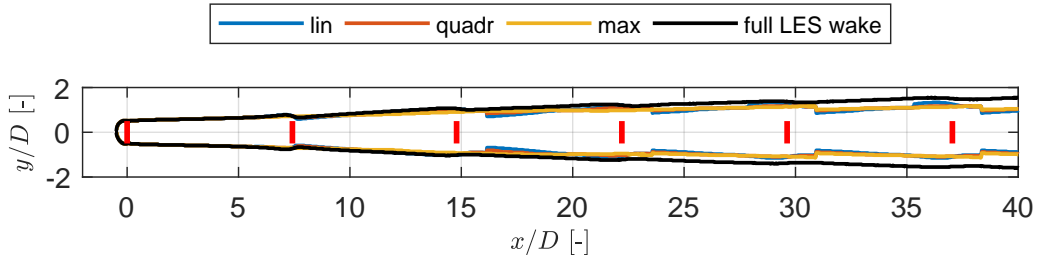


Figure 8.9: Wake boundary of the full LES wake (Case A5) and the superposed wake field, making use of the single LES wakes of Case A1, B2 and C1.

As mentioned before, the inflow conditions of the third to the sixth wake are not optimal. Therefore, the superposition of the following single wake combination is discussed as well.

- Wake 1: $U_0 = 14 \text{ m.s}^{-1}$ and $\text{TI}=3.6\%$ (Case A1, normalised with $U_0 = 14 \text{ m.s}^{-1}$)
- Wake 2-6: $U_0 = 11.2 \text{ m.s}^{-1}$ and $\text{TI}=8.6\%$ (Case B2, normalised with $U_0 = 11.2 \text{ m.s}^{-1}$)

The rotor averaged wind speed is shown in Figure 8.10. Focussing on the third to sixth wake, the trend in the rotor averaged wind speed is better with using a single wake with a higher turbulence intensity compared to the single wake with a low turbulence intensity. Again, due to the too short domain of the single wakes, the velocity should be lower behind the jumps, which has the biggest effect on the linear superposition method. Comparing Figure 8.7 and Figure 8.10 shows that the turbulence intensity has a bigger influence on the wake recovery than the inflow wind speed and therefore also the C_T value. The differences between the horizontal wind speed fields and the wake boundary are shown in Appendix D.1. Again, also with the use of these single wakes, the wake boundary of the superposed fields is smaller than the full LES field.

When the rotor averaged wind speed at the wind turbines of the full LES wake is compared to the results of the LES wake superposition results, the trends are different this time due to using another single wake, as can be seen in Figure 8.11. Now, the linear superposition method shows the best result with an overestimation of the rotor averaged wind speed of 2% for the sixth wind turbine. It has to be noted that the trend for the linear superposition is not the same as the one of the full LES simulation. The biggest difference is at the third wind turbine with an underprediction of 5% for the wind speed.

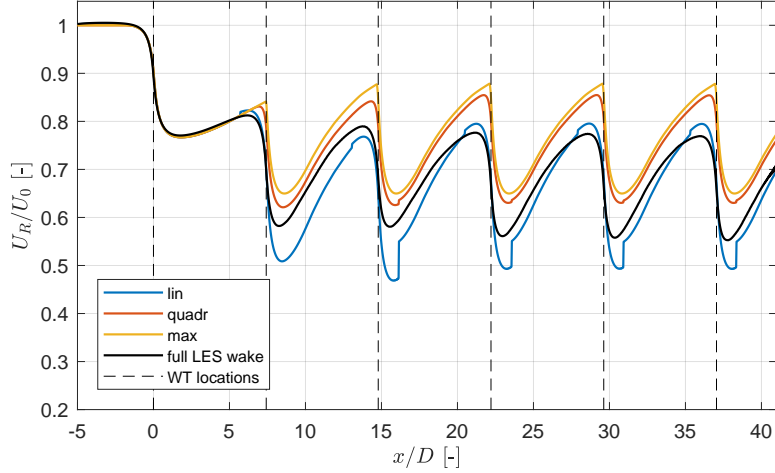


Figure 8.10: Rotor averaged wind speed of the full LES wake (Case A5) and the wakes constructed out of single LES wakes. The LES superposition is carried out making use of the single LES wakes of Case A1 and B2.

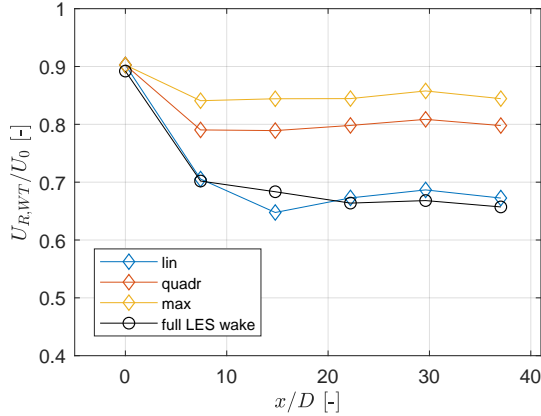


Figure 8.11: Rotor averaged wind speed at the wind turbine locations $U_{R,WT}$ of the full LES wake (Case A5) and the superposed wake fields. The LES superposition is carried out making use of the single LES wakes of Case A1 and B2.

8.3.2 Case A6: 13 wind turbines

In Case A6, 13 wind turbines are present with a spacing of $3.3D$ and an inflow wind speed of 14 m.s^{-1} . The mean horizontal wind speed at hub height and turbulence of the first single wake are shown in Figure 8.12 with an indication of the second wind turbine. The second wind turbine is still in the near wake of the first wind turbine. The streak/lobes in the wind speed due to the tip vortices are still present at the location of the second wind turbine. The wind speed and turbulence intensity at the location of the second wind turbine are 11.6 m.s^{-1} and 6.8% respectively. The C_T -value for this wind speed is 0.63. Comparing this with the C_T -value of 0.65 for a wind speed of 11.2 m.s^{-1} , gives a small difference. Therefore Case B2 (scaled with $U_0 = 11.2 \text{ m.s}^{-1}$) is chosen as the second wake.

A similar procedure is followed to define the wind speed and turbulence intensity at the location of the third wind turbine in the second wake. This wind speed and turbulence intensity are

calculated in the single wake of Case B2 as this single LES wake is used for the second wake, at the location of the third wind speed with respect to the second wind turbine, i.e. $3.3D$. This results in a wind speed of 7.4 m.s^{-1} and turbulence intensity of 18%. The single LES wake of Case B2 with an indication of the third wind turbine with respect to the second wind turbine and the calculation of the wind speed and turbulence intensity is given in Appendix D.2.

As shown in the results for Case A5 (Section 8.3.1), the turbulence intensity is more important for the trend and wake recovery of the single wake than the C_T -value. Therefore Case B2 is chosen as the third to 13th wake, but more ideally a single wake with even a higher turbulence intensity should be chosen.

To summarize, the single LES wakes used in the LES superposition for Case A6 are:

- Wake 1: $U_0 = 14 \text{ m.s}^{-1}$ and $\text{TI}=3.6\%$ (Case A1, normalised with $U_0 = 14 \text{ m.s}^{-1}$)
- Wake 2-13: $U_0 = 11.2 \text{ m.s}^{-1}$ and $\text{TI}=8.6\%$ (Case B2, normalised with $U_0 = 11.2 \text{ m.s}^{-1}$)

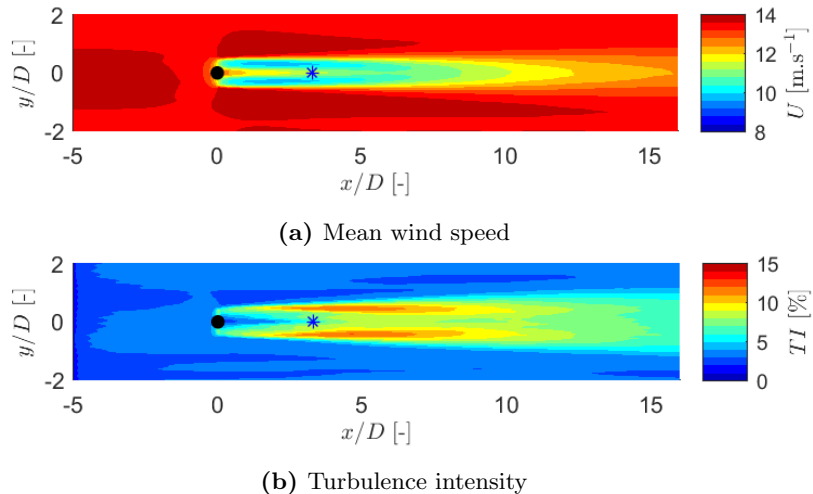


Figure 8.12: Illustration of the calculation of the mean wind speed and turbulence intensity at the location of the second wind turbine with a spacing of $3.3D$ and inflow wind speed of 14 m.s^{-1} (Case A1). The first and second wind turbine are indicated in black and blue respectively.

Figure 8.13 shows the rotor averaged wind speed. It is very clear that none of the superposition methods predicts the trend of the individual wakes well. Also, the rotor averaged wind speed at the wind turbines is not in correspondence with the full LES results, as can be seen in Figure 8.14. The induction zone, based on Figure 8.2 equals $0.6D$, which is approximately 18% of the distance between the wind turbines. This is not especially higher than for larger spacings. Therefore the reason for the non-matching results can maybe be found in the fact that the downstream wind turbines are positioned in the near wake of their first upstream wind turbine. The velocity deficit in the near wake is dominant over the velocity deficit in the induction zone, which can clearly be seen for the quadratic superposition method. In this method, small additional velocity deficits are suppressed due to the square root of the sum. In these results, the velocity only drops at the location of the wind turbine and not upstream of the wind turbines. On top of this, a single wake with a much higher turbulence intensity is needed to conclude if LES superposition can be made possible. The full wind speed fields, differences with the full LES simulation and wake boundary plots can be found in Appendix D.2. The wake boundary of the superposed field is smaller than the one of the full LES field, but this time the wake

boundary is different for every superposition method.

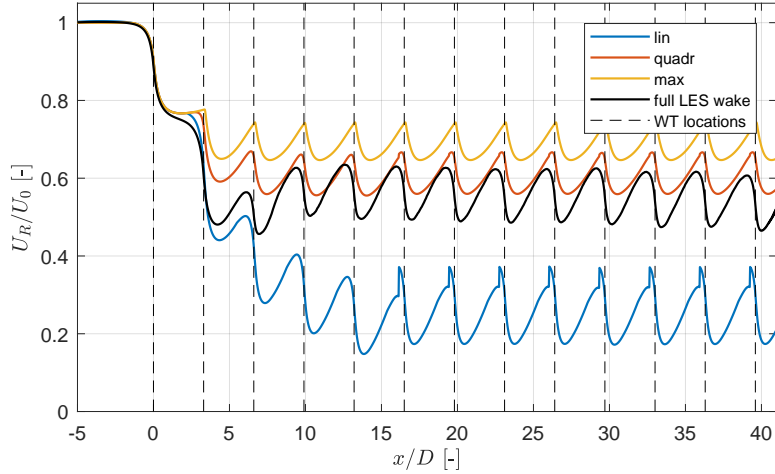


Figure 8.13: Rotor averaged wind speed of the full LES wake (Case A6) and the wakes constructed out of single LES wakes. The LES superposition is carried out making use of the single LES wakes of Case A1 and B2.

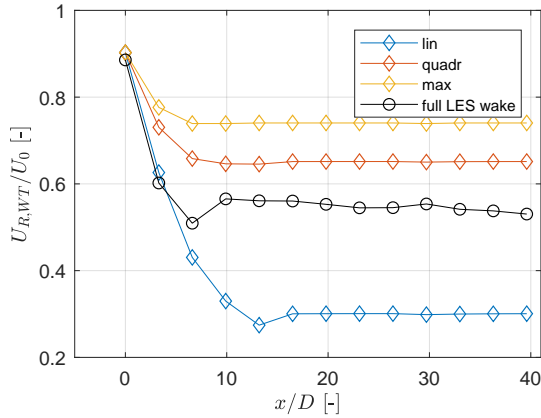


Figure 8.14: Rotor averaged wind speed at the wind turbine locations $U_{R,WT}$ of the full LES wake (Case A6) and the superposed wake fields. The LES superposition is carried out making use of the single LES wakes of Case A1 and B2.

8.4 Summary

Based on the single LES wakes used in the LES superposition, the conclusion can be made that the turbulence intensity of the single wakes is of more importance than the inflow wind speed or C_T -value when superposing single LES wakes to approach a full LES wake. The linear superposition method is for a certain choice of single wakes and a large wind turbine spacing in fairly well agreement with the full wake LES results. These results, however, are not in line with the results for a small wind turbine spacing.

More cases should be analysed to conclude if the superposition of single LES wakes can indeed be used. The recommendations for future research are given in Chapter 10.

Chapter 9

Optimization superposition method

As indicated in the Research Questions (Section 1.4), it is assumed that (one of) the superposition methods used in Chapter 7 and 8 are ‘true’. In Chapter 8, it is not clear if single LES wakes can be superposed and the results are much dependent on the single wakes used. In this chapter, two optimization methods are discussed. Using the methods gives an insight into the correctness of the different superposition methods. Section 9.1 describes the two different optimization methods. Next, the results are discussed in Section 9.2.

9.1 Methodology

Two different methods are developed, with a slightly different point of view. Both methods use the rotor averaged wind speed of an LES as the target and only one single wake is used with the same inflow conditions as the target.

As a first step, a single wake is chosen and the rotor averaged wind speed is computed and translated to a normalized wake deficit. Afterwards, this wake deficit is moved to all the wind turbine locations. If the domain of the single wake is not long enough to cover the full domain including all wind turbines, the wake deficit is linearly extrapolated. Figure E.1 in Appendix E shows an example of the extrapolation of the rotor averaged wind speed of a single wake.

The single wakes are numbered from W_1 to W_N , with N the number of wind turbines, as can be seen in Figure 9.1. Figure 9.1a and Figure 9.1b show the use of single LES and Park wakes respectively, but these can also be single wakes from different models or tools. The target, the rotor averaged wind speed of an LES with multiple wind turbines, is called $M(x)$.

The optimization function is

$$\min \left(\sum_i (M(x_i) - f(W_n, x_i))^2 \right) \quad (9.1)$$

with

$$M(x) = 1 - \frac{U_{R,target}(x)}{U_0} \quad \text{and} \quad W_n(x) = 1 - \frac{U_{R,n}(x)}{U_0} \quad (9.2)$$

The optimization method¹ fits the (non)-linear function $f(W, x)$ to $M(x)$ in a least-squares sense. The function $f(x)$ is dependent on the wake deficits and the streamwise location x and is different for both methods discussed in the next sections. If the optimization coefficients, which result from the optimization method, can be generalized for different wind turbine spacings, they can be used for other wind turbine spacings, without knowing the target.

¹The Matlab function `lsqcurvefit` is used: <https://nl.mathworks.com/help/optim/ug/lsqcurvefit.html>

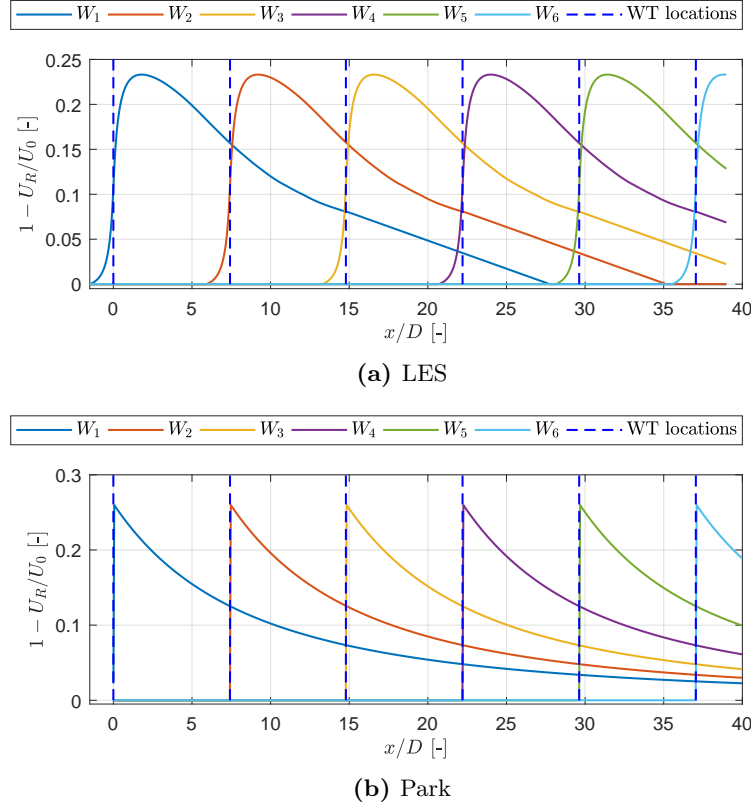


Figure 9.1: Illustration of the single wakes W_n , moved to the wind turbine locations, making use of a single (a) LES and (b) Park wake.

9.1.1 Method A

The first method is based on a full optimization of the rotor averaged wind speed and a specific superposition method is examined. Each wake deficit W_n is multiplied with a coefficient α_n . If the linear superposition method is tested, the function $f(x)$ is

$$f_{A,L}(x) = \alpha_1 W_1(x) + \alpha_2 W_2(x) + \alpha_3 W_3(x) + \dots + \alpha_N W_N(x) \quad (9.3)$$

$$= \sum_{n=1}^N (\alpha_n W_n(x)) \quad (9.4)$$

If, on the other hand, the quadratic superposition method is tested, the function becomes

$$f_{A,Q}(x) = \sqrt{(\alpha_1 W_1(x))^2 + (\alpha_2 W_2(x))^2 + (\alpha_3 W_3(x))^2 + \dots + (\alpha_N W_N(x))^2} \quad (9.5)$$

$$= \sqrt{\sum_{n=1}^N ((\alpha_n W_n(x))^2)} \quad (9.6)$$

Eq. (9.4) or Eq. (9.6) are then combined with Eq. (9.1) to calculate the optimization coefficients α_n . If the proposed superposition methods, i.e. linear and quadratic, are correct, then the coefficients α_n should (approximately) equal one. If a better method exists, based on the rotor averaged wind speed, the coefficients α_n differ from one.

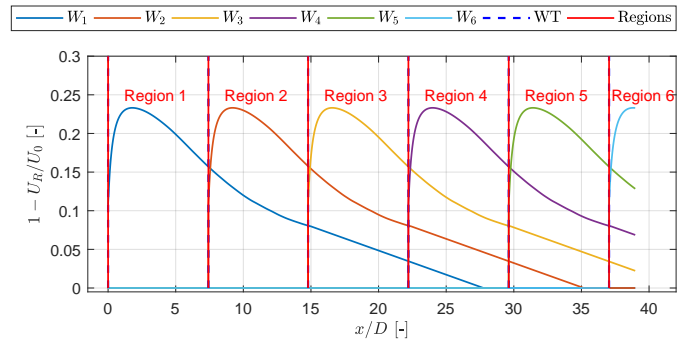
9.1.2 Method B

For the second optimization method, the domain is split up into different regions and for each region, the function $f(x)$ differs. An example of the different regions is given in Figure 9.2. The regions can be defined based on the position of the wind turbines (Figure 9.2a) or the regions can also include a part of the induction zone (Figure 9.2b).

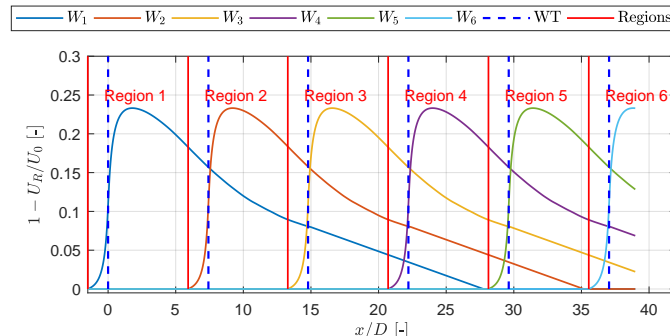
For each region, the wake deficit of the first upstream wake is multiplied with the coefficient β_1 , the second upstream wake with coefficient β_2 , etc. This is expressed by the equation below:

$$f_B(x) = \begin{cases} \beta_1 W_1(x), & \text{if } x \text{ in region 1} \\ \beta_1 W_2(x) + \beta_2 W_1(x), & \text{if } x \text{ in region 2} \\ \beta_1 W_3(x) + \beta_2 W_2(x) + \beta_3 W_1(x), & \text{if } x \text{ in region 3} \\ \beta_1 W_4(x) + \beta_2 W_3(x) + \beta_3 W_2(x) + \beta_4 W_1(x), & \text{if } x \text{ in region 4} \\ \dots, & \dots \\ \sum_{n=1}^N (\beta_i W_{N-i+1}(x)), & \text{if } x \text{ in region N} \end{cases} \quad (9.7)$$

Combining this equation with Eq. (9.1) gives a solution for the coefficients β_n . This optimization method might give an answer on the question whether or not the linear superposition method is ‘the correct’ optimization method, but it gives also an insight in how many upstream wakes should actually be taken into account. If, for example, the coefficients from β_5 to β_N are zero, or close to zero, the contribution of the fifth wake and further upstream wakes is zero or very small and the difference between including or excluding those wakes might be limited.



(a) Region boundaries at the locations of the wind turbines



(b) Region boundaries including the induction zone.

Figure 9.2: Illustration of the regions, used in optimization method B, for single LES wakes.

9.2 Discussion

The different optimization methods are tested on LES results with multiple wind turbines and different wind turbine spacings, i.e. Case A3 to A6 with an inflow wind speed of 14 m.s^{-1} (described in Chapter 6). Making use of these cases, the optimization coefficients α and β can be calculated for method A and B respectively. Below, the results are discussed for using a single LES wake and for a single Park wake. If a single LES wake is used, Case A1 is used as the inflow wind speed equals 14 m.s^{-1} . The single Park wake is modelled for $C_T = 0.45$ and $k = 0.03$, based on the results of Section 7.1.

9.2.1 Method A

The results for optimization method A with a single LES wake and a single Park wake are described below.

Single LES wake

The single wake of Case A1 is used as it has the same inflow wind speed and turbulence intensity as Case A3 to A6. Figure 9.3 gives the solution of optimization method A if a single LES wake is used. The RMSE equals 0.029 and 0.040 for the linear and quadratic method respectively. The solutions overpredict the deficit in the far and underpredict the deficit in the near wake. This means that the fluctuations/peaks of the rotor average wind speed are less strong.

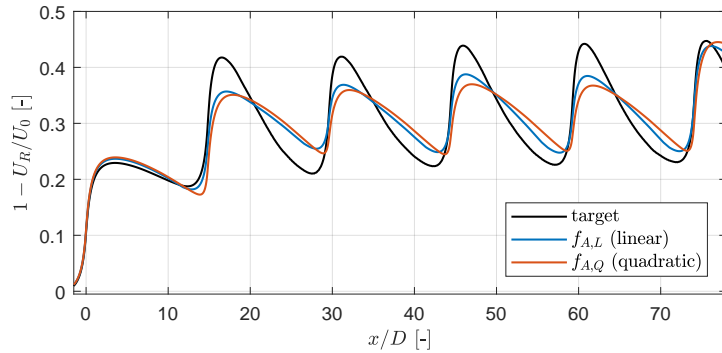


Figure 9.3: Result of optimization method A with a single LES wake for Case A5 as the target.

The α -coefficients for Case A3 to A6 are shown in Figure 9.4, both for the linear ($f_{A,L}$ of Eq. (9.4)) and the quadratic ($f_{A,Q}$ of Eq. (9.6)) superposition method tested. It is clear that the α -coefficients have a trend to converge for long rows of wind turbines, seen for a spacing of $3.3D$. It has to be noted that the last coefficient of every case can be neglected because the wake behind the last turbine is limited due to the end of the domain. The convergence of the coefficients can also be seen for a wind turbine spacing of $7.4D$ and six wind turbines.

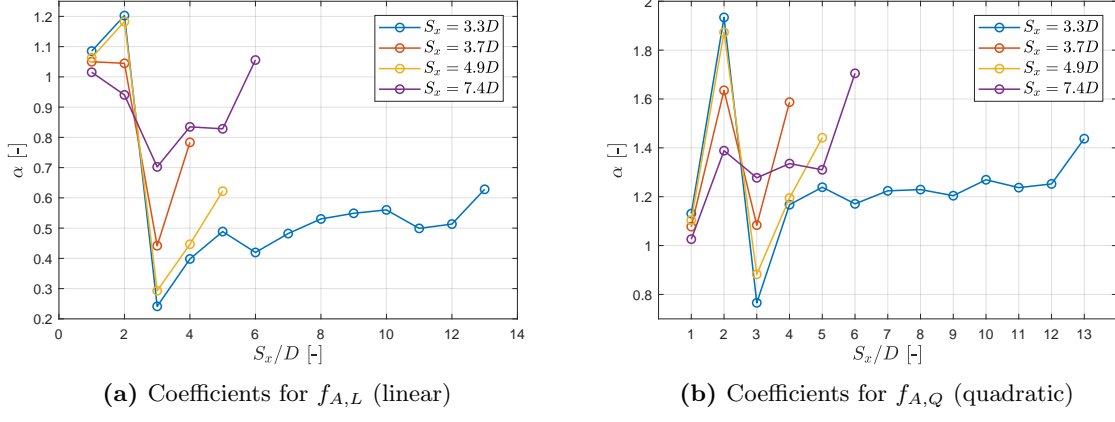


Figure 9.4: α -coefficients for (a) $f_{A,L}$ and (b) $f_{A,Q}$ for different wind turbine spacings if a single LES wake is used.

As the coefficients in both cases do not equal one, it can be concluded that neither linear or quadratic superposition is the ‘correct’ method if one single wake is used. The coefficients for $f_{A,L}$ are smaller than one, which means that the superposition should be less than linear, while the coefficients for $f_{A,Q}$ are bigger than one, meaning that the superposition should be larger than quadratic. The contribution of each wake is shown in Figure 9.5 with a spacing of $6.6D$ and the coefficients for $f_{A,L}$ as an example. It can be seen that in the region behind each wind turbine also that specific wake deficit has the largest contribution: e.g. in between the third and fourth wind turbine, W_3 has the biggest contribution.

Figure 9.6 shows the α -coefficients as a function of the spacing S_x . Both for $f_{A,L}$ and $f_{A,Q}$ is α_1 rather constant, decreases α_2 and increases α_3 for an increasing wind turbine spacing. The trend of the fourth and fifth coefficient is less unambiguous.

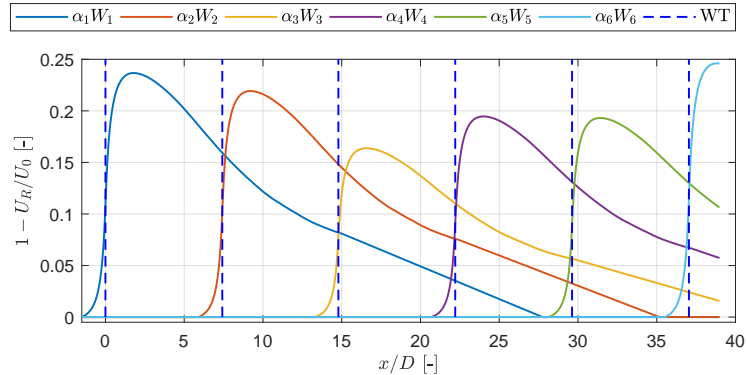


Figure 9.5: Contribution of the single wakes for Case A5 with the α -coefficient for $f_{A,L}$. The blue dashed line indicates the location of the wind turbines.

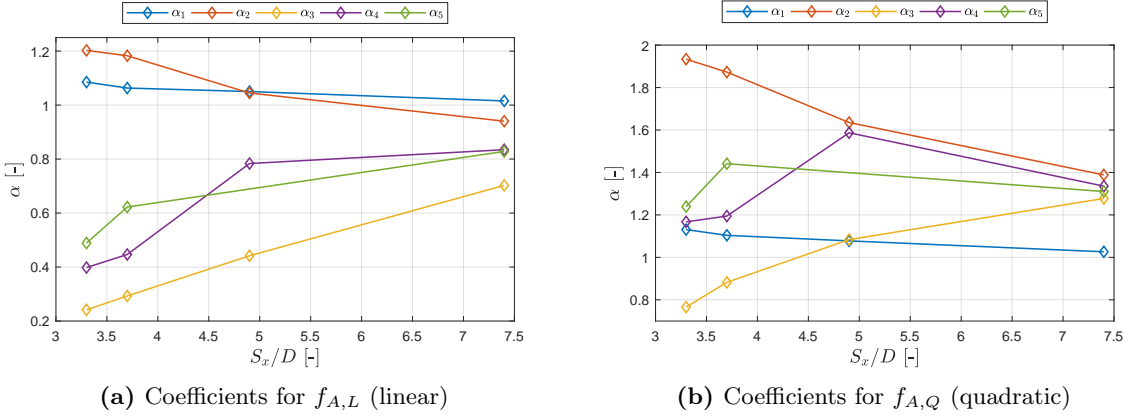


Figure 9.6: The coefficients α_1 to α_5 as a function of the spacing.

Single Park wake

Instead of using a single LES wake, a single Park wake can be used as well. In this case, a single Park wake for an inflow wind speed of 14 m.s^{-1} and $k = 0.03$ is used to comply with the inflow wind speed of the full LES simulations. The results for the rotor averaged wind speed deficit of Case A5 are shown as an example in Figure 9.7. Using a single Park wake expresses the peaks and fluctuation of the rotor averaged wind speed better than when using a single LES wake. The RMSE equals 0.033 for the linear method and 0.031 for the quadratic method. This means that the overall match between the rotor averaged wind speed of Case A5 and the result of the optimization method with a single Park wake is less good than with a single LES wake and the linear method, but better than with a single LES wake and the quadratic method. However, the difference might be due to the region upstream of the first wind turbine as these regions are matched very well with a single LES wake and not with a single Park wake.

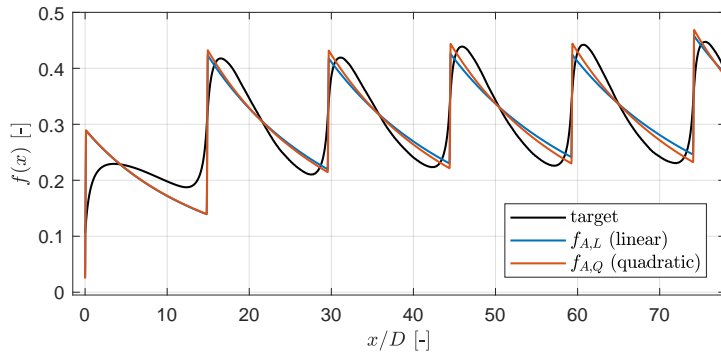


Figure 9.7: Result of optimization method A with a single Park wake for Case A5 as the target.

The α -coefficients for Case A3 to A6 are shown in Figure 9.8 and the same conclusions can be made as for a single LES wake: less than linear superposition or more than quadratic superposition should be applied. Figure 9.9 shows the trend of the α -coefficients as a function of the wind turbine spacing. For all coefficients is a clear trend visible.

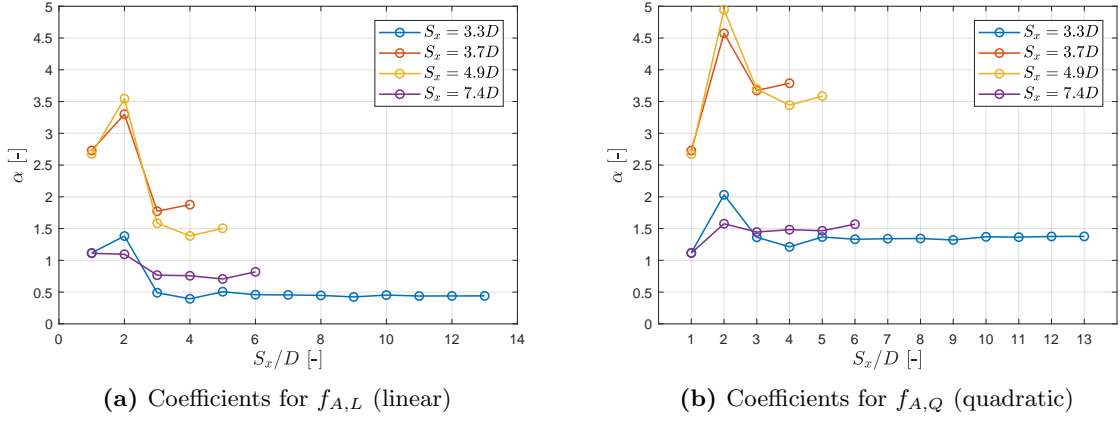


Figure 9.8: α -coefficients for (a) $f_{A,L}$ and (b) $f_{A,Q}$ for different wind turbine spacings if a single Park wake is used.

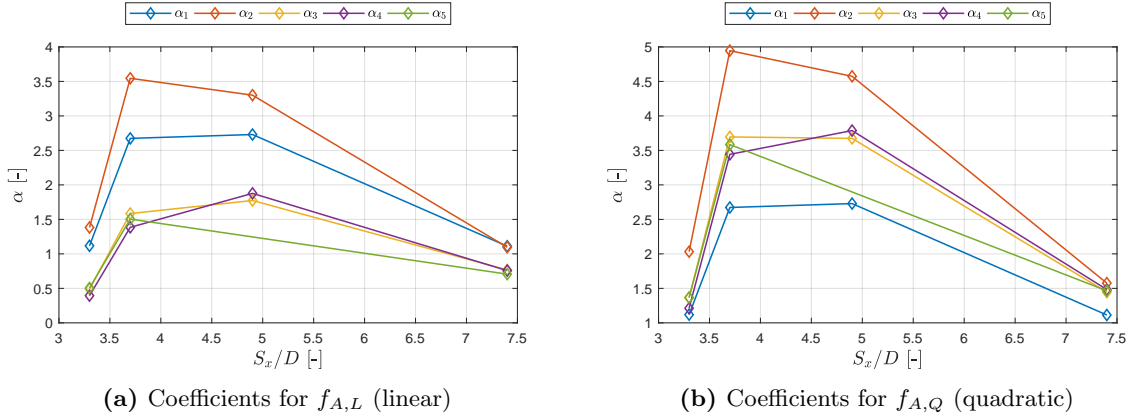


Figure 9.9: The coefficients α_1 to α_5 as a function of the spacing for optimization method A making use of a single Park wake.

Comparison of α -coefficients for single LES and Park wake

The α -coefficients for the use of a single LES wake and a single Park wake are compared. Here is focussed on Case A5 and A6 as the wind turbine spacing is large and small respectively and both cases include six wind turbines or more. It is clear that, regardless of which single wake is used, the trend of both α -sets is generally the same.

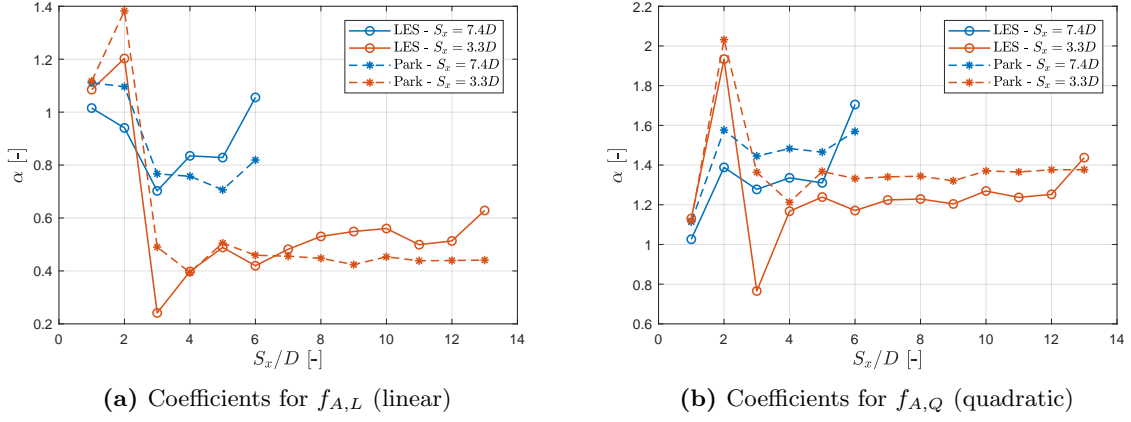


Figure 9.10: Comparison of the α -coefficients for (a) $f_{A,L}$ and (b) $f_{A,Q}$ if a single Park and single LES wake are used (for Case A5 and A6).

Interpolation of α -coefficients

Appendix E.2 discusses the differences in the results if the coefficients for $S_x = 4.9D$ would not be known and be interpolated between the known coefficients.

9.2.2 Method B

In this section, the results for optimization method B are discussed. Also for this method, a single LES or single Park wake can be used. First, the results are discussed for method B, making use of a single LES wake. Afterwards a single Park wake is used.

Single LES wake

As already discussed in Section 9.1.2, the induction zone can be included in the different regions, or the boundaries of the regions can coincide with the locations of the wind turbines. This changes the results for optimization method B, as can be seen in Figure 9.11. The RMSE without and with induction zone equals 0.031 and 0.034 respectively. If the induction zone is taken into account, the solution is discontinuous at the location of the region boundaries, which is not optimal as this is not physical.

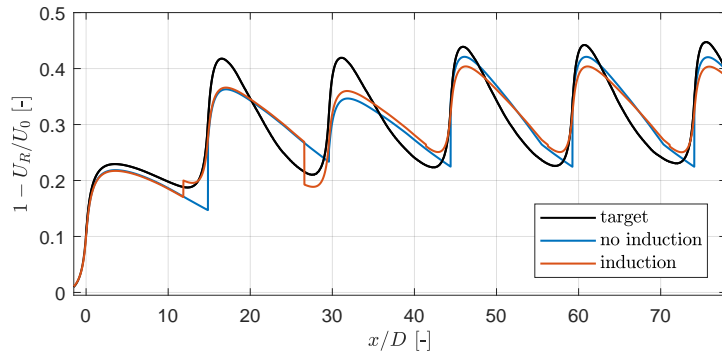


Figure 9.11: Result of optimization method B with a single LES wake for Case A5 as the target.

The solution for the β -coefficients for f_B (Eq. (9.7)) are shown in Figure 9.12 for Case A3 to A6. For both β -coefficient sets, the coefficients converge to zero for long wind turbine rows. The last coefficient before the coefficients become zero is generally large. Even though this coefficient is large, the contribution might be small due to the velocity deficit almost being zero. E.g. when looking at the coefficients for $S_x = 7.4D$, the fourth coefficient is large. If the deficit for a point in e.g. region 5 is calculated, β_4 corresponds with W_2 , which is partly zero in region 5 (Figure 9.2).

Figure 9.13 shows the first five coefficients as a function of the wind turbine spacing. β_1 and β_2 are rather constant. β_4 varies a lot, but this might not influence the results that much because the contribution might be small as discussed above.

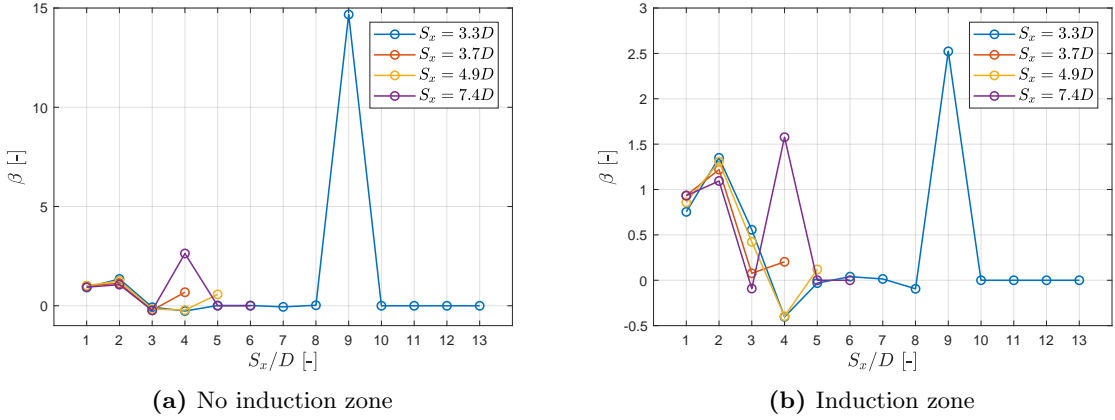


Figure 9.12: β -coefficients for f_B and a single LES wake if the regions (a) do not include an induction zone and (b) include the induction zone.

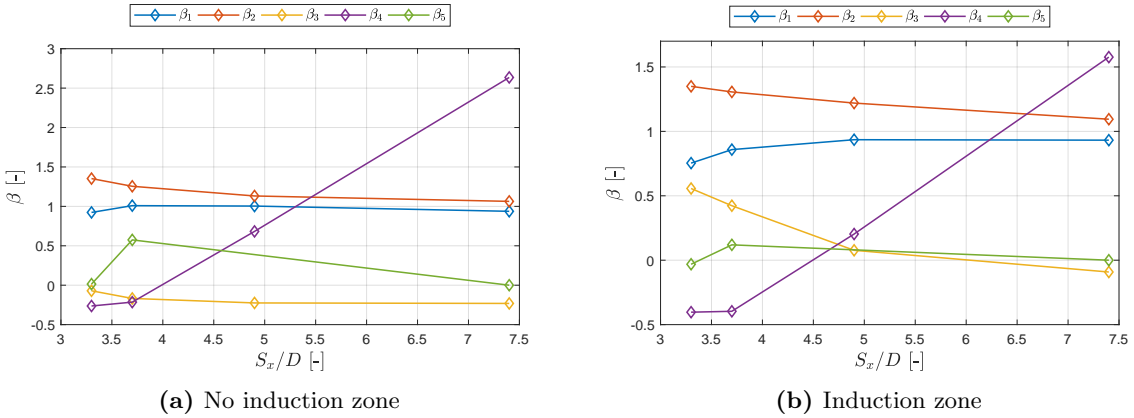


Figure 9.13: β_1 to β_5 as a function of the wind turbine spacing if the regions (a) do not include an induction zone and (b) include the induction zone. Optimization method B is carried out with using a single LES wake.

Single Park wake

If a single Park wake is used, the solution for the rotor averaged wind speed deficit looks like shown in Figure 9.14. Again, the solution is discontinuous when the induction zone is included. The RMSE is 0.032 if the induction zone is not included and 0.031 if the induction zone is

included.

The β -coefficients are shown in Figure 9.15. Now, the last coefficients are not strictly zero as the deficit in the far wake of a single Park wake does not equal zero, but they are close to zero. The β -coefficients as a function of the wind turbine spacing are shown in Figure 9.16. Comparing the results to the previous section, the trend of the β -coefficients is not linear.

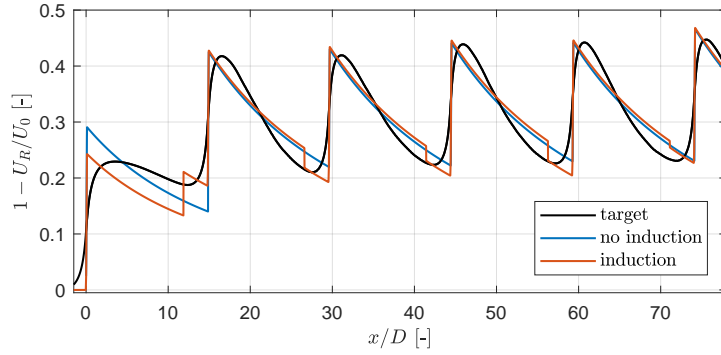


Figure 9.14: Result of optimization method B with a single Park wake for Case A5 as the target.

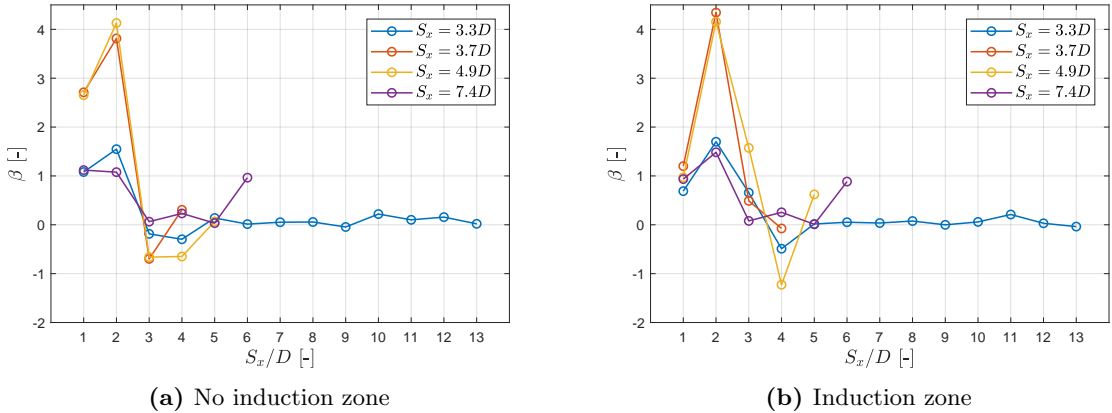


Figure 9.15: β -coefficients for f_B and a single Park wake if the regions (a) do not include an induction zone and (b) include the induction zone.

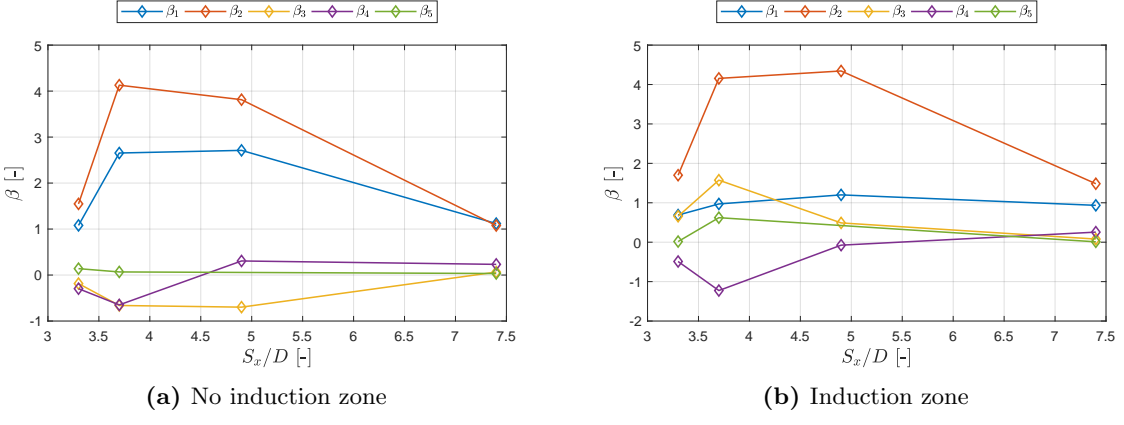


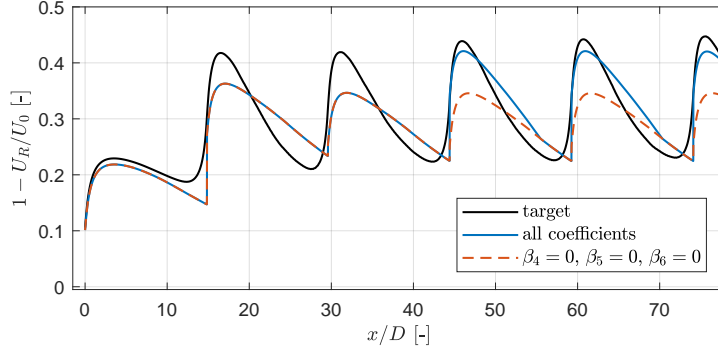
Figure 9.16: β_1 to β_5 as a function of the wind turbine spacing if the regions (a) do not include an induction zone and (b) include the induction zone. Optimization method B is carried out with using a single Park wake.

Putting the last β -coefficients to zero

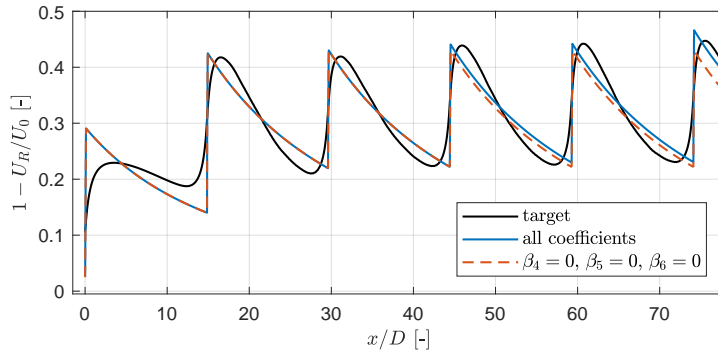
As the coefficients do not equal one, it means that the proposed (linear) superposition method is not correct, but the last coefficients being (nearly) zero means that the wake deficit at a certain downstream distance is only influenced by a limited amount of wakes. The difference in the results can be tested by putting the β -coefficients from β_4 equal to zero. The result is shown in Figure 9.17 for a wind turbine spacing of $7.4D$ and six wind turbines (Case A5). The boundaries of the regions coincide with the wind turbine positions.

The results show that for optimization method B with a single Park wake (Figure 9.17b), the results do not change a lot when the coefficients β_4 to β_6 are zero. The maximum difference is 0.036 and the RMSE increases from 0.032 to 0.033.

The difference is larger, however, when a single LES wake is used as the deficit of the fourth upstream wake is still 0.04 at the start of every region. The maximum difference between the original result and the new one equals 0.09. The RMSE increases from 0.034 to 0.047, which is a rather big increase if looked at the difference between the RMSE of the full solution with LES wake and Park wake. This means that the last non-zero coefficient, β_4 in this case, cannot just be put equal to zero. All RMSE values are summarized in Table 9.1.



(a) Single LES wake



(b) Single Park wake

Figure 9.17: Results for method B for Case A5 if $\beta_4 = \beta_5 = \beta_6 = 0$ for (a) a single LES wake and (b) a single Park wake.

Table 9.1: RMSE of the original solution and the solution with $\beta_4 = \beta_5 = \beta_6 = 0$.

	LES wake	Park wake
Original	0.034	0.032
$\beta_4 = \beta_5 = \beta_6 = 0$	0.047	0.033

9.3 Summary

Two different optimization methods are developed based on the rotor averaged wind speed, which use a particular single wake to approach a full LES wake. The method is tested for a single LES wake and a single Park wake for different wind turbine spacings and a uniform inflow profile. The optimization coefficients show a converging trend for large wind turbine rows and show that neither the linear superposition or quadratic superposition method is the ‘correct’ superposition method. They might need to be scaled to fit the target the best. The second method, which splits the full domain into different regions, shows that only a certain number (five to six, depending on the wind turbine spacing) of upstream wakes is of importance when calculating the wake deficit at a certain point. When a target is not known, the optimization coefficients of the study above could be used to calculate the full wake making use of just one single wake with the same inflow conditions.

As this study is still a preliminary study for a possible alternative superposition method, more research is needed. Some recommendations are given in Chapter 10.

Chapter 10

Conclusions

In the study to define the reference dataset, the LES results are chosen to serve as the reference over the large-scale BEACon measurement data, but more research is needed to define why the differences between the datasets occur. The LES results are more in line with expected trends, based on the known input parameters. The differences might be due to the turbulence intensity, the close proximity of land, atmospheric stability, or the scanning and post-processing method of the BEACon measurement campaign. To simplify the wind profile, a uniform inflow profile without veer and with low turbulence intensity is chosen to test the superposition methods.

To answer the question if the best superposition method in combination with a single wake model changes if the inflow wind speed is around rated wind speed or below rated wind speed, not enough relevant datasets are available. But multiple LES results are available for a uniform inflow wind speed around rated wind speed and for wind turbine rows with different wind turbine spacings. Multiple superposition approaches exist in literature, but only the linear, quadratic and maximum deficit method are used in this study. The superposition methods are tested with the Park model because this model is easy to implement and used in the industry as well. Not a predefined wake model, such as Park 1 [26] or Park 2 [33], is used, but the wake reflection, correction factor and wake decay coefficient can be chosen.

The maximum deficit method (without a correction factor) performs the best for wind turbine rows with small wind turbine spacings. The choice of the best superposition method is less obvious when the wind turbine spacing is larger. Both the quadratic and maximum deficit (without correction factor) method perform well. The results are compared based on the rotor averaged wind speed, horizontal wind field at hub height, the power and the wake recovery.

The wake recovery is based on the change in rotor averaged wind speed in the streamwise direction. The linear superposition method gives an overestimation of the wake recovery, but the quadratic and maximum deficit give a good estimation. The wake expansion of the LES results is higher than the one calculated with the Park model and this is independent of the superposition used. The further apart the wind turbines are spaced, the smaller the underestimation of the Park wake recovery is.

It has to be noted that the conclusions above regarding the best superposition method, wake recovery and wake expansion are based on the Park model, with the wake decay coefficient calibrated for a single wake. Other conclusions might be drawn when the superposition methods are combined with another single wake engineering model.

Apart from comparing LES results with the superposition of a simple engineering wake model, single LES wakes are superposed as well to examine if in this way the flow behind multiple wind turbines can be mimicked. The linear, quadratic and maximum deficit superposition approaches are used and the superposition is based on the horizontal wind field at hub height. No definitive

conclusions can be drawn to say if it is possible or not. When the wind turbines are placed closely together, none of the superposition methods gives a result in agreement with the full LES results. On the other hand, the linear superposition method gives good results for larger wind turbine spacings, but only if a smart choice of single LES wakes is made. It seems that the inflow turbulence intensity of the single LES wakes has a larger influence on the wake field than the inflow wind speed.

As none of the used superposition methods is necessarily ‘true’, two optimization methods are developed to check if the existing superposition approaches need to be adapted or if an alternative approach exists. The methods minimize the difference between the rotor averaged wind speed of a full reference wake and the superposition of a single wake.

The first optimization method tests the linear and quadratic superposition method and based on the results, it seems that both methods need to be scaled/corrected to achieve better results, i.e. the superposition should be done less than linear or more than quadratic. The optimization coefficients, which can be used for this scaling/correction, depend on the wind turbine spacing. The second method shows that if only a certain amount (five to six) of upstream wakes are taken into account, the results do not change a lot, but only if the wake deficit of the ignored wake is small enough in the region of interest.

Regardless of the single wake that is used, in this study a single LES wake and a single Park wake, the optimization coefficients of both methods show the same trends. This shows that these coefficients can possibly be generalized for the use of other single wakes.

Recommendations & Further Research

During the comparison between the large-scale measurement data from the BEACon campaign and the LES results with a similar inflow profile, the reasons why the wind speed field looks different are unclear. Therefore, a more thorough study is needed to define how those data can be compared and which inflow/boundary conditions should be adapted in the simulations.

All the studies, i.e. comparison of the full LES results with the Park superposition methods, the superposition of single LES wakes and the superposition optimization methods, are performed for no shear inflow conditions. Therefore, all the results need to be tested for a sheared inflow profile as well. The cases with an inflow wind speed below rated wind speed include only three wind turbines, therefore no conclusions could be made regarding the superposition methods. It is useful to perform the same simulations with long rows of wind turbines and different spacings.

Comparison between LES and engineering model

The comparison between the LES data and the Park model with multiple superposition methods is done for wind turbine rows with a uniform inflow and wind turbine rows aligned with the wind direction. If the wind turbine row is not aligned with the wind direction, the wakes might partly overlap and other conclusions might possibly be drawn. As mentioned above, a sheared inflow and/or a wind speed below rated wind speed for long wind turbine rows might change the most optimal optimization method. Other simple engineering models, e.g. the Larsen, Frandsen or Bastankhah and Porté-Agel models, in combination with (other) superposition methods might give good, or even better, results as well.

Superposition of single LES wakes

In the study of the superposition of single LES wakes, it could be seen that the turbulence intensity has a big influence on the trend and results of the superposition. Therefore, it would be advised to perform the LES superposition study again with more different single LES wakes available to be able to conclude if the superposition of single LES wakes can be used.

Superposition optimization method

During the calculations of the superposition method, the focus is on the rotor averaged wind speed. This is an arbitrary choice as the focus can also be on the full wind field or the (rotor averaged) wind speed at the wind turbine locations. Another option is to give different weights throughout the regions, e.g. a higher weight to the rotor position and far wake, but a lower weight to the induction zone and the near wake. An interesting study would be to see if and how the optimization coefficients would change.

The optimization coefficients are compared for a single LES wake and a single Park wake. The study should be extended by taking into account single wakes of other wake models (e.g. a single Fuga wake, a single Larsen wake etc.), different turbulence intensities and/or thrust coefficient. If the inflow wind speed changes, the C_T -value changes as well, which might change the optimization coefficients. Instead of using one single wake, multiple single wakes can be chosen as well.

For the full LES results, all the wind turbines are aligned with the wind direction and no partial wake overlap occurs. The optimization coefficients for different spacings could possibly be combined by taking the relevant coefficients for each wake. Possibly, the coefficients can be scaled according to the overlapping area, but both these options need to be examined.

References

- [1] 4C Offshore. SWT-6.0-154. <http://www.4coffshore.com/windfarms/turbine-siemens-swt-6.0-154-tid127.html>, 2017. [Online; accessed 09-12-2017].
- [2] 4C Offshore. Westermost Rough Offshore Wind Farm. <http://www.4coffshore.com/windfarms/westermost-rough-united-kingdom-uk34.html>, 2017. [Online; accessed 09-12-2017].
- [3] H. Aagaard Madsen, C. Bak, U. Schmidt Paulsen, M. Gaunaa, P. Fuglsang, J. Romblad, N. Olesen, P. Enevoldsen, J. Laursen, and L. Jensen. *The DAN-AERO MW Experiments*. Danmarks Tekniske Universitet, Risø Nationallaboratoriet for Bæredygtig Energi, 2010.
- [4] J. F. Ainslie. Calculating the flowfield in the wake of wind turbines. *Journal of Wind Engineering and Industrial Aerodynamics*, 27(1):213–224, 1987.
- [5] S. J. Andersen, B. Witha, S.-P. Breton, J. N. Sørensen, R. F. Mikkelsen, and S. Ivanell. Quantifying variability of large eddy simulations of very large wind farms. *Journal of Physics: Conference Series (online)*, 625(1):012027, 2015.
- [6] C. Bak, F. Zahle, R. Bitsche, T. Kim, A. Yde, L. C. Henriksen, A. Natarajan, and M. H. Hansen. *Description of the DTU 10MW reference wind turbine*. DTU Wind Energy, 2013.
- [7] M. Bastankhah and F. Porté-Agel. A new analytical model for wind-turbine wakes. *Renewable Energy*, 70:116–123, 2014.
- [8] S. Frandsen. On the wind speed reduction in the center of large clusters of wind turbines. *Wind Energy. Technology and Implementation. Part 1: Papers of the Parallel Sessions*, pages 375–380, 1992.
- [9] S. Frandsen, R. Barthelmie, S. Pryor, O. Rathmann, S. E. Larsen, J. Højstrup, and M. Thøgersen. Analytical modelling of wind speed deficit in large offshore wind farms. *Scientific Proceedings*, pages 6–11, 2004.
- [10] M. Gaumond, P.-E. Réthoré, A. Bechmann, S. Ott, G. C. Larsen, A. Peña Diaz, and K. S. Hansen. Benchmarking of wind turbine wake models in large offshore windfarms. 2012.
- [11] P. M. O. Gebraad, F. W. Teeuwisse, J. W. van Wingerden, P. A. Fleming, S. D. Ruben, J. R. Marden, and L. Y. Pao. Wind plant power optimization through yaw control using a parametric model for wake effects - a CFD simulation study. *Wind Energy*, 19(1):95–114, 2016.
- [12] T. Göçmen, P. van der Laan, P.-E. Réthoré, A. Peña Diaz, G. C. Larsen, and S. Ott. Wind turbine wake models developed at the Technical University of Denmark: A review. *Renewable and Sustainable Energy Reviews*, 60:752–769, 2016.
- [13] International Electrotechnical Commission. IEC 61400-1 Wind Turbines - Part 1: Design requirements. IEC, 2006.

- [14] N. O. Jensen. A note on wind generator interaction, 1983.
- [15] A. Jimenez, A. Crespo, and E. Migoya. Application of a LES technique to characterize the wake deflection of a wind turbine in yaw. *Wind Energy*, 13(6):559–572, 2010.
- [16] I. Katić, J. Højstrup, and N. O. Jensen. A simple model for cluster efficiency. *Ewec'86. Proceedings. Vol. 1*, pages 407–410, 1987.
- [17] M. C. Kelly. Uncertainty in vertical extrapolation of wind statistics: shear-exponent and WAsP/EWA methods, 2016.
- [18] G. C. Larsen. *A simple wake calculation procedure*, volume 2760. Risø, 1988.
- [19] G. C. Larsen. A simple stationary semi-analytical wake model. 2009.
- [20] G. C. Larsen, H. Aagaard Madsen, T. J. Larsen, and N. Troldborg. *Wake modeling and simulation*. Technical University of Denmark, Risø National Lab. for Sustainable Energy. Wind Energy Div, Technical Univ, 2008.
- [21] G. C. Larsen, H. Madsen Aagaard, F. Bingl, J. Mann, S. Ott, J. N. Sørensen, V. Okulov, N. Troldborg, N. M. Nielsen, K. Thomsen, T. J. Larsen, and R. Mikkelsen. Dynamic wake meandering modeling. 2007.
- [22] T. J. Larsen, G. C. Larsen, H. Aagaard Madsen, and S. M. Petersen. Wake effects above rated wind speed. An overlooked contributor to high loads in wind farms, 2015.
- [23] B. P. Leonard. A stable and accurate convective modelling procedure based on quadratic upstream interpolation. *Computer Methods in Applied Mechanics and Engineering*, 19(1):59–98, 59–98, 1979.
- [24] J. Mann. The spatial structure of neutral atmospheric surface-layer turbulence. *Journal of Fluid Mechanics*, 273(-1):141–68, 141–168, 1994.
- [25] J. A. Michelsen and DTU. *Block structured multigrid solution of 2D and 3D elliptic PDE's*, volume 94-06. 1994.
- [26] N. G. Mortensen, L. Landberg, I. Troen, E. Lundtang Petersen, O. Rathmann, and M. Nielsen. Wind atlas analysis and application program (WAsP), 1999.
- [27] N. G. Nygaard, F. E. Brink, J. S. Gretlund, B. Hirth, J. Schroeder, and J. Guynes. Wake measurements in an offshore wind farm using dual-Doppler radars.
- [28] N. G. Nygaard and A. C. Newcombe. Wake behind an offshore wind farm observed with dual-doppler radars. In *Journal of Physics: Conference Series*, volume 1037, page 072008. IOP Publishing, 2018.
- [29] S. Ott, J. Berg, and M. Nielsen. Linearised CFD models for wakes, 2011.
- [30] A. Peña Diaz. Sensing the wind profile, 2009.
- [31] A. Peña Diaz, P.-E. Réthoré, C. B. Hasager, and K. S. Hansen. Results of wake simulations at the Horns Rev I and Lillgrund wind farms using the modified Park model, 2013.
- [32] S. Pope. *Turbulent Flows*. Cambridge University Press, 2000.

- [33] O. S. Rathmann, B. O. Hansen, J. M. Leon, K. S. Hansen, and N. G. Mortensen. Validation of the revised WAsP park model. 2017.
- [34] D. J. Renkema. Validation of wind turbine wake models - Using wind farm data and wind tunnel measurements. MSc thesis, TU Delft, 2007.
- [35] B. Sanderse, S. P. van der Pijl, and B. Koren. Review of computational fluid dynamics for wind turbine wake aerodynamics. *Wind Energy*, 14(7):799–819, 2011.
- [36] Siemens AG. Wind Turbine SWT-6.0-154, Technical specifications. <https://www.siemens.com/global/en/home/markets/wind/turbines-and-services/swt-6-0-154.html>, 2016. [Online; accessed 09-12-2017].
- [37] Siemens AG. Wind Turbine SWT-6.0-154, Technical specifications. https://www.siemens.com/content/dam/internet/siemens-com/global/market-specific-solutions/wind/data_sheets/data-sheet-wind-turbine-swt-6.0-154.pdf, 2016. [Online; accessed 09-12-2017].
- [38] J. Smagorinsky. General circulation experiments with the primitive equations. *Monthly Weather Review*, 91(3):99–164, 1963.
- [39] J. N. Sørensen, R. F. Mikkelsen, D. S. Henningson, S. Ivanell, S. Sarmast, and S. J. Andersen. Simulation of wind turbine wakes using the actuator line technique. *Philosophical Transactions of the Royal Society A: Mathematical, Physical and Engineering Sciences*, 373(2035):20140071 (16 pp.), 2015.
- [40] J. N. Sørensen and W. Z. Shen. Numerical modelling of wind turbine wakes. *Journal of Fluids Engineering*, 124(2):393–399, 2002.
- [41] N. N. Sørensen. General purpose flow solver applied to flow over hills, 1995.
- [42] L. Ta Phuoc, R. Lardat, M. Coutanceau, and G. Pineau. Recherche et analyse de modèles de turbulence de sous maille adaptés aux écoulements instationnaires décollés. *LIMSI Report 93074*, 1994.
- [43] N. Troldborg. Actuator line modeling of wind turbine wakes. 2009.

Appendix A

Sensitivity study of the Park model

A.1 Influence of wake decay coefficient and spacing

In this case, the sensitivity of the wake decay coefficient k and the distance between the wind turbines is examined. The fictitious wind farm consists out of three equally spaced wind turbines with a spacing S_x . The superposition method used is quadratic superposition, the correction factor is implemented and the first C_T -curve is used (Figure 4.8). The sensitivity study is carried out twice: with and without including wake reflection. The parameters are summarized in Table A.1.

The border for which wake reflection of the upstream wind turbines influences the wind speed deficit at hub height of the third wind turbine can also be defined analytically:

$$-(z + H) + \frac{D}{2} + k \cdot 2S_x = 0 \quad (\text{A.1})$$

The results, shown in Figure A.2a and A.2b, show the wind speed deficit at the hub of the third wind turbine, indicated in blue in Figure A.1. Figure A.3 shows the difference between the two results:

$$\Delta \left(\frac{\Delta U}{U_0} \right) = \frac{\Delta U_{\text{without WR}}}{U_0} - \frac{\Delta U_{\text{with WR}}}{U_0}$$

As expected, the difference is zero below the first analytical border and the wind speed deficit without wake reflection is smaller than the wind speed deficit with wake reflection above the analytical border. The wind speed deficit decreases also for increasing k and increasing S_x .

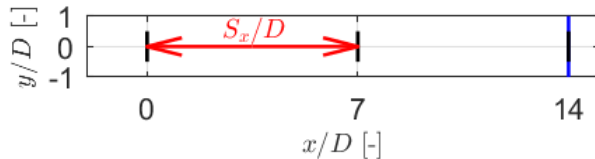


Figure A.1: Wind farm lay-out for the sensitivity study of the wake decay coefficient and wind turbine spacing.

Table A.1: Input parameters for sensitivity study of the wake decay coefficient and wind turbine spacing.

U_0 [m.s $^{-1}$]	k [-]	S_x [m]	Superposition	Correction Factor	Wake reflection	C_T
10	Variable	Variable	Quadratic	True	False/True	curve 1

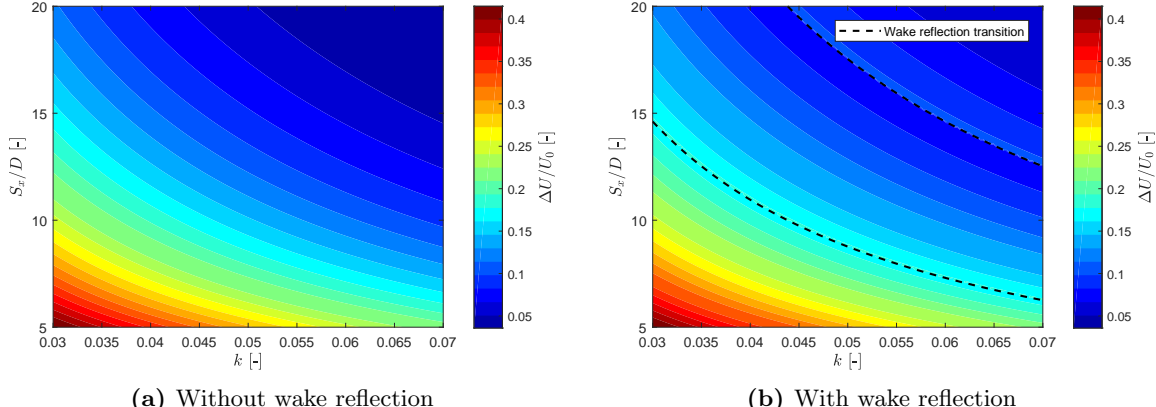


Figure A.2: Wake deficit at third wind turbine for different wind turbine distances S_x and wake coefficients k (a) without wake reflection and (b) with wake reflection.

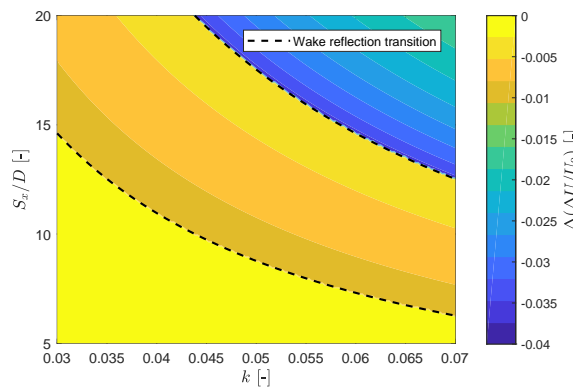


Figure A.3: Difference in wake deficit between including and not including wake reflection.

A.2 Influence of thrust coefficient

The influence of the thrust coefficient is examined in two different ways. In the first case, the wake deficit at a fixed distance behind a single wind turbine with a variable C_T -value is calculated. In the second case, a wind farm lay-out is considered and the wake deficit at these wind turbines is calculated. The C_T -value is not fixed this time, but two different C_T -curves are looked at. Both cases are summarized in Table A.2.

Table A.2: Input parameters for sensitivity study of the thrust coefficient.

U_0 [m.s ⁻¹]	k [-]	S_x [m]	Superposition	Correction Factor	Wake reflection	C_T
- 8,10,12	Variable 0.04	- $7D$	- Quadratic	True True	True True	Variable Variable curves

The wake deficit at a fixed distance ($x = 7D$, indicated in blue in Figure A.4) behind a single wind turbine is calculated making use of the Park model for varying values of C_T and k . The inflow wind speed and superposition method are not important because the deficit behind a

single wind turbine is calculated for a predefined C_T -value (Table A.2, first line). Figure A.5 shows that the higher the value of C_T , the higher the wake deficit is. The conclusion for the variation in wake deficit when k varies is the same as seen before: the higher k , the lower the wake deficit.

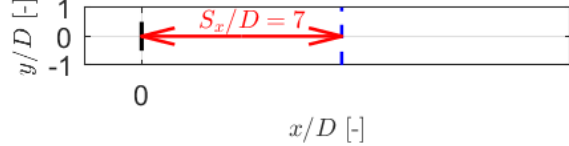


Figure A.4: Wind farm lay-out for the sensitivity study of the wake decay coefficient and wind turbine spacing.

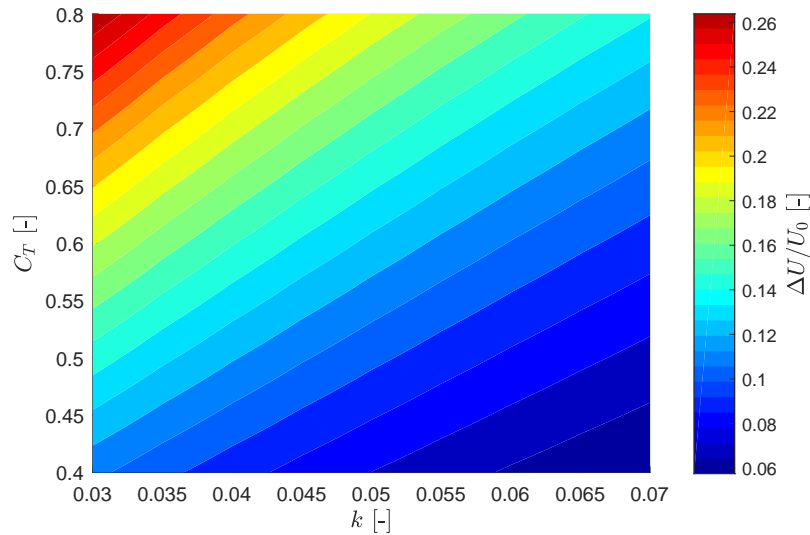


Figure A.5: Wake deficit at $7D$ behind wind turbine for different values of C_T and k .

Next to examining the sensitivity due the C_T -value for a single wind turbine, the sensitivity of the wake deficit for different C_T -curves and multiple wind turbines is examined. The two C_T -curves used are plotted in Figure 4.8. The wind turbine distance is fixed to $7D$ and the wake decay coefficient k is equal to 0.04. Quadratic superposition, wake reflection and the correction factor are used (Table A.2, second line). The results are shown in Figure A.6a, Figure A.6b and Figure A.6c for a wind speed of 8 m.s^{-1} , 10 m.s^{-1} and 12 m.s^{-1} respectively. These inflow conditions are (just) below and above rated wind speed. Even if the difference of C_T value between the two C_T -curves is only 0.04 (for $U_0 = 8 \text{ m.s}^{-1}$), the difference in wind speed deficit at the seventh wind turbine ($x = 42D$) is 0.05, which is a difference of about 12.5%.

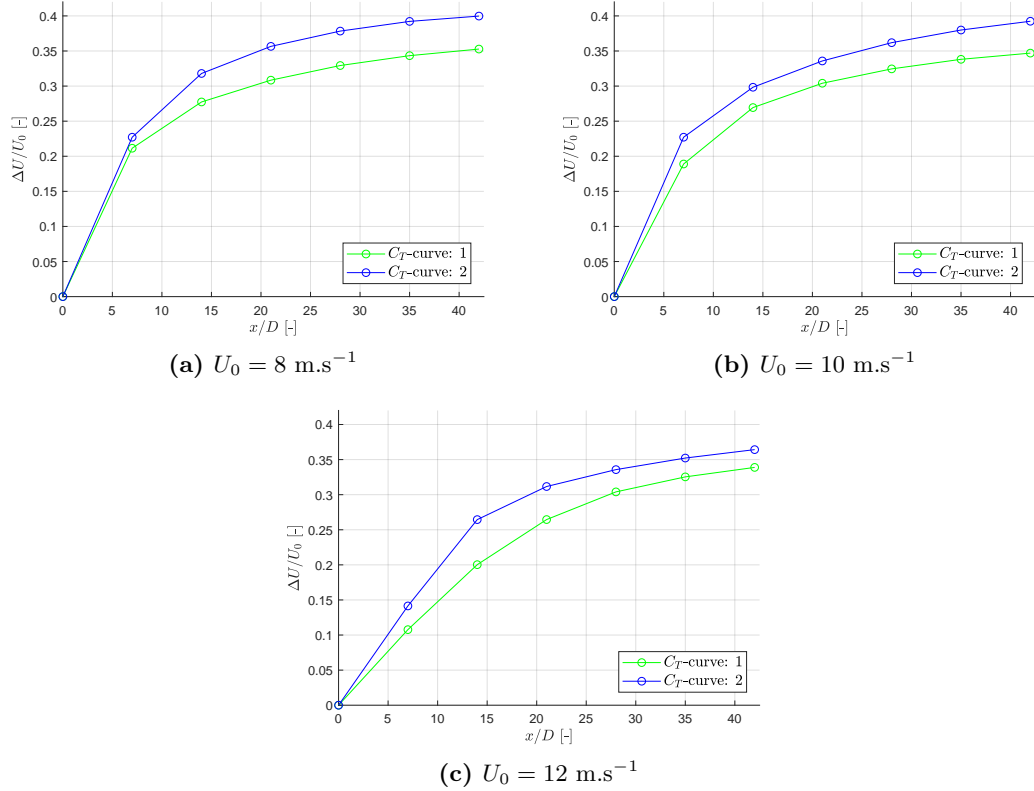


Figure A.6: Wake deficit at the wind turbines for an upstream wind speed of (a) 8 m.s^{-1} , (b) 10 m.s^{-1} and (c) 12 m.s^{-1} .

Appendix B

Calibration of single Park wake

B.1 Case A1: $U_0 = 14 \text{ m.s}^{-1}$

Figure B.1 shows the horizontal plane at hub height of the LES result and the single Park wakes for different wake decay coefficients k , with an inflow velocity of 14 m.s^{-1} and turbulence intensity of 3.6%.

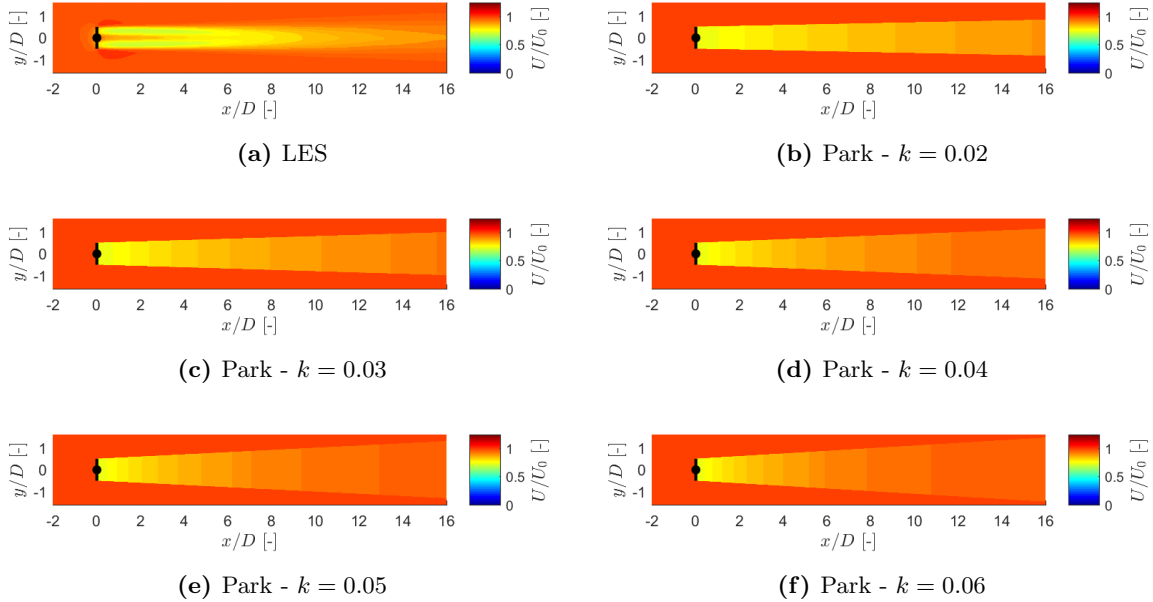


Figure B.1: Horizontal wind speed field at hub height for the LES results of Case A1 and the single Park wakes with different wake decay coefficients.

B.2 Case B1: $U_0 = 11.2 \text{ m.s}^{-1}$

Figure B.2 shows the horizontal plane at hub height of the LES result and the single Park wakes for different wake decay coefficients, with an inflow velocity of 11.2 m.s^{-1} and turbulence intensity of 3.6%.

Figure B.3 shows the wake boundary of the single LES wake and the single Park wakes for different k values. Figure B.4 shows the difference between the single LES wake boundary and the different single Park wake boundaries.

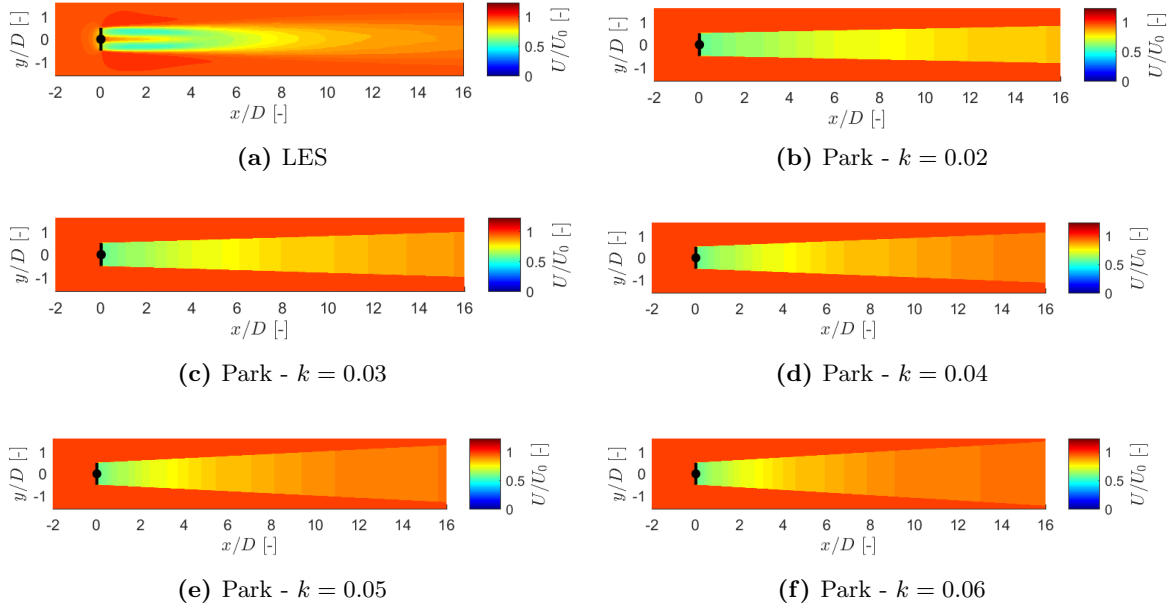


Figure B.2: Single wakes with an inflow wind speed of 11.2 m.s^{-1} (Case B1) of (a) LES simulation and (b-f) single Park model with different wake coefficients k .

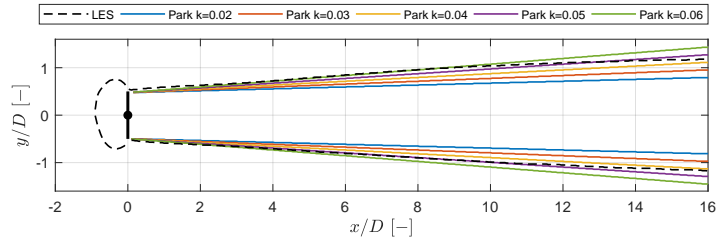


Figure B.3: Wake boundary of the LES simulation and Park model results with different wake coefficients k for Case B1.

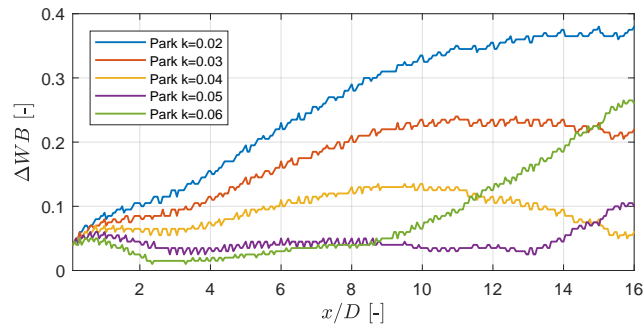


Figure B.4: Difference in wake boundary between the LES results and Park model results with different wake coefficients k for Case B1.

Appendix C

Comparison LES and Park

C.1 Inflow wind speed at rated wind speed

C.1.1 Case A2: 3 wind turbines

Figure C.1 shows the horizontal wind field at hub height of the LES result including three wind turbines ($S_x = 7.4D$) and the Park model with different superposition methods. The inflow wind speed is 14 m.s^{-1} and the turbulence intensity equals 3.6%.

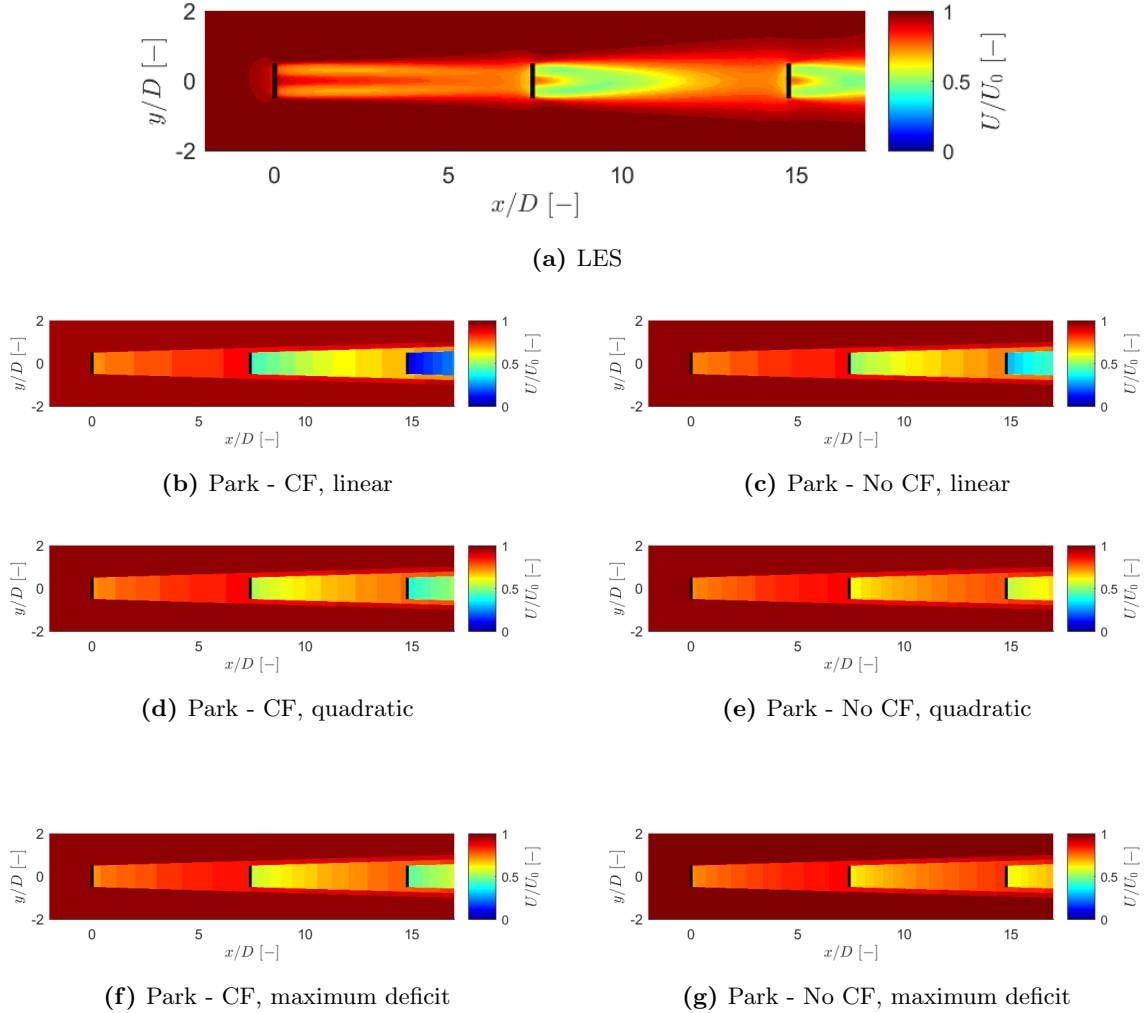


Figure C.1: Horizontal wind speed field at hub height for Case A2 (three wind turbines with a spacing of $7.4D$).

C.1.2 Case A3: 4 wind turbines

Figure C.2 shows the horizontal wind field at hub height of the LES result including four wind turbines ($S_x = 4.9D$) and the Park model with different superposition methods. The inflow wind speed is 14 m.s^{-1} and the turbulence intensity equals 3.6%.

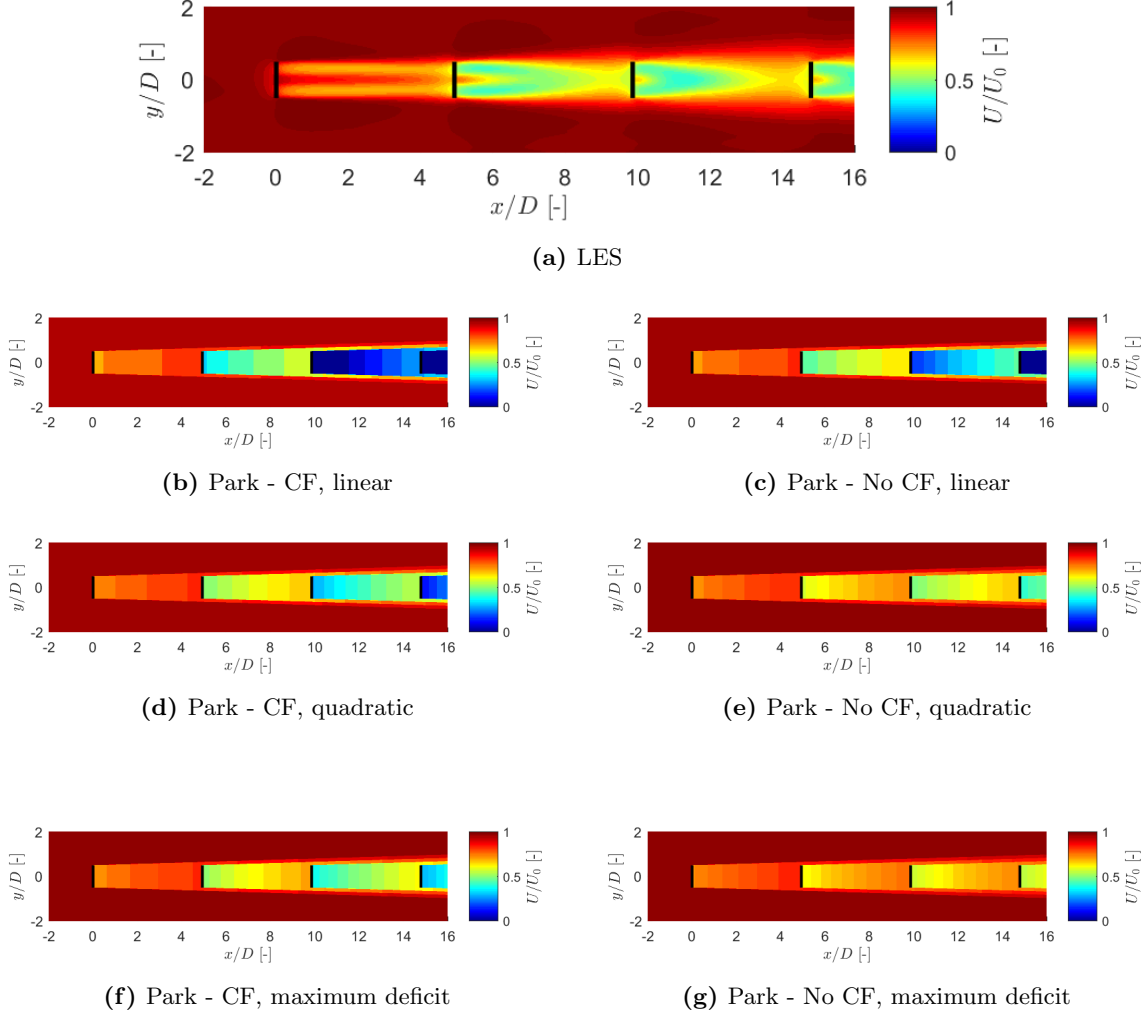


Figure C.2: Horizontal wind speed field at hub height for Case A3 (four wind turbines with a spacing of $4.9D$).

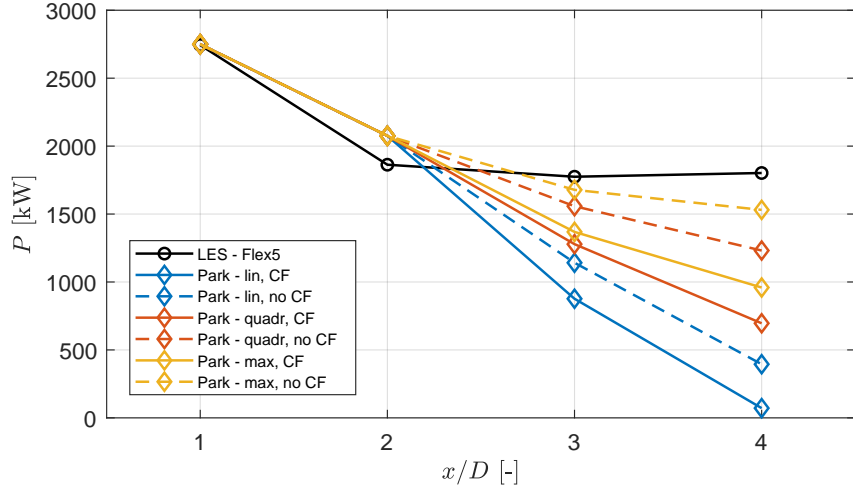
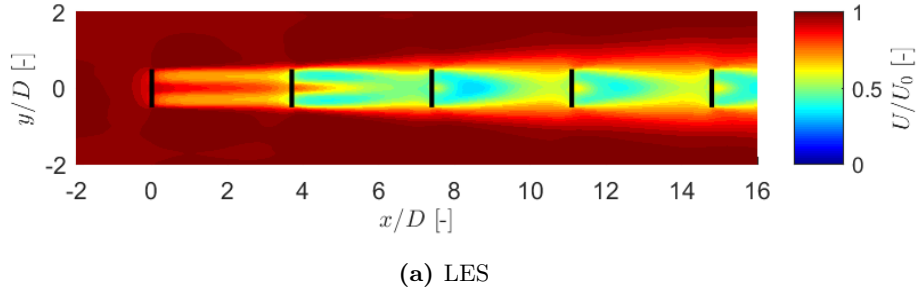


Figure C.3: Power of the LES simulation and Park models for Case A3.

C.1.3 Case A4: 5 wind turbines

Figure C.4 shows the horizontal wind field at hub height of the LES result including five wind turbines ($S_x = 3.7D$) and the Park model with different superposition methods. The inflow wind speed is 14 m.s^{-1} and the turbulence intensity equals 3.6%. When the wind speed is negative, which is physical not possible, the numerical results are “Not a number” and this is shown in white in the figures.

Figure C.5 shows the power of the LES result and the Park models.



(a) LES

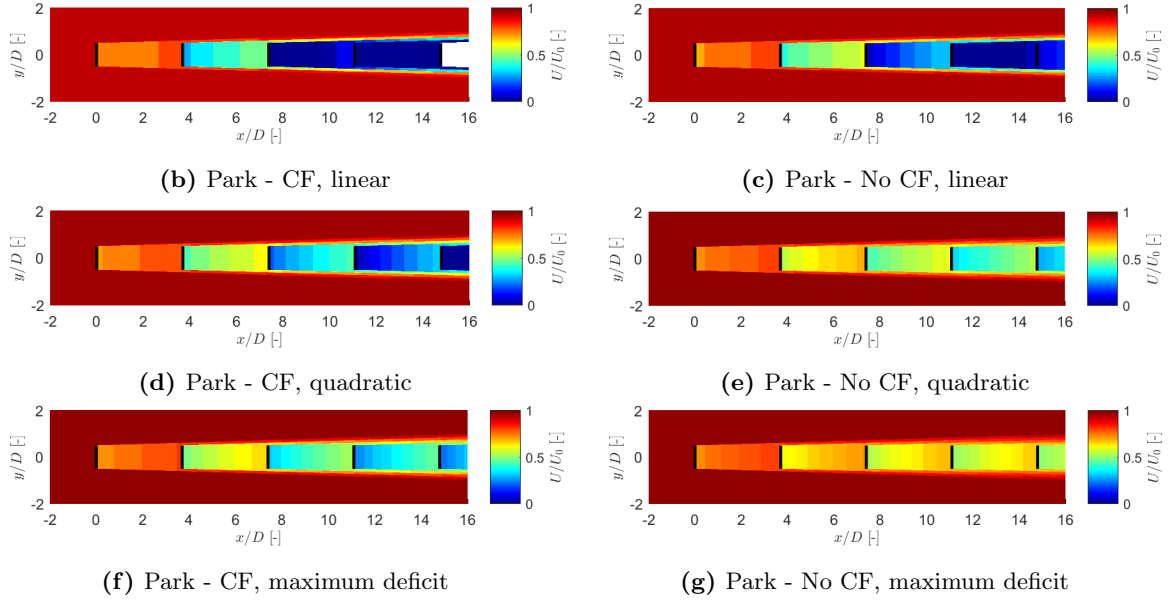


Figure C.4: Horizontal wind speed field at hub height for Case A4 (five wind turbines with a spacing of $3.7D$). The white areas indicate where a negative wind speed is obtained.

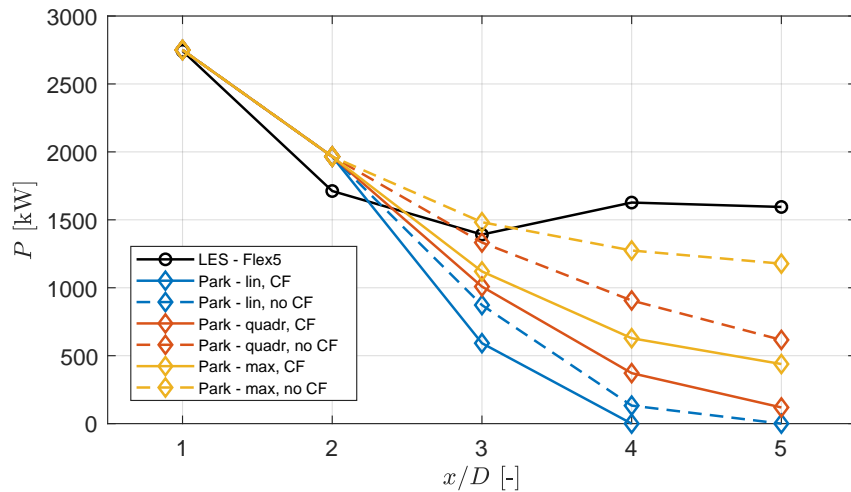
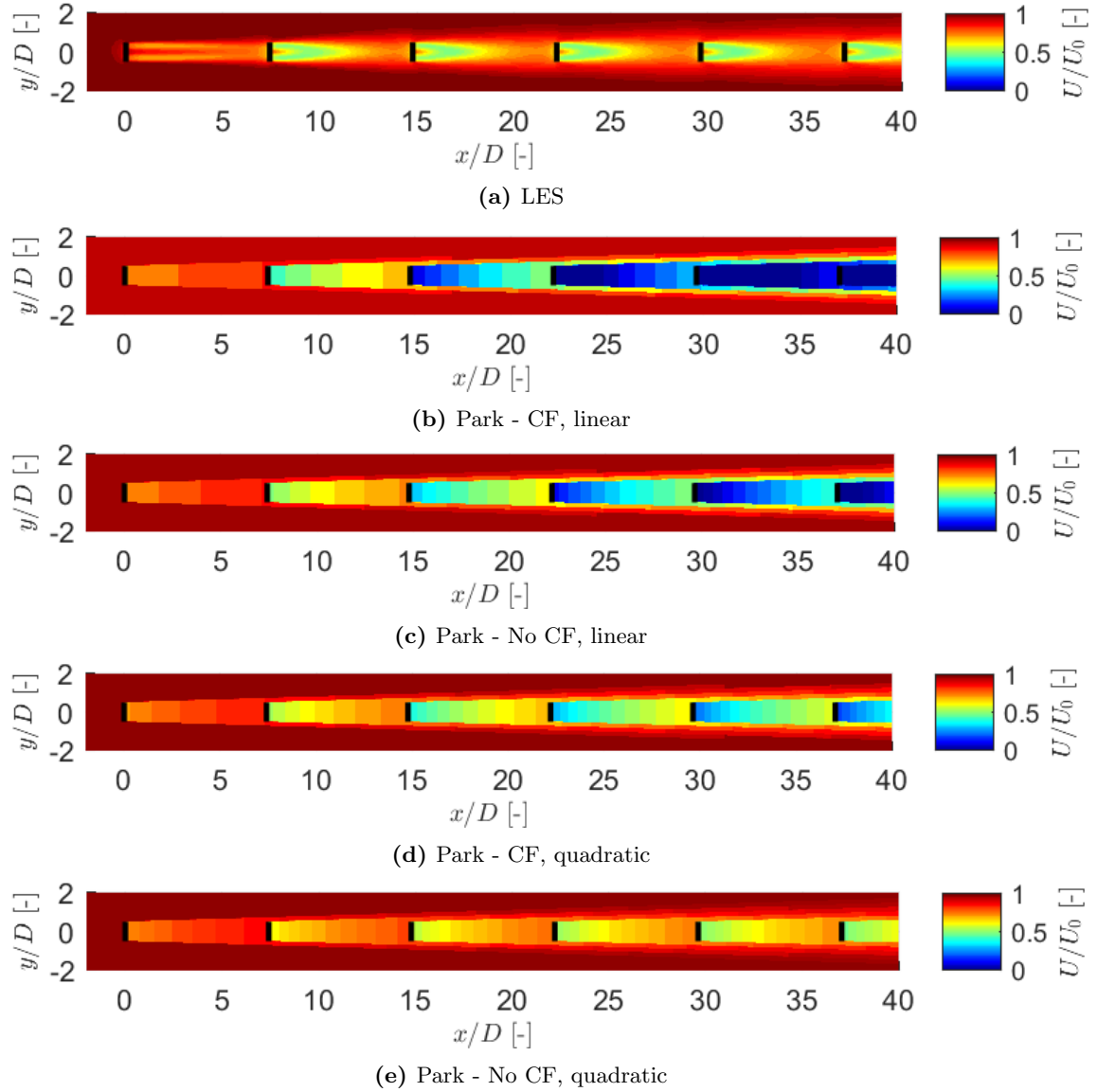
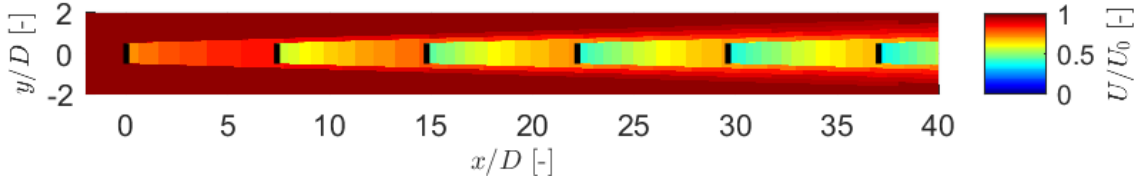


Figure C.5: Power of the LES and Park models for Case A4.

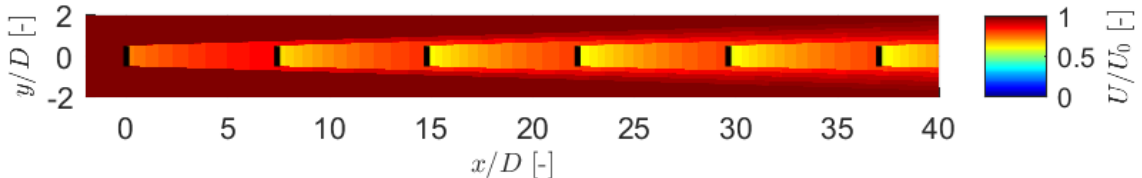
C.1.4 Case A5: 6 wind turbines

Figure C.6 shows the horizontal wind field at hub height of the LES result including six wind turbines ($S_x = 7.4D$) and the Park model with different superposition methods. The inflow wind speed is 14 m.s^{-1} and the turbulence intensity equals 3.6%.





(f) Park - CF, maximum deficit

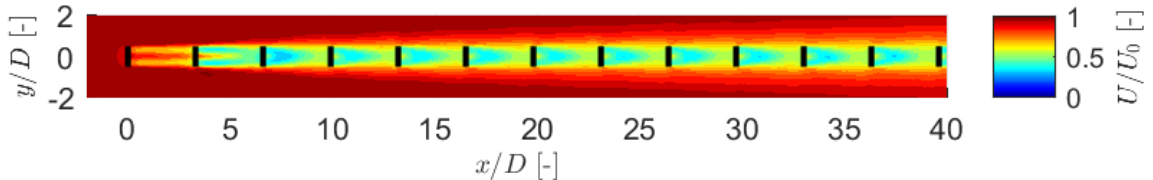


(g) Park - No CF, maximum deficit

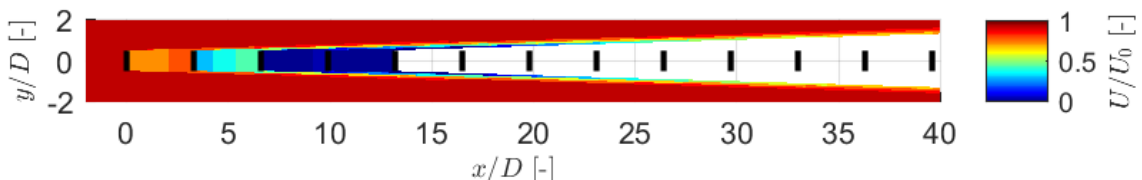
Figure C.6: Horizontal wind speed field at hub height for Case A5 (six wind turbines with a spacing of $7.4D$).

C.1.5 Case A6: 13 wind turbines

Figure C.7 shows the horizontal wind field at hub height of the LES result including 13 wind turbines ($S_x = 3.3D$) and the Park model with different superposition methods. The inflow wind speed is 14 m.s^{-1} and the turbulence intensity equals 3.6%. When the wind speed is negative, which is physical not possible, the numerical results are “Not a number” and this is shown in white in the figures.



(a) LES



(b) Park - CF, linear

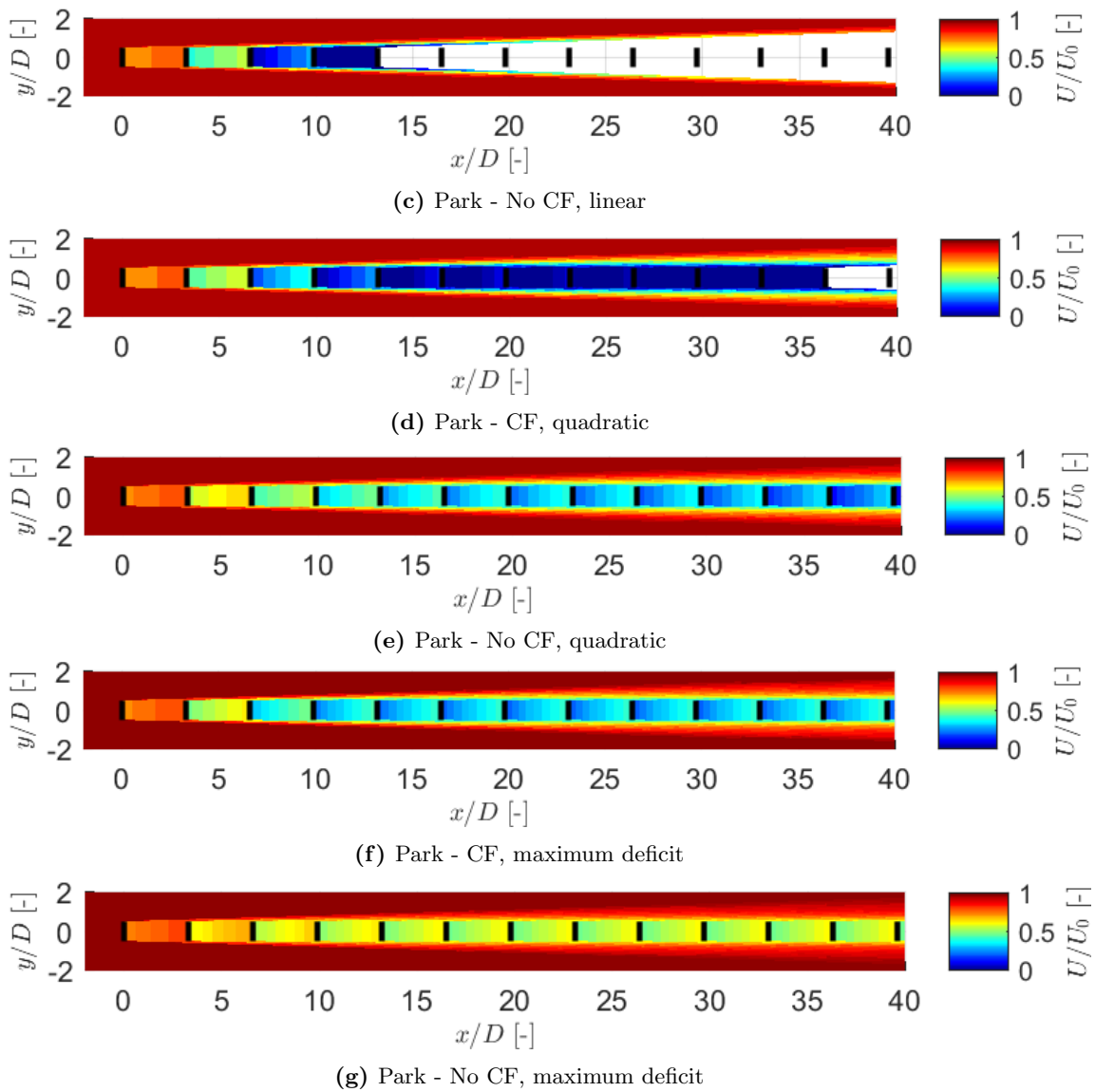


Figure C.7: Horizontal wind speed field at hub height for Case A6 (13 wind turbines with a spacing of $3.3D$). The white areas indicate where a negative wind speed is obtained.

C.2 Case B: $U_0 = 11.2 \text{ m.s}^{-1}$

C.2.1 Case B3: 3 wind turbines

Figure C.8 shows the horizontal wind field at hub height of the LES result including three wind turbines ($S_x = 7.4D$) and the Park model with different superposition methods. The inflow wind speed is 11.2 m.s^{-1} and the turbulence intensity equals 3.6%.

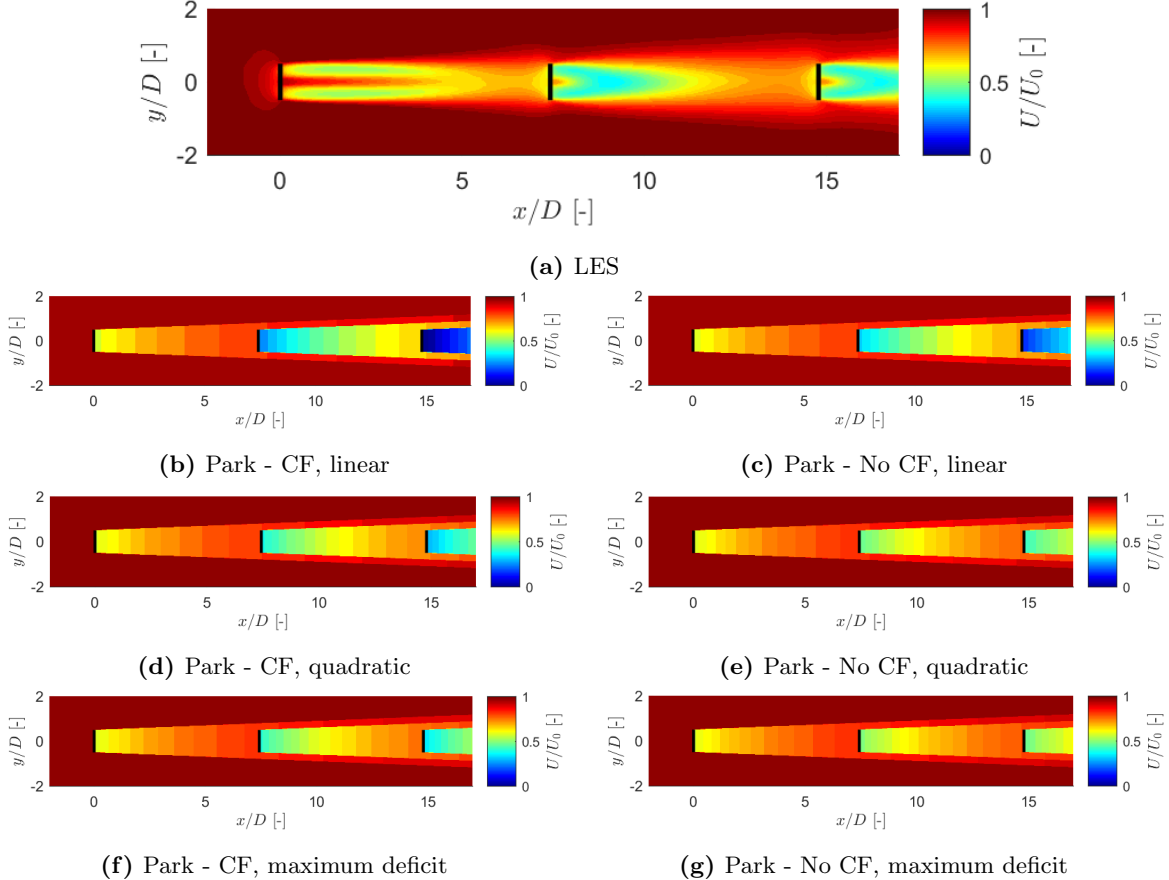


Figure C.8: Horizontal wind speed field at hub height for Case B3 (three wind turbines with a spacing of $7.4D$).

Appendix D

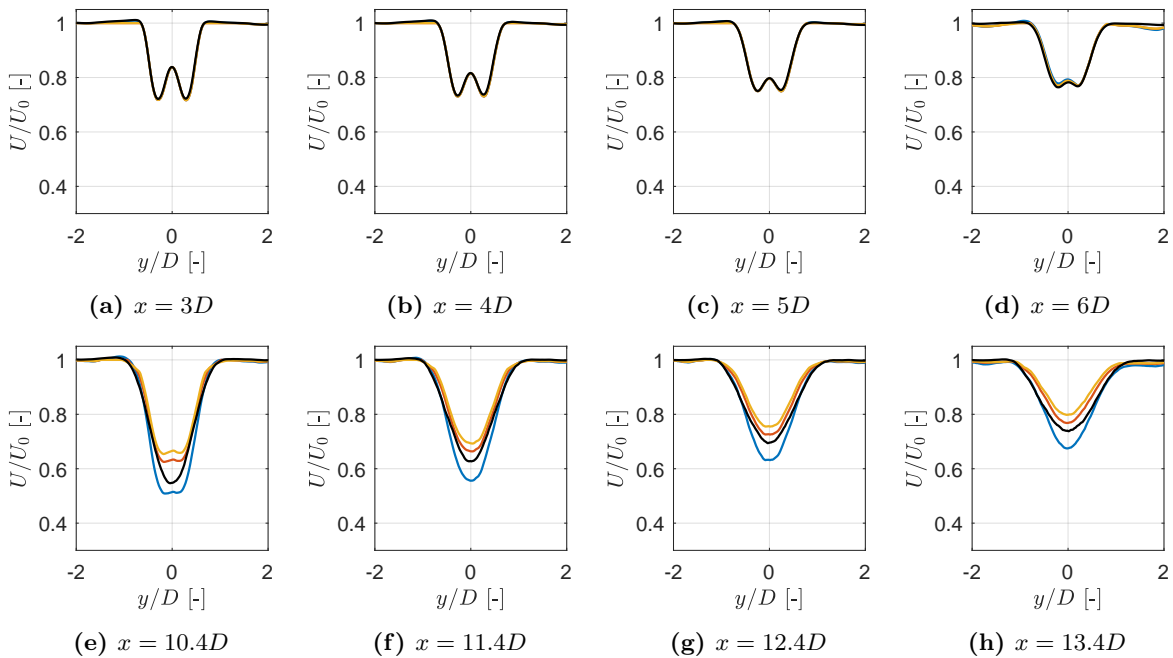
LES superposition

D.1 Case A5

The figures below are for the LES superposition method with the following normalized single wakes chosen:

- Wake 1: $U_0 = 14 \text{ m.s}^{-1}$ and TI=3.6% (Case A1)
- Wake 2: $U_0 = 11.2 \text{ m.s}^{-1}$ and TI=8.6% (Case B2)
- Wake 3-6: $U_0 = 8.6 \text{ m.s}^{-1}$ and TI=3.6% (Case C1)

Figure D.1 shows the horizontal wind profiles $3D$, $4D$, $5D$ and $6D$ behind the wind turbines.



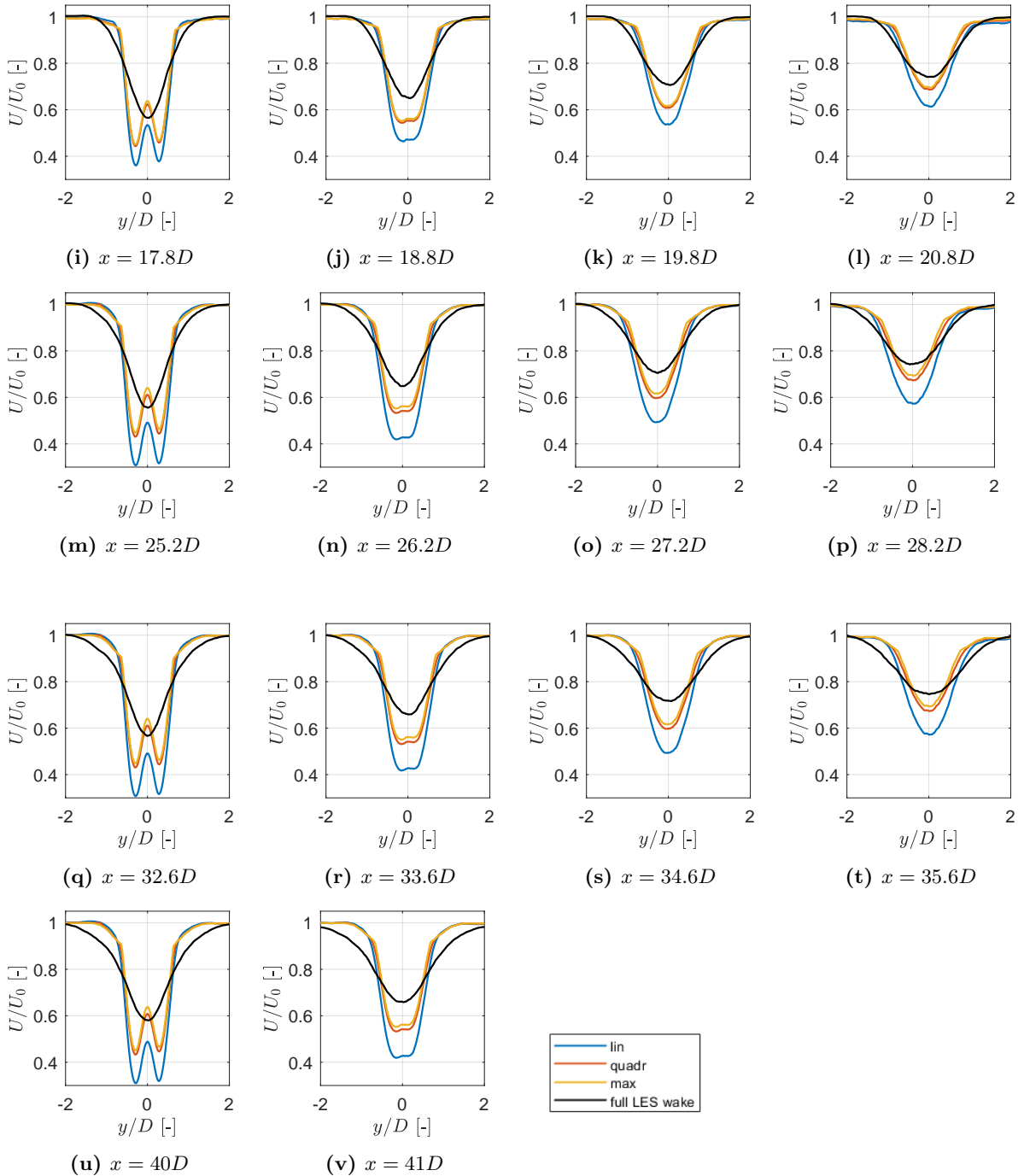


Figure D.1: Horizontal profiles at hub height of the original LES simulation with 6 wind turbines (Case A5) and the fields constructed out of single wake LES simulations. The LES superposition is carried out making use of the single LES wakes of Case A1, B2 and C1.

The figures below are for the LES superposition method with the following normalized single wakes chosen:

- Wake 1: $U_0 = 14 \text{ m.s}^{-1}$ and TI=3.6% (Case A1)
- Wake 2-6: $U_0 = 11.2 \text{ m.s}^{-1}$ and TI=8.6% (Case B2)

Figure D.2 shows the difference in the horizontal wind fields at hub height between the full LES

wake and the wind fields of the superposition of single LES wakes. Figure D.3 shows the wake boundary of the full LES wake and superposed wake fields.

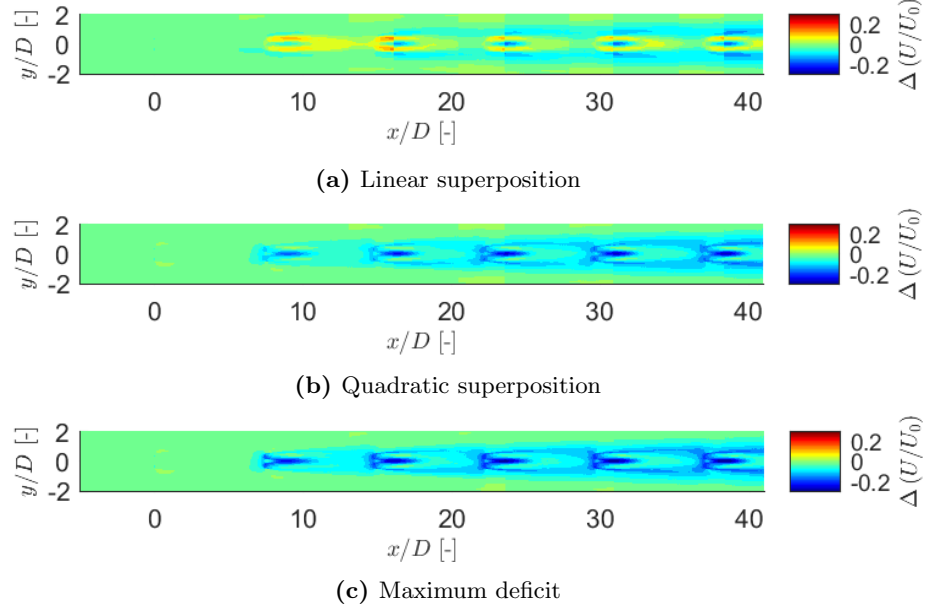


Figure D.2: Difference in the horizontal wind speed fields at hub height of the full LES wake and the superposed LES wakes, making use of (a) linear, (b) quadratic and (c) maximum deficit superposition. The second to the sixth single wake have an inflow wind speed of 11.2 m.s^{-1} and turbulence intensity of 8.6%.

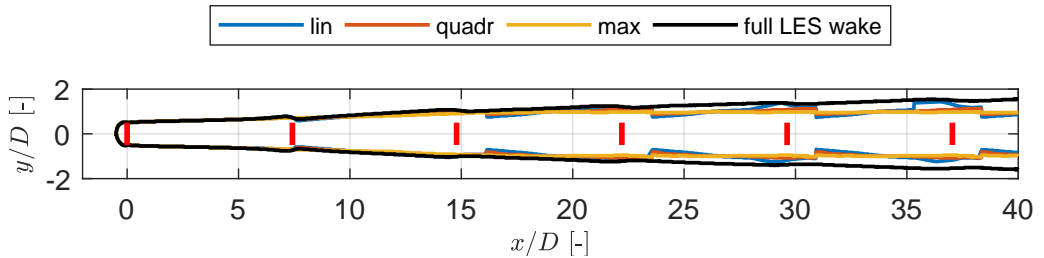


Figure D.3: Wake boundary of the full LES wake (Case A5) and the superposed wake field, making use of the single LES wakes of Case A1 and B2.

D.2 Case A6

Figure D.4 illustrates the calculation of the mean wind speed and turbulence intensity at the location of the third wind turbine with respect to the second wind turbine. The single wake has an inflow wind speed of 11.2 m.s^{-1} and a turbulence intensity of 8.6 %.

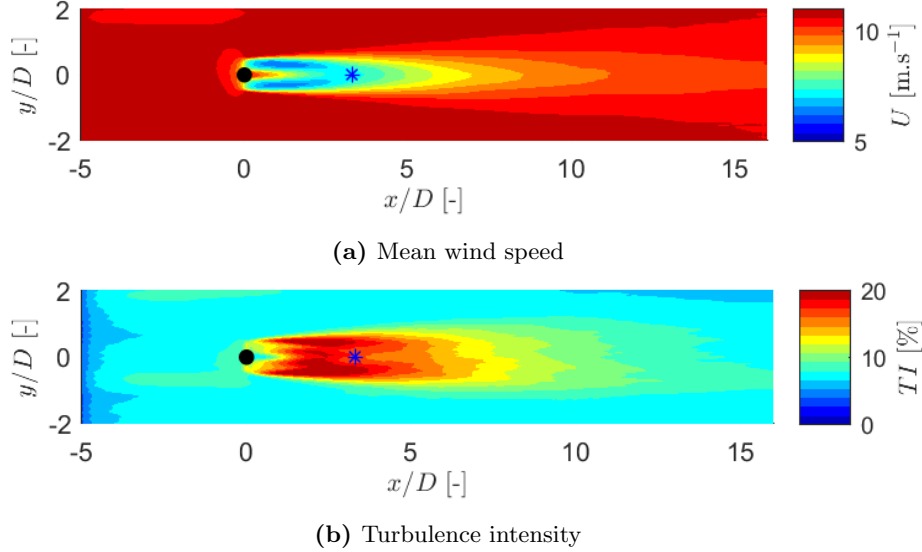


Figure D.4: Illustration of the calculation of the mean wind speed and turbulence intensity at the location of the third wind turbine with respect to the first wind turbine ($3.3D$) in the single LES wake with an inflow wind speed of 11.2 m.s^{-1} and $TI=8.6\%$ (Case B2).

The figures shown below are for the LES superposition methods with the following single wakes chosen:

- Wake 1: $U_0 = 14 \text{ m.s}^{-1}$ and $TI=3.6\%$ (Case A1)
- Wake 2-13: $U_0 = 11.2 \text{ m.s}^{-1}$ and $TI=8.6\%$ (Case B2)

Figure D.5 shows the horizontal wind fields at hub height of the full LES wake and the superposed wind fields. Figure D.6 shows the difference between those wind fields. Figure D.7 shows the wake boundary of the full LES wake and superposed wake fields.

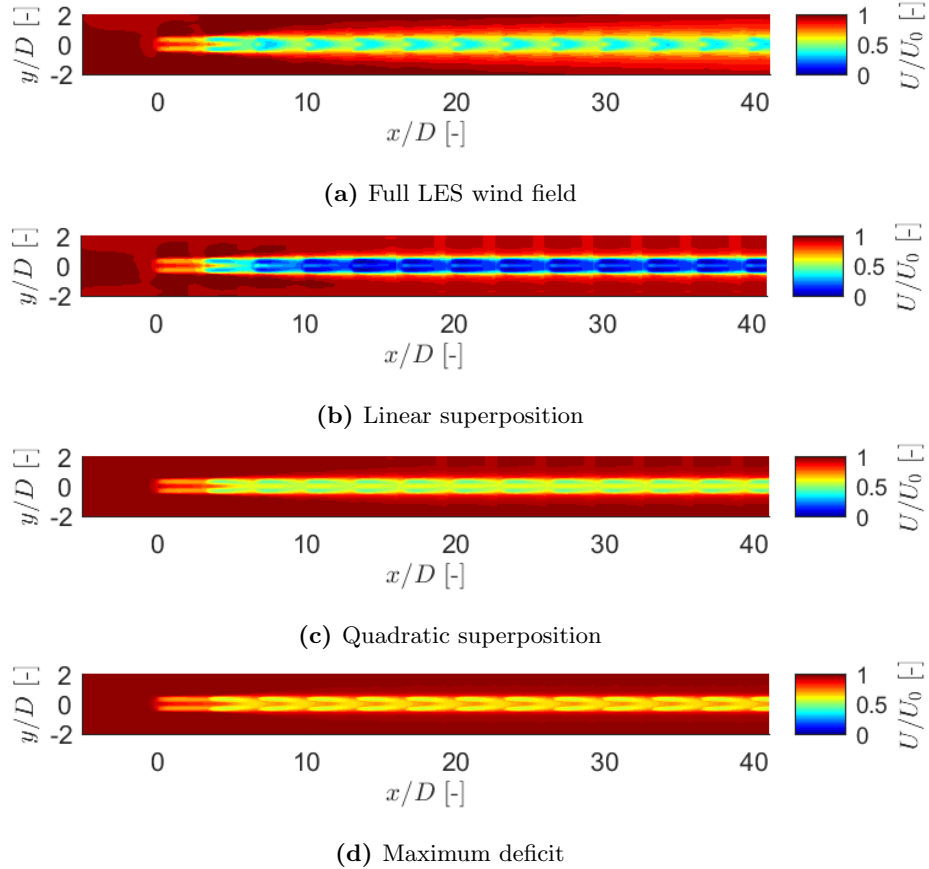


Figure D.5: Horizontal wind speed fields at hub height of (a) the full LES wake, followed by the superposed LES wakes, making use of (b) linear, (c) quadratic and (d) maximum deficit superposition. The LES superposition is carried out making use of the single LES wakes of Case A1 and B2.

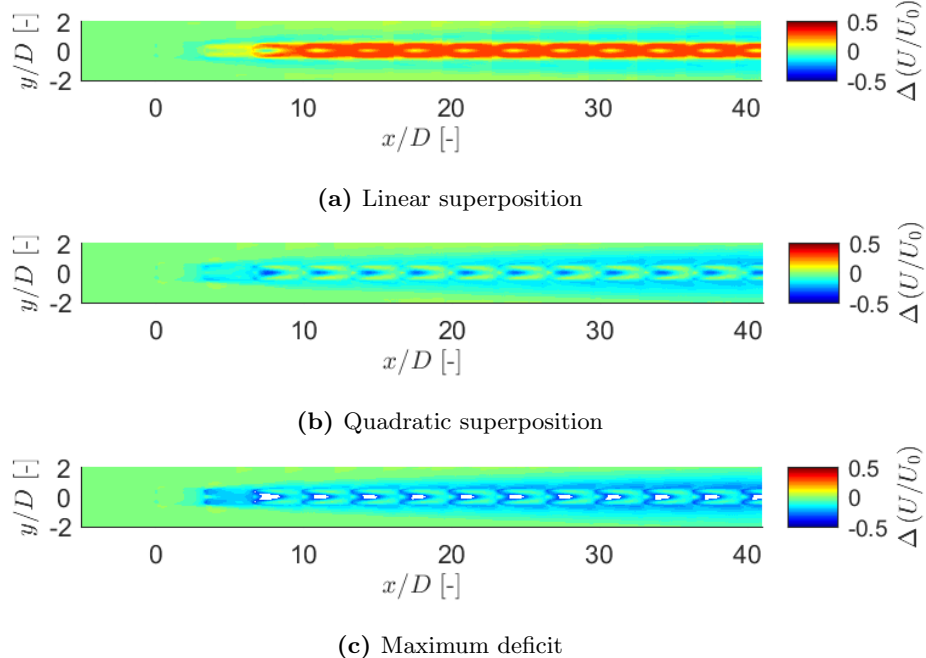


Figure D.6: Difference in the horizontal wind speed fields at hub height of the full LES wake results and the superposed LES wakes, making use of (a) linear, (b) quadratic and (c) maximum deficit superposition. The LES superposition is carried out making use of the single LES wakes of Case A1 and B2.

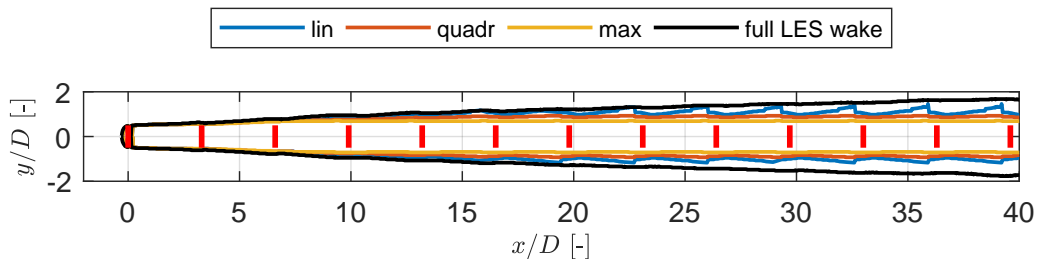


Figure D.7: Wake boundary of the full LES wake (Case A6) and the superposed wake field, making use of the single LES wakes of Case A1 and B2.

Appendix E

Optimization method

E.1 Methodology

Figure E.1 shows the linear extrapolation of a single wake with an inflow wind speed of 14 m.s^{-1} and turbulence intensity of 3.6 %.

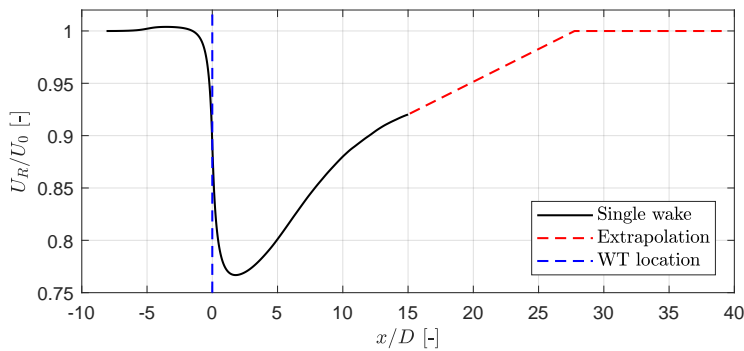


Figure E.1: Linear extrapolation of a single LES wake (Case A1).

E.2 Method A: Interpolation of α -coefficients

In Section 9.2.1, the results are shown for wind turbine spacings of $3.3D$, $3.7D$, $4.9D$ and $7.4D$ and trends could be seen for each coefficient as a function of the spacing. Now is looked at the change in result if only two or three of these coefficient sets were available.

In a first step, the difference in the result is looked at if the α -coefficients for a spacing of $3.3D$, $3.7D$ and $7.4D$ would be known and the coefficients for a spacing of $4.9D$ are interpolated (interpolation 1). Figure E.2a shows the original results (full line), as discussed before, and the results without the coefficient of $4.9D$ (dashed line). The black points indicate the interpolated values of the α -coefficients for a spacing of $4.9D$. By comparing the full lines and the interpolated points, the difference in the coefficients can be calculated.

The same procedure can be followed if only the coefficients for a wind turbine spacing of $3.3D$ and $7.4D$ are known and the coefficients for a spacing of $3.7D$ and $4.9D$ are interpolated (interpolation 2), which is shown in Figure E.2b.

Table E.1 summarizes the different α -coefficients for $f_{A,L}$, i.e. the original coefficients and the coefficients calculated with interpolation 1 and interpolation 2. Figure E.3 shows both the original optimization method solution for the rotor averaged wind speed deficit and the results with the interpolated coefficients. The difference in the coefficients is the largest for α_4 , which is

manifested in the highest difference in the rotor averaged wind speed downstream of the fourth wind turbine.

The RMSE of the target (Case A3) and the original solution equals 0.029. The RMSE of interpolation 1 and interpolation 2 equal 0.0325 and 0.0327 respectively. As the difference between the coefficient of interpolation 1 and interpolation 2 is small, the difference between the solution of the rotor averaged wind speed is small as well.

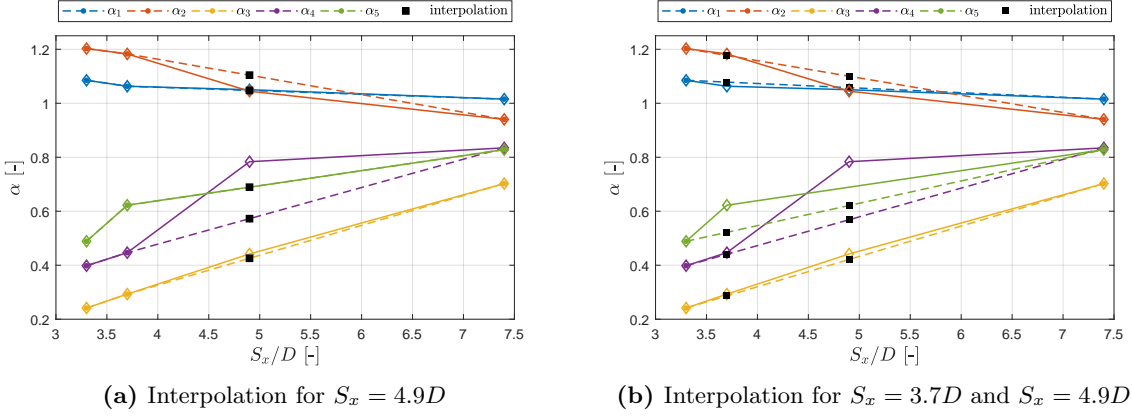


Figure E.2: The original α -coefficients for $f_{A,L}$ are plotted in full lines. The interpolated coefficients are plotted in black for (a) $3.3D$, $3.7D$ and $7.4D$ known (interpolation 1) and (b) $3.3D$ and $7.4D$ known (interpolation 2).

Table E.1: Original α -coefficients for $f_{A,L}$ and the coefficients calculated by interpolation, together with the RMSE for all solutions.

	α -coefficients for $f_{A,L}$				RMSE
	α_1	α_2	α_3	α_4	
original	1.050	1.045	0.442	0.784	0.0285
interpolation 1	1.048	1.104	0.426	0.573	0.0325
interpolation 2	1.058	1.100	0.421	0.569	0.0327

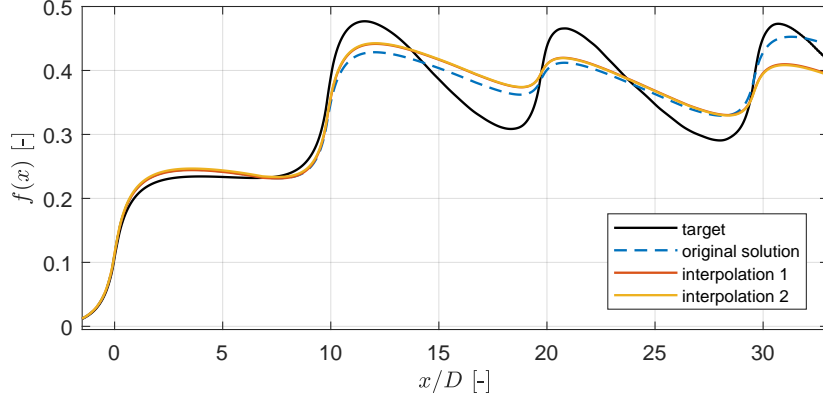


Figure E.3: Solution of the rotor averaged wind speed deficit with interpolated α -coefficients for $4.9D$ with the coefficients for (a) $3.3D$, $3.7D$ and $7.4D$ known (interpolation 1) and (b) $3.3D$ and $7.4D$ known (interpolation 2).

The solution with interpolation for the coefficients of $f_{A,Q}$ (Eq. (9.6)) (quadratic) are shown in Figure E.4, Figure E.5 and Table E.2. The conclusions are similar: the difference in the coefficients is the highest for α_4 and therefore is also the difference the highest for the fourth wake. The RMSE for the rotor averaged wind speed increases from 0.037 to 0.042 and 0.043 from the original solution to the solution with the interpolation coefficients.

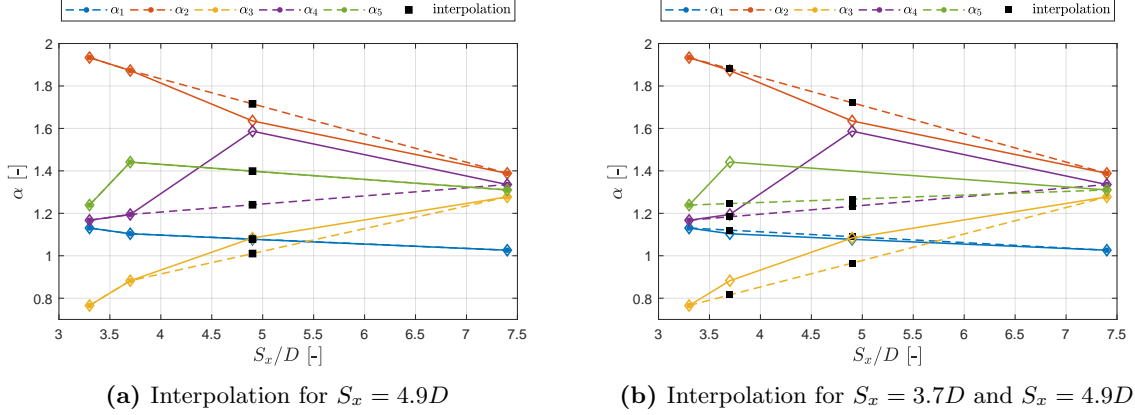


Figure E.4: The original α -coefficients for $f_{A,Q}$ are plotted in full lines. The interpolated coefficients are plotted in black for (a) $3.3D$, $3.7D$ and $7.4D$ known (interpolation 1) and (b) $3.3D$ and $7.4D$ known (interpolation 2).

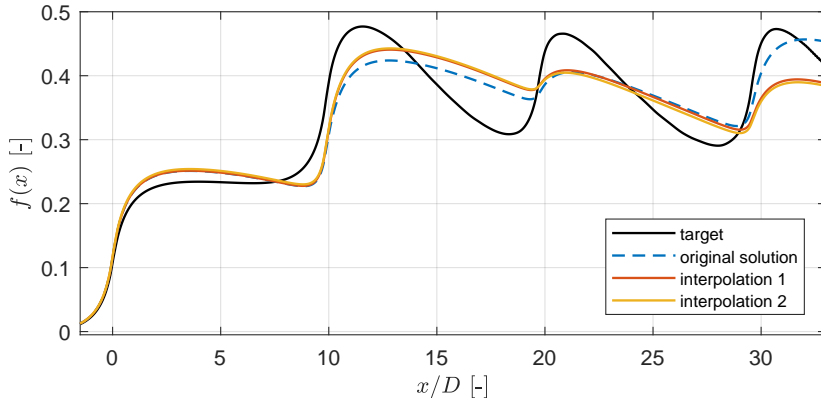


Figure E.5: Solution of the rotor averaged wind speed deficit with interpolated α -coefficients of $f_{A,Q}$ for $4.9D$ with the coefficients for (a) $3.3D$, $3.7D$ and $7.4D$ known (interpolation 1) and (b) $3.3D$ and $7.4D$ known (interpolation 2).

Table E.2: Original α -coefficients for $f_{A,Q}$ and the coefficients calculated by interpolation, together with the RMSE for all solutions.

	α -coefficients for $f_{A,Q}$				RMSE
	α_1	α_2	α_3	α_4	
original	1.078	1.635	1.084	1.587	0.0366
interpolation 1	1.079	1.716	1.011	1.240	0.0419
interpolation 2	1.090	1.721	0.965	1.233	0.0429

The interpolation of the α -coefficients if a single Park wake is used, would give larger differences

as the trends of these coefficients are not linear. Therefore, more points are needed to fit a non-linear curve.

